DETERMINING THE FATE OF METHANE RELEASED FROM THE SEAFLOOR IN DEEP AND SHALLOW WATER ENVIRONMENTS

A Dissertation

by

MENGRAN DU

Submitted to the Office of Graduate and Professional Studies of
Texas A&M University
in partial fulfillment of the requirements for the degree of

DOCTOR OF PHILOSOPHY

Chair of Committee,	John Kessler
Co-Chair of Committee,	Shari Yvon-Lewis
Committee Members,	Thomas Bianchi
	Brendan Roark
	Meixun Zhao
Head of Department,	Debbie Thomas

August 2014

Major Subject: Oceanography

ABSTRACT

Marine gas seeps and accidental marine oil spills are sources of methane (CH_4) to the ocean, and potentially to the atmosphere, though the magnitude of the fluxes and dynamics of these systems are poorly defined. For example, the ultimate capacity of aerobic CH_4 oxidation, a process converting CH_4 to carbon dioxide (CO_2) and biomass in most ocean waters, is unknown. Deeper water environments may provide a longer conduit for CH_4 to transit before atmosphere emission and thus a higher likelihood for an oxidative fate. Shallow water environments may provide a shorter conduit for CH_4 to transit before being emitted to the atmosphere, however, these environments often have some of the highest rates of primary production causing pCO_2 to be undersaturated. Thus the biochemical conversion of CH_4 to CO_2 may not enable this released carbon to be emitted to the atmosphere. To better constrain these variables in natural environments, studies of dissolved oxygen (DO) concentration, CH_4 concentration and stable isotopic ratios were conducted at two contrasting sites: the Deepwater Horizon (DWH) oil spill in the Gulf of Mexico (GoM) and the natural seep field near Coal Oil Point (COP), CA.

The investigation of 1316 DO profiles measured from 11 May until 20 September 2010 revealed the spatial and temporal variability of bulk hydrocarbon respiration in these deep and intermediate plumes since DO is removed during hydrocarbon respiration. These analyses suggest that the general movement of these plumes was toward the southwest, and that a total mass of 0.18 ± 0.05 Tg hydrocarbon in the plume layers was fully respired

to CO_2, and 0.10 ± 0.08 Tg hydrocarbon was incorporated into biomass (i.e. conversion efficiency 0.36 ± 0.11 mg biomass/mg hydrocarbon). A stable isotope model incorporating measurements of CH_4 concentrations, CH_4 oxidation rates, and current velocity was developed to determine CH_4 oxidation rates, as well as the flow rate from the seafloor. This model was tested on 20 samples taken from 1 to 12 km from the wellhead from 11 June through 20 June 2010 during the DWH oil spill. Results suggest that the rate of CH_4 oxidation ranged from 22 to 844 nM d^{-1} in mid-June 2010 and that the rate of flow from the Macondo well was 8.4×10^7 moles d^{-1}, both of which are in agreement with previous estimates determined independently.

High-resolution measurements of sea surface CH_4 and CO_2 concentrations and air-sea fluxes were conducted at the COP seep field. Results suggest that the diffusive air-sea fluxes of CH_4 and CO_2 were 0.18 ± 0.19 mmol m^{-2} day^{-1} and -1.65 ± 1.23 mmol m^{-2} day^{-1}, respectively, and that the extent of microbial oxidation of CH_4 was insufficient to change this shallow water environment from a sink of atmospheric CO_2 to a source.

The seeps at COP released CH_4 into waters at a rate that was an order of magnitude less than that from the DWH oil spill, and resulted a plume area that was also an order of magnitude less. In total, these results suggest that microbial oxidation provides the dominant sink of the released CH_4 at both sites.

DEDICATION

To

My Parents

Xiaomei Chen & Jinchun Du

in recognition of their unconditional

love, support, guidance, encouragement.

ACKNOWLEDGEMENTS

I would like to express my sincere gratitude to my committee chair, Dr. John Kessler, my committee co-chair Dr. Shari Yvon-Lewis, and my committee members, Dr. Thomas Bianchi, Dr. Brendan Roark, and Dr. Meixun Zhao, for their guidance and support throughout the course of this research. I extend special thanks to John who has taught me more than I ever thought possible. Special thanks also go to Shari for all the encouragement she has given me. It has been an absolute pleasure working with them.

I want to thank the department faculty and staff for making my time at Texas A&M University a great experience. I also want to extend my gratitude to the National Education Foundation, the Gulf of Mexico Research Initiative, and the China Scholarship Council, for providing financial support.

Lastly I would like to thank my friends and family for always believing in me, always encouraging me, and always loving me. My parents, Xiaomei Chen and Jinchun Du, receive my deepest gratitude and love for their dedication throughout my life.

NOMENCLATURE

CH_4	Methane
CO_2	Carbon Dioxide
COP	Coal Oil Point
CRDS	Cavity Ring-Down Spectroscopy
DWH	Deepwater Horizon
FID	Flame Ionization Detector
GC	Gas Chromatography
GoM	Gulf of Mexico
IRMS	Isotope-ratio Mass Spectrometry

TABLE OF CONTENTS

Page

Page

LIST OF FIGURES

Page

Page

LIST OF TABLES

Page

1. INTRODUCTION AND LITERATURE REVIEW

Methane (CH_4) is the most abundant component of volatile organic carbon (VOC) in the atmosphere [*Wuebbles and Hayhoe*, 2000] and an important greenhouse gas, which warms the Earth 23 times more than carbon dioxide (CO_2) over a 100-year timescale [*Forster et al.*, 2007; *Ramaswamy et al.*, 2001]. Though the present concentration of CH_4 in the atmosphere is ~200 times lower than that of carbon dioxide, the CH_4 concentration has risen by ~150% since pre-industrial times, and this is ~5 times faster than the rate of change of carbon dioxide, and continues to rise [*Forster et al.*, 2007]. Despite the fact that the ocean contributes only ~1% to the global atmospheric budget [*Wuebbles and Hayhoe*, 2002], the ocean is the largest global reservoir of CH_4 and has the potential to increase its emissions with changing oceanographic conditions as implied from the geologic record, e.g., the Paleocene-Eocene Thermal Maximum [*Dickens et al.*, 1995]. The complexity of migration pathways of CH_4 in the sediments and in the waters makes the quantification of CH_4 dynamics remarkably challenging. It is necessary to understand each of these processes to better understand the fate of CH_4 in different environments.

1.1 Methane Cycling in the Ocean

In continental margins, a large amount of CH_4 is preserved in clathrate hydrates, anoxic sediments, thawed permafrost, and deep petroleum reservoirs. Methane in marine sediments originates from two main sources: microbial degradation of organic matter in shallow sediments and thermocatalytic breakdown of complex organic matter in deep

sediments. Methanogenesis generally occurs beneath the sulfate-reduction zone, which is typically a few tens of meters deep, and in some circumstances several hundred meters beneath the seafloor [*Parkes et al.*, 1990]. In contrast, thermogenic CH_4 usually occurs at depths exceeding 1,000 m [*Floodgate and Judd*, 1992] as part of the petroleum-generating processes [*Judd*, 2004] under conditions of high temperature and pressure.

Microbial and thermogenic CH_4 may dissolve in pore waters, remain trapped, or migrate upward. In deep water environments, upward migration may be inhibited where conditions of temperature and pressure are favorable for the formation of gas hydrates, an ice-like clathrate structure. Methane hydrates occur in thick onshore permafrost, the shallow Artic shelf, the upper edge of the stability zone, deep water sediments, and seafloor mounds. Deep water sediments are by far the most abundant, containing 95.5% of the global CH_4 hydrate reservoir [*Ruppel*, 2011]. When gas hydrates dissociate, or CH_4 underneath them migrates upward, most of the CH_4 will be anaerobically oxidized in the near-seafloor sediments [*Hinrichs and Boetius*, 2002; *Knittel and Boetius*, 2009; *W. S. Reeburgh*, 2007; *Treude et al.*, 2003]. At active seeps, excess CH_4 is released to the seafloor.

The ocean acts as a filter of seepage CH_4 since dissolution, oxidation and physical processes, such as currents, may restrict CH_4 from reaching the atmosphere. Methane is found to compose ~90% of most bubbles released from seeps at the seafloor, but only ~60-70% of the bubbles reaching the sea surface [*Clark et al.*, 2003; *Leifer et al.*, 2000]. Methane is lost in the water column through dissolution, a process that is dependent on

the initial bubble size, the water depth, the presence of upwelling, etc. In locations with seafloor depths greater than 100 m, CH_4 in rising bubbles may be completely replaced by DO and nitrogen in the water [*McGinnis et al.*, 2006]. The dissolved CH_4 is mostly utilized by microbes as part of their metabolic processes [*Mau et al.*, 2012; *Mau et al.*, 2007]. Thus, the presence of gas seeps supports localized benthic biological communities. It seems to imply that only the CH_4 released from shallow seeps is able to reach the atmosphere. However, there are several exceptions. For instance, at petroleum reservoirs, oil coating the bubbles inhibits the loss of CH_4 to dissolution and oil-coated bubbles may even reach the sea surface [*Sassen et al.*, 2001]. At seeps that occur within the gas hydrate stability zone (GHSZ), bubbles are coated by gas hydrates that protect bubbles until they reach the limit of the GHSZ [*Cranston et al.*, 1994].

Methane released from seeps may enter the atmosphere either directly through bubble injection at the sea surface or indirectly by diffusion from dissolved CH_4 in surface waters. Estimates of the contribution by seeps to the atmospheric CH_4 budget rely on the knowledge of seep distribution, gas flux rates at the seafloor, biological activity in the water, and survivability of rising bubbles [*Cranston et al.*, 1994; *Hornafius et al.*, 1999; *Mau et al.*, 2007]. Despite the fact that a large number of natural gas seeps have been recorded globally, only a few seepage flux measurements at the seafloor have been done due to the technical difficulties (such as the difficulty in deploying measuring equipment) and costs involved [*Boles et al.*, 2001; *Dimitrov*, 2002; *Hornafius et al.*, 1999; *Judd et al.*, 2002].

1.2. Microbial Oxidation of Methane

1.2.1 Indicators of Microbial Activity

Dissolved Oxygen

Dissolved oxygen (DO) in the surface ocean is generally close to equilibrium with the atmosphere. The DO level drops quickly below the surface mixed layer where DO is utilized for the remineralization of organic matter descending from above. At deeper depths, oxygen gradually increases as lower temperature increases the solubility of oxygen, and advection brings cold and oxygen-rich deep waters from polar regions (Figure 1.1A).

DO profiles can be affected under certain conditions. For instance, hypoxia, defined as zones of DO concentration less than 2 mg/L, has been reported in shallow waters in the northern Gulf of Mexico due to stratification and eutrophication [*Rabalais and Turner*, 2001]. However similar reduction of DO has not been reported in deep waters of the Gulf of Mexico. Interestingly, A particular circumstance is spike drops of DO when a large amount of hydrocarbons was were released into the deep ocean of the Gulf of Mexico during the DWH oil spill, large drops of DO were observed in the deepwaters (Figure 1.1B), e.g. [Valentine et al., 2010; Du and Kessler, 2012]. A possible explanation for the abrupt deficiencies of DO is microbial oxidation of the emitted hydrocarbons, a process that removes DO simultaneously and quantitatively.

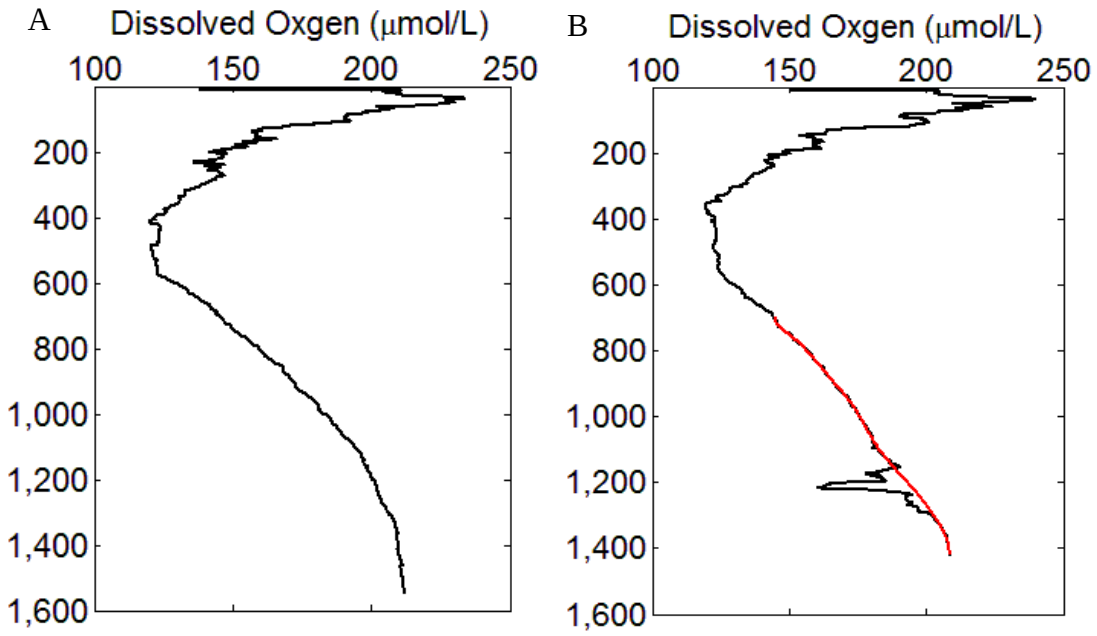

Figure 1.1 DO profile under normal and abnormal conditions: (A) normal condition; (B) affected by microbial CH_4 oxidation.

DO profiles are normally recorded by an electrode-based oxygen sensor (SBE-43) on a CTD. A polynomial can be fit to each DO profile providing a background from which the anomalous DO anomaly loss could can be calculated as the difference between the data and corresponding background [*Valentine et al.*, 2010]. Thus, the DO anomaly can be used to quantify the mass of hydrocarbons that have been released and respired when the mass fraction of individual hydrocarbons in deep water plume and their stoichiometric relationship with DO are known.

Stable Isotopes

As a fingerprint of the carbon reservoir, measurements of stable isotopes of ^{13}C-CH_4 in the ocean have been used to suggest whether the CH_4 was formed by thermogenic or biogenic processes [*Whiticar*, 1999]. Overall, CO_2 reduction and acetogenesis processes produce CH_4 that is some of the isotopically lightest carbon forms on earth, and hydrothermal dissociation produces relatively heavier CH_4 in the ocean.

However, $\delta^{13}C$-CH_4 in oceans is further altered when bacterial oxidation of CH_4 occurs [*Barker and Fritz*, 1981]. During microbial CH_4 oxidation processes, methanotrophs preferentially utilize the lighter molecule $^{12}CH_4$ over the heavier molecule $^{13}CH_4$, resulting in the residual CH_4 being enriched in ^{13}C. Thus, incorporating CH_4 isotopes into Rayleigh distillation equations [*Bigeleisen and Wolfsberg*, 1958; *Rayleigh*, 1896] provides a way to estimate the fraction of CH_4 that has been oxidized [*Kessler et al.*, 2006; *Kinnaman et al.*, 2007].

1.2.2 Methods for Measuring Methane Oxidation Rate

CH_4 oxidation rates have been measured by tracer incubation methods [*Pack et al.*, 2011; *Valentine et al.*, 2010], and by *in-situ* water mass tracking methods [*Heeschen et al.*, 2004; *Kadko et al.*, 1990; *Pack et al.*, 2011; *Rehder et al.*, 1999; *Scranton and Brewer*, 1978]. The radioisotope tracer methods measure the incorporation of ^{14}C-CH_4 or ^{3}H-CH_4 tracers in the oxidation product during incubation. These are currently the most sensitive methods and most commonly used [*Heintz*, 2012]. However problems arise from dealing with radio

tracers due to difficulties with shipping of radioisotopes and strict safety regulations. The water mass tracking methods determine CH_4 oxidation rates by comparing changes in CH_4 concentration with water mass ages. However, these methods are less sensitive than the tracer addition methods. Also, the tracer addition methods determine the specific CH_4 oxidation rates, but the water mass tracking methods provide integrative rates. Moreover, costly procedures are normally associated with most of these measurements and greatly limit the implementation of these techniques in field.

1.3 Study Objectives

The goal of this study was to investigate how water depth affects the fate of CH_4 released from the seafloor in deep and shallow water environments. Two sites were chosen for this study: the Deepwater Horizon (DWH) oil spill in the Gulf of Mexico and the shallow natural seep field near Coal Oil Point (COP), California. Seeing that no significant amount of CH_4 has been reported to escape to the atmosphere from natural deep seeps [*Hu et. al.*, 2012], the high powered DWH emission in deep waters would provide a unique opportunity to study the capacities of the ocean in constraining the released CH_4 from entering the atmosphere.

1.3.1 Deepwater Horizon Oil Spill in the Gulf of Mexico

On 20 April 2010, an explosion on an oil rig was caused by a blowout at the Macondo well. That explosion was visible for over 35 miles and killed 11 people. The platform then caught fire and burned for 2 days until 22 April when the platform sank. Since the

platform was still attached by the oil pipe to the seafloor, that pipe had to be cut away and oil and natural gas HCs began being emitted directly from the well into the deep waters of the Gulf of Mexico. The oil continued flowing until 15 July 2010, when the environmental release was finally terminated.

The DWH oil spill provided the opportunity to investigate how the ocean responds to a large release of oil and gas. The blowout caused an intrusion of a fluid mixture containing ~24% of gas and ~76% of oil by mass [*Reddy et al.,* 2011] to the deepwaters of the Gulf of Mexico. A large fraction of the wellhead fluids were either dissolved or trapped at depths, resulting in hydrocarbons plumes at ~1 km depth [*Ryerson et al.,* 2011; *Socolofsky et. al.,* 2011] that stimulated and sustained a bacterial bloom for several months [*Kessler et al.,* 2011b].

This spill also provided a unique opportunity to study how efficient the microorganisms were in removing the plume hydrocarbons in the Gulf of Mexico. Reductions in background DO concentrations [*Valentine et al.,* 2010] were observed due to the microbial respiration of ethane and propane in the early to middle periods of this disaster. Later in this disaster, it appears that CH_4 was the dominant driver of DO loss [*Kessler et al.,* 2011b, *Du and Kessler,* 2012]. Thus, a DO approach was developed to make an assessment of the amount of hydrocarbons that was released to the deep waters of the GoM, oxidized by methanotrphic bacteria, and incorporated into microbial biomass. A natural stable isotope

approach was also developed to provide an effective way to study the rate of CH_4 oxidation and the rate of flow from the DWH oil spill.

1.3.2 Shallow COP Seep Field

While the ocean acts as an efficient filter for CH_4 released at the seafloor, the filtration capacity is greatly reduced in shallow waters, such as the seep field at COP, California. As one of the world's largest seeps region, a significant sea-to-air emission of CH_4 has been found at the COP seep field [*Mau et al.*, 2007].

The COP seep field is located in bottom depths of 5 to 70m along the northern continental shelf of the Santa Barbara Chanel. The total gas emission at the COP seep field has been estimated using a sonar technique [*Hornafius et al.*, 1999; *Quigley*, 1999]. Methane flux at the seafloor was estimated to be in the range of 1.9 to 6.0 $\times 10^6$ mol d^{-1} [*Mau et al.*, 2007]. A model study estimated released CH_4 dissolving in the water at a rate of 3.6×10^6 mol d^{-1}, and a similar amount of being directly emitted to the atmosphere [*Clark et al.*, 2000]. Two distinct plumes [*Mau et al.*, 2012] have been identified in this seep field: one at ~40m depth and another one at ~200m depth. These two plumes result in high CH_4 concentrations in the surface water and the turnover time with respect to microbial oxidation of plume hydrocarbons was found to be shorter with increasing seafloor depth [*Mau et al.*, 2012]. Advection and horizontal turbulent diffusion greatly affect the propagation of these two plumes. Some of the CH_4 in the plumes is removed by microbes.

Most of the released CH_4 is transported down-current away from the seep field [*Clark et al.*, 2000] for further microbial oxidation and air-sea exchange.

Several studies have reported the air-sea fluxes of CH_4 from the COP seep field. However all of those are based on coarse sampling grids from which variations in surface water CH_4 concentration within a plume may not be captured. A study with continuous recording of the air-sea fluxes of CH_4 and CO_2 within the Santa Barbara Basin would provide a high resolution view of the distribution of dissolved CH_4 and carbon dioxide, as well as a more accurate amount of total diffusive air-sea flux of these two greenhouse gases from this seep field.

1.3.3 Comparison of the Two Sites

Comparing the DWH oil spill in the Gulf of Mexico in 2010 to the shallow natural seeps at COP, California, is a unique opportunity to see how differently oceans respond to the release of CH_4 at deep and shallow depths. Both the DWH oil spill in the Gulf of Mexico and natural seepage at the shallow COP seep field resulted in plumes of CH_4 in the water columns, but they tend to make significantly different contributions to the atmospheric CH_4 budget. Though the primary production (i.e., a process that removes CO_2 from the ocean and decreases surface ocean pCO_2) in the coastal waters near COP is much higher than that at the more open waters of GoM, there is a possibility of CO_2 produced from CH_4 oxidation making it to the atmosphere.

The study of bacterial activity during the oil spill will give us some of the fundamental capacities of microorganisms to consume released oil and natural gas, including CH_4, and some fundamental knowledge that is able to translate what we have learned from this disaster to other disasters that might occur at other areas on this planet. The study at the COP seep field not only provides a high-resolution view of air-sea fluxes of CH_4, but also tests the hypothesis that the microbial oxidation of dissolved CH_4 to CO_2 influences the dynamics of these greenhouse gases.

2. AN ASSESSMENT OF THE SPATIAL AND TEMPORAL VARIABILITY OF BULK HYDROCARBON RESPIRATION FOLLOWING THE DEEPWATER HORIZON OIL SPILL*

Following the Deepwater Horizon (DWH) blowout, the respiration of hydrocarbons dissolved and trapped in the deep and intermediate waters of the Gulf of Mexico imparted a significant reduction in dissolved oxygen (DO) concentration and stimulated a bloom of bacteria biomass. The investigation of 1316 DO profiles measured from 11 May until 20 September 2010 revealed the spatial and temporal variability of bulk hydrocarbon respiration in these deep and intermediate plumes. These analyses suggest that while there were occasional reversals in direction, the general movement of these plumes was toward the southwest and that the cumulative loss of DO peaked from 14 August through 18 September at a value of 18.9±3.8 Gmol. These oxygen-based analyses were extended to determine a first-order estimate of the total release of hydrocarbon mass to the environment that must be less than or equal to the true release based on the inherent assumptions; these analyses estimate a total environmental release of 0.47±0.09 Tg of analyses estimate a total mass of 0.18±0.05 Tg hydrocarbons in the plume layers fully respired to CO_2, 0.10±0.08 Tg hydrocarbons incorporated into biomass, and the hydrocarbons (60±19% of the official estimate based on acoustic techniques). These

*Reprinted with permission from Du, M. and Kessler, J. D. (2012), Assessment of the spatial and temporal variability of bulk hydrocarbon respiration following the Deepwater Horizon oil spill, Environmental science & technology, 46(19), 10499-10507. Copyright 2014 American Chemical Society.

biomass/hydrocarbon conversion efficiency of 0.36 ± 0.11 mg biomass/mg hydrocarbon. These analyses also suggest that CH_4 was the dominant hydrocarbon controlling the bulk respiration rates, and that the addition of dispersants to the wellhead effectively accelerated hydrocarbon respiration.

2.1 Introduction

Previous studies of well blowouts in deep water have shown the formation of hydrocarbon plumes in the water column [*Scott A Socolofsky and Adams*, 2005; *Yapa and Chen*, 2004]. The Deepwater Horizon incident in the Gulf of Mexico in 2010 was no exception. Hydrocarbons in the plumes, substrates for bacterial respiration, sustained a bacterial bloom for several months [*Camilli et al.*, 2010; *Hazen et al.*, 2010; *Valentine et al.*, 2012]. Several reports displayed data of hydrocarbon perturbations dissolved and trapped in plumes of unquantified mass in intermediate and deep waters [*Camilli et al.*, 2010; *Hazen et al.*, 2010; *Joye et al.*, 2011; *Kessler et al.*, 2011a; *Kessler et al.*, 2011b; *S. A. Socolofsky et al.*, 2011; *Valentine et al.*, 2012; *Valentine et al.*, 2010; *Yvon-Lewis et al.*, 2011], and reductions in background dissolved oxygen (DO) concentrations caused by the microbiological respiration of the plume hydrocarbons [*Camilli et al.*, 2010; *Joye et al.*, 2011; *Kessler et al.*, 2011a; *Kessler et al.*, 2011b; *Valentine et al.*, 2012; *Valentine et al.*, 2010]. Chemical components of the dispersants injected at the wellhead were found enriched in these deep plumes behaving in a conservative manner [*Kujawinski et al.*, 2011], however no data has been presented displaying a correlation between the addition of dispersants at the wellhead and hydrocarbon respiration rates. While natural seepage

has been shown to influence dissolved organic carbon profiles in ocean waters [*Pohlman et al.*, 2010; *Wang et al.*, 2001], most likely by a combination of direct and indirect (e.g. respiration byproducts) influence, natural seepage in the Gulf of Mexico has not been shown to influence water column profiles of DO in a similar manner to what was observed following the Macondo Well blowout (Figure 2.1, 2.2A,B) [*DiMarco et al.*, 2001; *Joye et al.*, 2011; *Kessler et al.*, 2011b; *Nowlin Jr.*, 2001; *Valentine et al.*, 2010]. Thus, we use these profiles to estimate respiration of the dissolved and trapped hydrocarbons released from the Deepwater Horizon. These oxygen-based analyses help constrain the direction of plume propagation, total amount of DO removed by hydrocarbon respiration, the total mass of hydrocarbons respired in the plume layers, the total mass of hydrocarbons incorporated into the biomass, bulk hydrocarbon respiration rates as a function of time, and the total mass of the environmental release from the well.

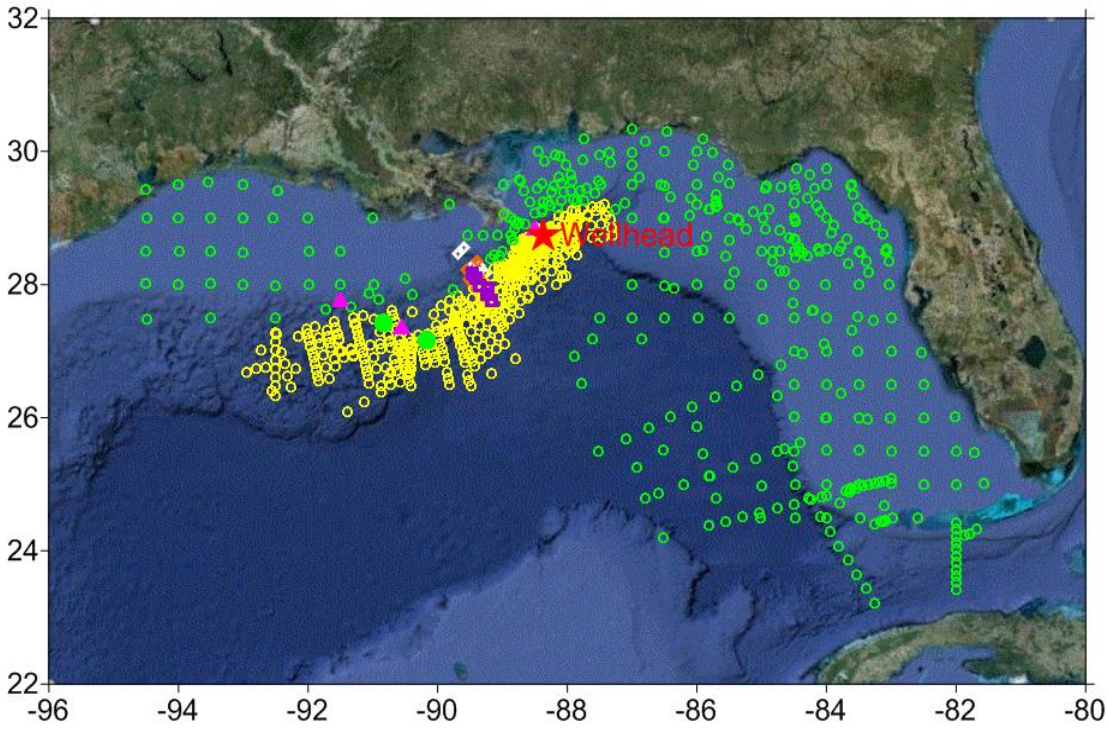

Figure 2.1 1316 CTD casts spanning from 11 May 2010 until 20 September 2010. Red star represents the wellhead; Pink triangles represent natural seeps (MC118, GC600 and GC185); Yellow Circles represent 936 during-spill DO stations in an area impacted by hydrocarbons dissolved and trapped in deep and intermediate plume layers (>700m) which covered an area of 73200 km^2; Green Circles represent 354 during-spill stations outside the chemically defined deep and intermediate plume showing no DO anomalies or stations of shallow depth (<700m); White (n=19) and orange (n=20) diamonds represent during-spill stations within the Mississippi Canyon showing DO anomalies and no DO anomalies, respectively; Green dots represent pre-spill DO stations [*DiMarco et al.*, 2001; *Nowlin Jr.*, 2001] close to the natural seeps (GC185 and GC600) showing no DO anomalies (see Figure 2B); Purple squares represent post-spill DO stations within the Mississippi Canyon showing no DO anomalies (see Figure 2.2B).

Figure 2.2 (A) During-spill dissolved oxygen profile (black) that showed DO removal at depth of 900m and 1110m and corresponding background (red): R/V Cape Hatteras h19 at 88.2947 ºW 28.6878 ºN on 16 June 2010. (B) Two pre-spill DO profiles [*DiMarco et al.*, 2001; *Nowlin Jr.*, 2001] close to the natural seeps (GC185 and GC600; see Figure 1; black) and six post-spill DO profiles (see Figure 1; blue) that showed no DO anomalies: station 309093 at 90.8360 ºW 27.4320 ºN on 14 November 1992, station 410097 at 90.1665 ºW 27.1625 ºN on 16 February 1993, station 3 at 89.1747 ºW 27.7653 ºN on 10 August 2012, station 10 at 89.2197 ºW 27.9378 ºN on 10 August 2012, station 11 at 89.3548 ºW 27.9753 ºN on 10 August 2012, station 12 at 89.4017 ºW 28.0920 ºN on 10 August 2012, station 14 at 89.2475 ºW 27.78528 ºN on 10 August 2012, and station 15 at 89.4575 ºW 28.1695 ºN on 10 August 2012. (C) During-spill DO profiles (n=21) within the northern Mississippi Canyon showing no DO anomaly [*Kessler et al.*, 2011b] (D) Contour Maps of the Mississippi Canyon with data spanning from 14 August through 18 September. White (n=19) and orange (n=21) diamonds represent during-spill stations within the Mississippi Canyon showing DO anomalies and no DO anomalies, respectively.

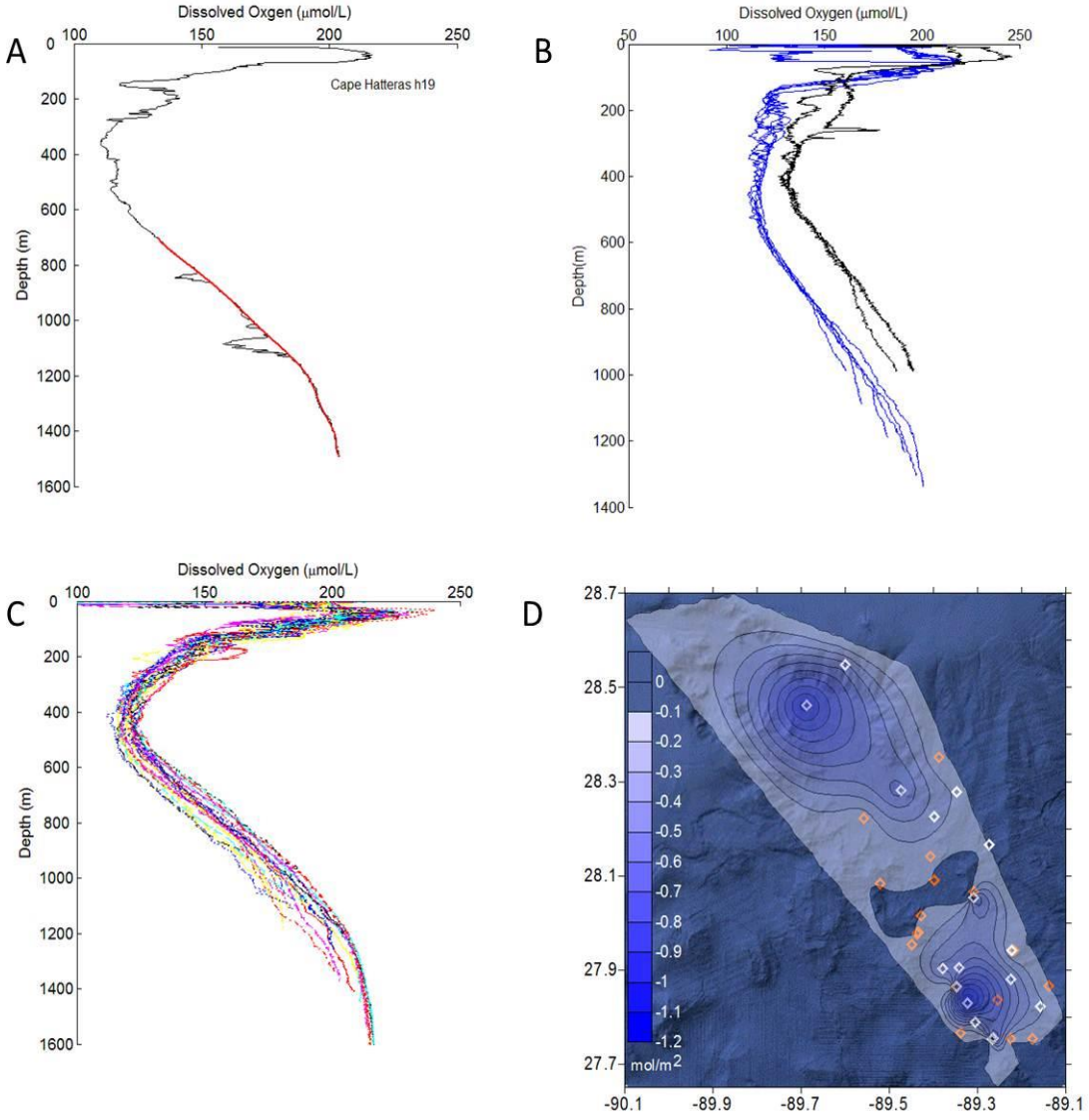
A
Dissolved Oxgen (µmol/L)
Cape Hatteras h19
Depth (m)
B
Dissolved Oxygen (µmol/L)
Depth(m)
C
Dissolved Oxygen (µmol/L)
Depth (m)
D
0
-0.1
-0.2
-0.3
-0.4
-0.5
-0.6
-0.7
-0.8
-0.9
-1
-1.1
-1.2
mol/m2

Hydrocarbon respiration rates and the influence on DO have previously been measured by laboratory experiments [*Hazen et al.*, 2010], incubating samples with an isotopic tracer [*Pack et al.*, 2011; *Valentine et al.*, 2001; *Valentine et al.*, 2010; *Ward et al.*, 1987] and with modeling studies [*Hazen et al.*, 2010; *Valentine et al.*, 2012]. However, the complex composition of the spilled hydrocarbons [*de Gouw et al.*, 2011; *Reddy et al.*, 2012; *Ryerson et al.*, 2012] and the costly procedures normally associated with the direct measurement of individual hydrocarbon respiration rates [*Pack et al.*, 2011; *Valentine et al.*, 2001; *Valentine et al.*, 2010; *Ward et al.*, 1987], greatly limit measurements of the temporal and spatial evolution of hydrocarbon respiration rates. Instead, by sacrificing compound specific rate determinations, we rely on profiles of DO that can be measured without the same restrictions surrounding the use of isotopic tracers in order to estimate parameters of bulk hydrocarbon respiration.

Previous studies have investigated DO anomalies produced from the respiration of spilled hydrocarbons dating back to the Amoco Cadiz spill [*A Aminot*, 1997; *A K Aminot, R.*, 1978] in March 1978. More recently, chemical composition data in the atmosphere [*de Gouw et al.*, 2011] has been compared with that dissolved in the water [*Camilli et al.*, 2010; *Hazen et al.*, 2010; *Joye et al.*, 2011; *Valentine et al.*, 2010], and emitted from the well [*Reddy et al.*, 2012] to estimate the mass fraction of individual hydrocarbons dissolved and trapped in the water column [*Ryerson et al.*, 2012]. The oxygen investigations presented here, when related to the mass fraction of individual emitted hydrocarbons dissolved and trapped in the deep water column [*Ryerson et al.*, 2012] and

their stoichiometric relationship with DO, as well as similar average parameters for the respiration of biomass, provide an effective sink-based approach of studying bulk plume hydrocarbon respiration and their environmental impact following the Deepwater Horizon oil spill.

2.2 Methods

2.2.1 Cumulative DO Anomaly

Determination of Cumulative DO Anomaly

During expeditions spanning from 11 May until 20 September 2010, DO profiles [*Camilli et al.*, 2010; *Kessler et al.*, 2011b; *NODC*, 2011] were recorded by an electrode-based oxygen sensor (SBE-43) on the Niskin bottle rosette (Figure 2.1) and periodic comparisons with Winkler titrations were conducted for validation and calibration of dissolved oxygen [*Kessler et al.*, 2011b; *Valentine et al.*, 2010]. Our initial investigations encompassed 1316 vertical profiles [*Camilli et al.*, 2010; *NODC*, 2011] to investigate the spatial (vertical and horizontal) distribution of the DO anomalies. Since the majority of the DO anomalies were identified in the deep waters, we limited the following analyses to waters with depths that extended into the plume layers (>700m; Figure 2.1) to investigate DWH hydrocarbon respiration in intermediate and deepwater. A 10th degree polynomial was fit to each DO profile providing a background from which the DO anomaly could be calculated (Figure 2.2A) as the difference between the data and corresponding background. The DO anomalies were integrated vertically, producing a quantity of moles of DO removed per area (Appendix Table A.1.).

To view the spatial and temporal distribution of DO removal, the integrated DO anomalies measured within an 11-day window surrounding a specific day were contour mapped using the Kriging Gridding method. We did contour plots of the DO anomalies for each day from 16 May to 18 September 2010 (Figure 2.3) and calculated the distance of the maximum DO removal from the wellhead (Figure 2.4). While there was a slight northeastern extension of the deepwater oxygen anomalies by 120 km from the well, the persistent direction was toward the southwest extending 505 km from the well. The summation of the gridded DO anomalies multiplied by the total plume area yielded the cumulative DO anomaly (CDOA) centered in each 11-day window from 16 May to 18 September 2010. However, the magnitude of the CDOA is partially controlled by the extent of the plume or the bounds of the contour analyses. For example, a previous study suggested that the greatest extent of the DO removal was 30 Gmol from 18 August to 2 September within the same boundary as was used in this study and 39 Gmol if the boundary was extended along the southern and western bounds by an additional 50km [*Kessler et al.*, 2011b]. Since only DO anomalies occurring at depths >700m were investigated in this study, the northern boundary was chosen in accordance with Gulf of Mexico bathymetric restrictions. The southern and western boundaries used here were chosen to encompass the greatest extent of the DO anomalies measured during this entire data set with an average additional extension of 50 km to account for decay to background levels. Our analysis does not suggest which boundary used previously [*Kessler et al.*, 2011b] is more accurate and we arbitrarily chose the more conservative of the two options.

During the contour analyses, portions of the northern Mississippi Canyon were excluded from the contouring (Figure 2.1, 2.2D, 2.3) because including this area caused the contoured deep DO anomalies to extend into the shallow (<700 m) waters adjacent to the canyon sides. In order to assess the influence of just the Mississippi Canyon on the total DO removal, analyses were performed on just the Mississippi Canyon during the times of greatest CDOA (14 August through 18 September). The contour gridding of the integrated DO profiles within the canyon (Figure 2.2C,D) suggests a DO removal of 0.32 ± 0.26 Gmol which accounts for less than 2% of the total DO removal during this plateau period. Due to its minimal influence, the hydrocarbon respiration in the northern Mississippi Canyon was ignored from further analyses.

A potential error in the contour analyses occurs when stations where profiles of DO were collected are not adequately or randomly distributed throughout the true location of the deep plume. This appears to be the case in early August when sampling stations were concentrated around the wellhead but the deepwater dissolved oxygen loss had propagated southwestward outside the sampling area. It is not until the sampling extends further south and west and reintersects the deep plume that the CDOA reconnects with the longer term trend with time (Figure 2.3, 2.5A). While few stations were sampled in the far-field (distance > 160km from the wellhead) southwest plume before August 2010, the CDOA still follows the longer term trend with time beginning at the inception of this event suggesting the stations adequately sampled the major areas of DO removal, except for early August.

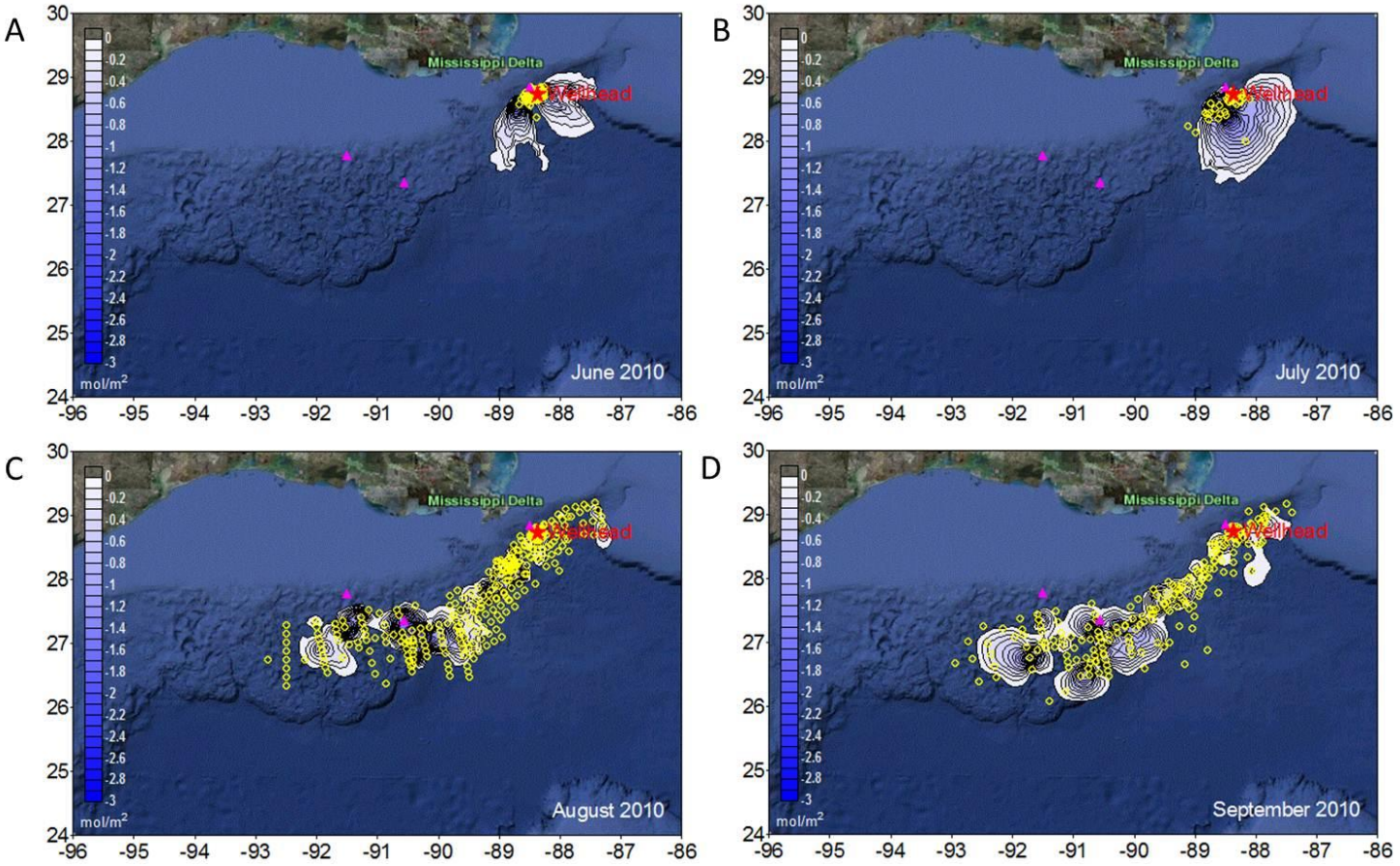

Figure 2.3 Contour maps of integrated DO anomalies (mol/m^2) using the Kriging Gridding method. (A) June 2010 (B) July 2010 (C) August 2010 (D) September 2010. Red star represents the wellhead; Pink triangles represent natural seeps (MC118, GC600 and GC185).

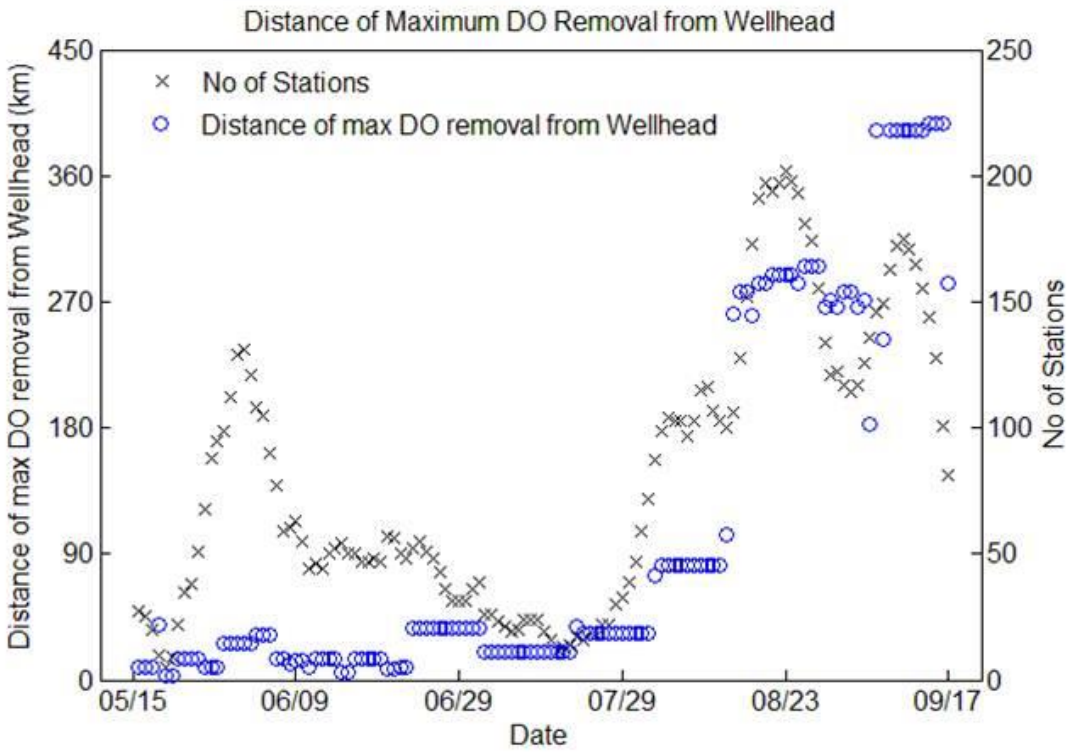

Figure 2.4 Distance of the maximum DO removal from the wellhead. The maximum DO removal displays deepwater current reversals during a general propagation toward the southwest. The maximum DO removal in mid-September was observed approximately 400km from the wellhead.

Error Analysis

Errors associated with this approach to calculate the CDOA were quantified with 2 techniques: statistical bootstrapping analysis and determination of the uncertainty associated with a polynomial fit to the data.

A. Bootstrapping Analysis

First, all profiles of integrated DO anomalies were divided into 4 time periods: May, June, and July, and the plateau (August 14 through September 18). Second, the profiles in each of the 4 time periods were randomly distributed into 3-5 bins for contour gridding with each bin containing 20 to 90 profiles. Third, a contour, gridding, and summation analysis was then conducted on each bin of data. Forth, the CDOA from each bin in a specific time period was used to determine the average and standard errors of the CDOA (Figure 2.5A, Table 2.1).

Since our data suggest the CDOA is increasing during May, June, and July, this upward trend will cause additional error in our bootstrapping analysis. In order to remove the error associated with the upward trend, we calculated the standard deviation of the polynomial fit to the data (see below). Errors from this trend were removed from the total bootstrapping error with a root-mean-square technique (Table 2.2).

$$\delta=\mathrm{Sqrt}[\mathrm{Stdev}_{BS}^{2}-\mathrm{Stdev}_{Fit}^{2}] \quad \text{(Eq. 2.1)}$$

where, δ is the standard deviation of the CDOA during each time period; Stdev_{BS} is the standard deviation of boot strapping analysis during each time period; Stdev_{Fit} is standard deviation of the polynomial fit to the data during each time period.

Figure 2.5 (A) Cumulative dissolved oxygen anomaly (CDOA) and estimation of the mass of hydrocarbon respired ($RHCM_{D\&T}$) based on the assumption that no hydrocarbon was incorporated into biomass growth. CODA and RHCM leveled off from 14 August to 18 September at 18.9±3.8 Gmol and 0.16±0.03 Tg, respectively. An interpolation to CDOA and $RHCM_{D\&T}$ (blue curves) from 16 May to 18 September 2010 was fit with a 13th degree Taylor Function Approximation to the Error Function (ERF, see Equation 2), of which the variation represents the standard errors of the constants from a least-squares fitting approach. CDOA data from 1 August to 13 August (green dots) were removed from the data interpolation analysis due to under sampling of the plume area during this time period. Red crosses represent the average and standard errors calculated with a statistical bootstrapping technique with the data from 16 May to 18 September. The gray cross represents the average and standard error associated with the data from 18 August to 4 October presented previously [*Kessler et al.,* 2011b]. (B) Hydrocarbon respiration rate. Colored curves represent the derivative of the ERF interpolation to the CDOA data and the different curves represent the errors associated with the least squares fitting of the CDOA data. The black curve represents CH_4 oxidation rates determined by multiplying the CH_4 concentration by the first-order rate constant presented previously [*Kessler et al.,* 2011b], but scaled to the official environmental release [*R Camilli et al.*, 2012; *McNutt et al.*, 2012] and CH_4 mass fraction estimates [*Reddy et al.*, 2012]. (C) The acceleration of DO removal (colored) and variation from average daily addition rate of dispersants at the Wellhead (black). The DO loss is accelerated at approximately the same time as the maximum daily addition rate of dispersants. The maximum acceleration occurs between 9 June and 16 June. For (B) and (C), the blue (σ = 25), red (σ = 28.5) and green (σ

= 32) curves represent the errors associated with the least-squares fitting of the CDOA data. (D) Correlation between the acceleration of DO removal (the second order derivative of the interpolations to CDOA) and variation from average daily addition rate of dispersants (the variation of daily dispersant addition from the regression fitting of cumulative dispersants addition): from 16 May to 17 May and 5 July to 15 July (grey dots), from 18 May to 2 June and from 17 June to 4 July (green dots), and from 3 June to 16 June (blue dots).

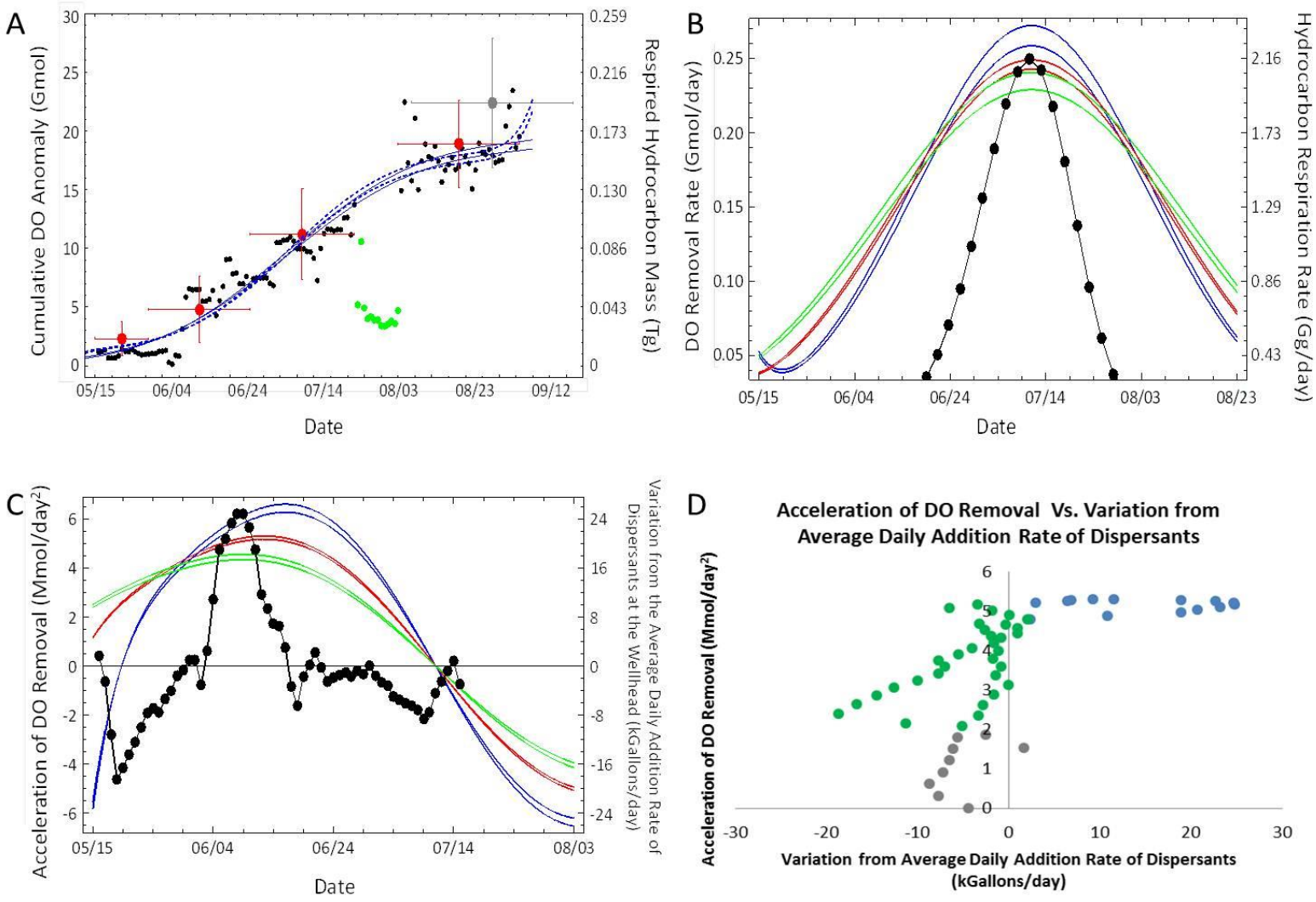
A
Cumulative DO Anomaly (Gmol)
Respired Hydrocarbon Mass (Tg)
Date
B
DO Removal Rate (Gmol/day)
Hydrocarbon Respiration Rate (Gg/day)
Date
C
Acceleration of DO Removal (Mmol/day²)
Variation from the Average Daily Addition Rate of Dispersants at the Wellhead (kGallons/day)
Date
D
Acceleration of DO Removal Vs. Variation from Average Daily Addition Rate of Dispersants
Acceleration of DO Removal (Mmol/day²)
Variation from Average Daily Addition Rate of Dispersants (kGallons/day)

Table 2.1 Standard errors of CDOA, THCM, $RHCM_D$ and $RHCM_{D\&T}$ based on the assumption that no hydrocarbon was incorporated into biomass growth (i.e. Scenario 1).

	CDOA (Gmol)	THCM (Tg)	RCM_D (Tg)	$RHCM_{D\&T}$ (Tg)
[a]16 May to 31 May	2.3 ±1.5	0.06 ±0.04	0.01 ±0.01	0.02 ±0.01
[a] 01 June to 30 June	4.8 ±3.2	0.12 ±0.08	0.03 ±0.02	0.04 ±0.03
[a] 01 July to 31 July	11.2 ±4.5	0.28 ±0.11	0.07 ±0.03	0.10 ±0.04
[a] 14 August to 18 September	18.9 ±3.8	0.47 ±0.09	0.12 ±0.02	0.16 ±0.03
[b] 14 August to 18 September	22.6 ±2.8	0.56 ±0.07	0.14 ±0.02	0.21 ±0.03
[a] Kessler et. al. 2011 Expedition 1	29.5 ±5.1	0.73 ±0.13	0.18 ±0.03	0.25 ±0.04
[b] Kessler et. al. 2011 Expedition 1	35.9 ±7.2	0.89 ±0.18	0.22 ±0.04	0.31 ±0.06
[a] Kessler et. al. 2011 Expeditions 1, 2 and 3	22.4 ±5.5	0.55 ±0.14	0.14 ±0.03	0.19 ±0.05
[b] Kessler et. al. 2011 Expeditions 1, 2 and 3	25.7 ±5.2	0.63 ±0.13	0.16 ±0.03	0.22 ±0.04

[a] indicates contouring within the yellow boundary.
[b] indicates contouring within the green boundary.

Table 2.2 Standard deviations from statistical bootstrapping analysis and polyfit to CDOA during each time period.

	$\delta_{\text{Boot Strapping}}$	[a] δ_1	[b]δ_2
16 May to 31 May	1.47	0.38	1.44
01 June to 30 June	3.19	1.86	2.83
01 July to 31 July	4.46	1.35	3.89
14 August to 18 September	3.78	1.90	3.73

[a] δ_1 is standard deviation of the residuals between the CDOA data and polynomial fitting data; δ_1 of the whole data set is 3.74.

[b]δ_2 removes the trend of the fitting from the total bootstrapping with a root-mean-square technique: $\delta=\text{Sqrt}[\text{Stdev}_{BS}^2-\text{Stdev}_{Fit}^2]$

B. Data Interpolation and Uncertainty Analysis

An interpolation to the time-series CDOA data from 16 May to 18 September 2010 was fit with a 13th degree Taylor Function Polynomial approximation to the Error Function (ERF; i.e. the integral of a Gaussian distribution; Equation 2; Figure 2.5A).

$$ERF = b + m\sum_{n=0}^{\infty}\frac{(-1)^n\left(\frac{x-X}{\sqrt{2\sigma^2}}\right)^{2n+1}}{n!(2n+1)} \qquad \text{(Eq. 2.2)}$$

where, X and σ are the mean and standard deviation of the distribution, respectively, and m and b are constants.

To assess the error in the interpolation of the CDOA data, the errors associated with the 4 fitting parameters were determined. Given the shape and duration of the profile, X was

determined with negligible uncertainty (X = day 57; i.e. 11 July 2010) and σ was determined to have moderate uncertainty (σ = day 28.5±3.5). With values for X and σ, the Taylor approximation to the ERF (Equation 2.2) was used to linearize the data enabling the coefficients of m and b, as well as their one standard deviation error, to be determined with a linear least-squares approach with conventional error propagation (m=9.97±0.6; b=9.56±0.1). The functions produced from these coefficients with their errors are displayed in Figure 2.5A.

2.2.2 Total Mass of Hydrocarbon Released and Respired

Plume hydrocarbons could be either fully respired to CO_2, or incorporated into cellular lipids [*Das and Chandran*, 2010] which could be remineralized after exhaustion of the degradable hydrocarbons [*Fritsche and Hofrichter*, 2009]. The total masses of hydrocarbons released and respired were assessed in three different scenarios:

Scenario 1 - All Plume Hydrocarbons Were Respired Directly to CO_2 With No Contribution to Biomass Growth

By knowing the mass fraction of individual hydrocarbons dissolved and trapped in the water column [*Ryerson et al.*, 2012] and their stoichiometric relationship with dissolved oxygen, the oxygen removing potential [*Ryerson et al.*, 2012] (ORP) of all plume (dissolved and trapped) hydrocarbons can be calculated as:

$$\text{ORP of Dissolved } HC_i \text{ (mol } O_2/g_T) = (F_i \times M_i \times S_i) / MW_i \qquad \text{(Eq. 2.3)}$$

where, HC_i = hydrocarbon i; F_i = fraction dissolved of HC_i; M_i = fraction of released mass for HC_i that was dissolved (g_i/g_T); S_i = stoichiometric ratio of O_2 to HC_i; MW_i = molecular weight of HC_i (g_i/mol)

$$\text{ORP of Trapped } HC_i \text{ (mol } O_2/g_T) = ((1-F_i) \times M_i \times S_i \times 0.14 \times 0.9610)/(MW_i \times F_x) \quad \text{(Eq. 2.4)}$$

where, 0.14 = fraction trapped relative to Toluene; 0.9610 = fraction dissolved of Toluene; $F_x = \Sigma[(1-F_i) \times M_i] / (\Sigma[(1-F_i) \times M_i] + [(1-\Sigma M_i) \times 1])$; ΣM_i = Sum of the mass fractions characterized for the MW-1 sample [*Ryerson et al.*, 2012] = 0.480169

$$\text{ORP of All plume HC (mol } O_2/g_T) = \Sigma \text{ [ORP of Dissolved } HC_i + \text{Trapped } HC_i] \quad \text{(Eq. 2.5)}$$

The total hydrocarbon mass (THCM) released, the dissolved hydrocarbon mass respired ($RHCM_D$), and the total hydrocarbon mass respired ($RHCM_{D\&T}$) can be estimated as:

$$\text{THCM} = \text{CDOA (mol } O_2) \div \text{ORP of All plume HC (mol } O_2/g_T) \quad \text{(Eq. 2.6)}$$

$$RHCM_D = \text{CDOA (mol } O_2) \div [\text{ORP of All plume HC (mol } O_2/g_T) \div F_D \text{ (g/ } g_T)] \quad \text{(Eq. 2.7)}$$

$$RHCM_{D\&T} = \text{CDOA (mol } O_2) \div [\text{ORP of All plume HC (mol } O_2/g_T) \div F_{D\&T} \text{ (g/ } g_T)] \quad \text{(Eq. 2.8)}$$

where, $F_D = \Sigma(F_i \times Mi)$; $F_{D\&T} = \Sigma[F_i \times M_i] + \Sigma[(1-F_i) \times M_i \times 0.14 \times 0.9610) / F_x]$

Inserting the appropriately measured values into Eq. 2.3-2.8, produces values for THCM, $RHCM_D$, and $RHCM_{D\&T}$ that are linearly related to CDOA [*Ryerson et al.*, 2012] (Figure 2.5A) by factors of 24.6815, 6.1382, and 8.6330 g/mol O_2, respectively. The derivatives

of the interpolations to CDOA, $RHCM_D$ and $RHCM_{D\&T}$ determined the time-dependent trends of DO removal rate, degradation rate of dissolved hydrocarbons, and degradation rate of total dissolved and trapped hydrocarbons, respectively (Figure 2.5B, Table 2.3). The second derivative of the interpolations to the CDOA - the acceleration of the DO removal - was compared with dispersants added directly at the wellhead [*Kujawinski et al.*, 2011] (Figure 2.5C,D) to assess the effectiveness of the application of dispersants on increasing hydrocarbon degradation rates.

Scenario 2 - All Plume Hydrocarbons Contributed to Biomass Growth and the Observed DO Anomaly Occurred Entirely from the Remineralization of the Biomass Bloom

Due to the complexity of biomass carbon molecules, we approximate biomass as a group of -CH2- radicals to assess the overall respiration of plume biomass. This assumption yields an oxygen/average biomass stoichiometric ratio of 1.5:1 which was used to estimate the total amount of biomass respired that is required to account for the total removal of oxygen.

Table 2.3 Peak values of DO removal and hydrocarbon respiration rates, acceleration of DO removal and variation from average daily addition rate of dispersants.

	DO Removal Rate (Gmol/day)	HC_D Respiration Rate (Gg/day)	[a]$HC_{D\&T}$ Respiration Rate (Gg/day)	Acceleration of DO Removal (Mmol/day^2)	[b]Dispersants (kGallons/day)
Date	11 July	11 July	11 July	9 June to 16 June	8 June
Value	0.25 ±0.02	1.54 ±0.13	2.16 ±0.19	5.46 ±1.13	24.81

[a]$HC_{D\&T}$ Respiration Rate: A previously study determined a similar maximum CH_4 oxidation rate of 2.16 Gg/day occuring on 10 July 2010 [*Kessler et al.*, 2011b].

[b]Dispersants: Variation from average daily addition rate of dispersants (kGallons/day) [*Lehr et al.*, 2010].

Scenario 3 - Part of the Hydrocarbon Was Fully Respired to CO_2 and Part Was Incorporated into Biomass, which Has Not Been Significantly Remineralized by Mid-September 2010

Comparing the results from scenarios 1 and 2 with the official estimate of mass released from the well and the fraction of mass dissolved and trapped in the deep Gulf waters [*R Camilli et al.*, 2012; *McNutt et al.*, 2012; *Ryerson et al.*, 2012] suggests that either a fraction of the released hydrocarbon mass was not respired or that it was incorporated into biomass which, by mid-September 2010, was not significantly remineralized. Here, we investigate the later possibility to provide an estimate of the biomass/hydrocarbon conversion efficiency (EF) for this event. By comparing our determinations of total hydrocarbon mass respired from Scenarios 1 and 2 with an estimate of total plume hydrocarbon mass determined by previously published results [*R Camilli et al.*, 2012; *McNutt et al.*, 2012; *Ryerson et al.*, 2012], EF can be estimated as:

$$EF = (OEHC_{D\&T} - \text{HC Fully Respired to } CO_2) / OEHC_{D\&T} \quad \text{(Eq. 2.9)}$$

2.3 Results and Discussion

Contour maps of the integrated DO anomalies measured from 11 May 2010 until 20 September 2010 suggest a southwest migration of the hydrocarbon plume that covered an area over 73,200 km^2 in the deep Gulf of Mexico (Figure 2.3). While the general plume propagation trend was toward the southwest, there were periodic current reversals moving the area of maximum DO removal closer toward the well (Figure 2.4), a process previously described as influencing the microbial community and accelerating hydrocarbon

respiration [*Valentine et al.*, 2012]. As more plume hydrocarbons were respired and the CDOA grew (Figure 2.5A), the estimation of the respired hydrocarbon mass increased and leveled off from 14 August to 18 September until our analyses became data limited (Figure 2.5A). Defined as the derivatives of the CDOA and RHCM, the DO removal and hydrocarbon respiration rates showed related trends, peaking on 11 July and dropping to zero in the late August (Figure 2.5B, Table 2.3).

The CDOA reached a plateau from 14 August through 18 September with a total quantity of 18.9±3.8 Gmol of DO removed, and the DO removal rate peaked at 0.25±0.02 Gmol/day on 11 July (Figure 2.5A,B). If we subject only the data presented previously [*Kessler et al.*, 2011b] (18 August to 4 October) to a contour and boot-strapping analysis within the identical plume boundary used here, we calculate a DO removal of 22.4±5.5 Gmol, which is consistent with total DO removal during the plateau in this study (Figure 2.5A). The slope of the regression line of the CDOA during the plateau is an estimate of the mixing rate of fresh oxygen into the plume assuming respiration was substrate limited during this time period. An average oxygen mixing rate of 0.0063 gigamoles of oxygen per day into the plume area was determined. Extending this fresh oxygen mixing rate to earlier periods before the wellhead shutdown indicates that during May through September 2010 the DO anomalies were not significantly replenished with fresh oxygen, but rather dispersed over a larger distance.

Based on the amount of total DO removal from 14 August through 18 September, and the assumption that no hydrocarbon was incorporated into biomass growth (i.e. Scenario 1), the mass of hydrocarbon respired (dissolved) and the mass of hydrocarbon respired (dissolved and trapped) were estimated as 0.12±0.02 Tg and 0.16±0.03 Tg (i.e. 15±3% and 21±6%, respectively, of the total environmental release determined previously by acoustic techniques [*R Camilli et al.*, 2012; *McNutt et al.*, 2012], Figure 2.5A, Equation 2.7). The close agreement between this estimate of hydrocarbon mass respired (dissolved and trapped) with an estimate of total plume hydrocarbon mass (0.28±0.03Tg) determined by previously published results [*R Camilli et al.*, 2012; *McNutt et al.*, 2012; *Ryerson et al.*, 2012], suggests that respiration removed the majority (60±19%) of the plume hydrocarbon mass; other processes such as dispersion, evasion to the atmosphere, and deposition on the seafloor likely occurred helping terminate the deep water hydrocarbon plume, however, respiration was the dominant processes that removed the majority of the plume mass. If we assume that all hydrocarbons dissolved and trapped in the deep and intermediate waters of the Gulf of Mexico were removed by respiration, we can calculate the total mass of 0.47±0.09 Tg hydrocarbons released to the environment (Equation 2.6). This analysis produces an estimate that is 60±19% of the official estimate based on acoustic techniques [*R Camilli et al.*, 2012; *McNutt et al.*, 2012]. Incorporating other processes that can remove plume hydrocarbons, and quantifying the incorporation of plume hydrocarbons into biomass growth, rectifies this 40±19% discrepancy. These analyses also suggest that the highest hydrocarbon respiration rates reached 1.54±0.13 Gg/day of dissolved hydrocarbon and 2.16±0.19 Gg/day of both dissolved and trapped

hydrocarbon on 11 July (Figure 2.5B). Similarly, a maximum CH_4 oxidation rate of 2.16 Gg/day was estimated to occur on 10 July by scaling a previous estimate [*Kessler et al.*, 2011b] to updated estimates of the total environmental hydrocarbon release [*R Camilli et al.*, 2012; *McNutt et al.*, 2012] and mass fraction of CH_4 in the emitted hydrocarbons [*Reddy et al.*, 2012]. The close agreement between the timing and extent of the maximum bulk hydrocarbon respiration rate and CH_4 oxidation rate suggest that CH_4 was the dominant hydrocarbon controlling the bulk respiration rate, a conclusion which is in agreement with CH_4 being the dominant hydrocarbon emitted and it being fully repired [*Kessler et al.*, 2011b; *Reddy et al.*, 2012].

The mass of biomass hydrocarbons respired based on the assumption that no hydrocarbon was directly respired to CO_2 (i.e. Scenario 2) was estimated as 0.18 ± 0.04 Tg, which is within the error of estimation in Scenario 1. While scenario 3 seems plausible, the results here do not suggest it is more probable than scenarios 1 and 2, mainly because it remains uncertain if the accumulated biomass was significantly remineralized by mid-September, 2010. For example, the slope of the CDOA profile would have been changed when more DO was removed from biomass remineralization, however a more uniform profile was observed (Figure 2.5A). Possible reasons for the absence of a CDOA "bump" could be either that remineralization of biomass developed in the early stage was negligible compared to full hydrocarbon respiration to CO_2 at that time, or that the remineralization of biomass did not occur by mid-September, 2010, or that biomass remineralization occurred at a steady rate concurrent with full hydrocarbon respiration. By comparing our

determinations of total hydrocarbon mass respired from Scenarios 1 and 2 with an estimate of total plume hydrocarbon mass determined by previously published results [*R Camilli et al.*, 2012; *McNutt et al.*, 2012; *Ryerson et al.*, 2012], we estimated the mass of hydrocarbons incorporated into the biomass of 0.18 ± 0.05 Tg, and the biomass/hydrocarbon conversion efficiency of 0.36 ± 0.11 mg biomass/mg hydrocarbon which is consistent with earlier studies [*Beolchini et al.*, 2010; *Yerushalmi and Guiot*, 1998].

To assess the effectiveness of dispersants added directly at the wellhead to increase the surface area, deepwater retention, and bioavailability of released hydrocarbons, we compared the acceleration of the DO removal with the quantity of dispersants added on a daily basis. Specifically, since the daily amount of dispersants added directly at the wellhead between 16 May and 15 July was relatively constant, we compared the difference between the actual and average daily dispersant injection at the wellhead [*Kujawinski et al.*, 2011] to the acceleration of DO removal. While the results suggest that DO removal accelerated reaching a maximum acceleration in early to mid-June, coincident with the time period of most aggressive dispersant addition (Figure 2.5C), an analysis of the acceleration of DO removal versus the quantity of daily dispersant addition reveals that the "saturation" quantity of dispersant addition, above which no further acceleration in respiration was observed, is roughly equal to the average daily addition rate (Figure 2.5D). In sum, DO anomaly analysis provides an easy and effective approach for the estimation of hydrocarbon release and bulk plume hydrocarbon respiration in response to an oil spill

event. A longer term campaign for future spills to sample an organized network, similar to the NOAA ‘clean sweep’ grid, would help quantify the total environmental release of hydrocarbons, recovery of the system, and the extent of environmental damage.

3. QUANTIFYING METHANE OXIDATION RATES AND FLUX DURING THE DEEPWATER HORIZON OIL SPILL WITH MEASUREMENTS OF METHANE STABLE ISOTOPIC RATIOS AND CENCENTRATIONS

Several independent techniques have been developed to measure the CH_4 oxidation rates and the flux from the seafloor. However, none of these methods measure them concurrently. Here we present a stable isotope model incorporating measurements of CH_4 concentrations, CH_4 stable isotopic isotopes, and current velocity, which can be used to determine CH_4 oxidation rates, as well as the flux from the seafloor. This model was tested on 20 samples taken from 1 to 12 km from the wellhead from 11 June through 20 June 2010 during the Deepwater Horizon oil spill. Results suggest that rate of CH_4 oxidation ranged from 22 to 844 nM d^{-1} in mid-June 2010 and that the flux from the seafloor was 8.4×10^7 moles d^{-1}. Both estimated here are in agreement with previous estimates determined independently.

3.1 Introduction

The blowout of the Macondo well on April 20, 2010 initiated the release of oil and natural gas into the deep waters of the Gulf of Mexico. The oil and gas was continuously added to the water for 83 days. A persistently dominant hydrocarbon plume was formed at 1000- to 1200-m depth to the southwest of the well head [*Camilli et al.,* 2010; *Du and Kessler,* 2012; *Joye et al.,* 2011; *Kessler et al.,* 2011b; *Ryerson et al.,* 2012; *Valentine et al.,* 2010;

Yvon-Lewis et al., 2011] As the dominant hydrocarbon released, CH_4 oxidation dominated the bulk hydrocarbon respiration [*Du and Kessler*, 2012; *Reddy et al.*, 2012].

Methane oxidation rates have previously been measured from ex situ tracer inoculation and incubation with radio- or stable- isotope tracers, and with in situ comparison of CH_4 concentration changes with water mass ages [*Heeschen et al.*, 2004; *Kadko et al.*, 1990; *Pack et al.*, 2011; *Rehder et al.*, 1999; *Scranton and Brewer*, 1978]. However, most of these techniques require measurements that are less routinely conducted in oceanography studies. The flow rate of CH_4 has been measured with in situ observation such as acoustic Doppler technique, optical plume velocimetry, particle image velocimetry, etc. [*Crone and Tolstoy*, 2010; *McNutt et al.*, 2012; *Reddy et al.*, 2012]. However, costly procedures are normally associated with these direct measurements. Moreover, none of these methods concurrently measure the flow rate of CH_4 into the waters and the biodegradation rates.

During microbial CH_4 oxidation processes, methanotrophs preferentially utilize $^{12}CH_4$ over $^{13}CH_4$, resulting in the residual CH_4 being enriched in ^{13}C (i.e., isotopic fractionation, [*Bigeleisen and Wolfsberg*, 1958; *Broecker and Oversby*, 1971; *Rayleigh*, 1896; *Whiticar*, 1999]. Measurement of CH_4 isotopes incorporated into Rayleigh distillation equations [*Bigeleisen and Wolfsberg*, 1958; *Rayleigh*, 1896] can be used to estimate the fraction of CH_4 that has been oxidized (e.g., [*Kinnaman et al.*, 2007]). However the conventional Rayleigh equations assume a closed system where a fixed amount of reactant is allowed to partially react [*Bigeleisen and Wolfsberg*, 1958]. Errors occur when mixing in a system

is not negligible. Here we present a stable isotope model incorporating measurements of CH_4 concentrations, CH_4 stable isotopic ratios, and current velocities in an open system (i.e. the Gulf of Mexico), that can be used to determine the oxidation rate of CH_4, as well as the flow rate of CH_4 during the DWH incident.

3.2 Methods

Samples for CH_4 concentration and stable isotope analysis were collected at 20 stations located from 1 to 12 km from the wellhead on the R/V Cape Hatteras from 11 June through 20 June 2010 (Figure 3.1). Samples for CH_4 concentration analysis were collected using a headspace equilibration technique and were analyzed by GC-FID onboard with a precision of 1.5% [*Valentine et al.*, 2010; *Yvon-Lewis et al.*, 2011]. Samples for CH_4 stable isotope analysis were collected using a stripping and trapping technique [*Kessler and Reeburgh*, 2005] and were measured by isotope-ratio mass spectrometry (IRMS) at the Woods Hole Oceanographic Institution with an average precision of 0.1‰.

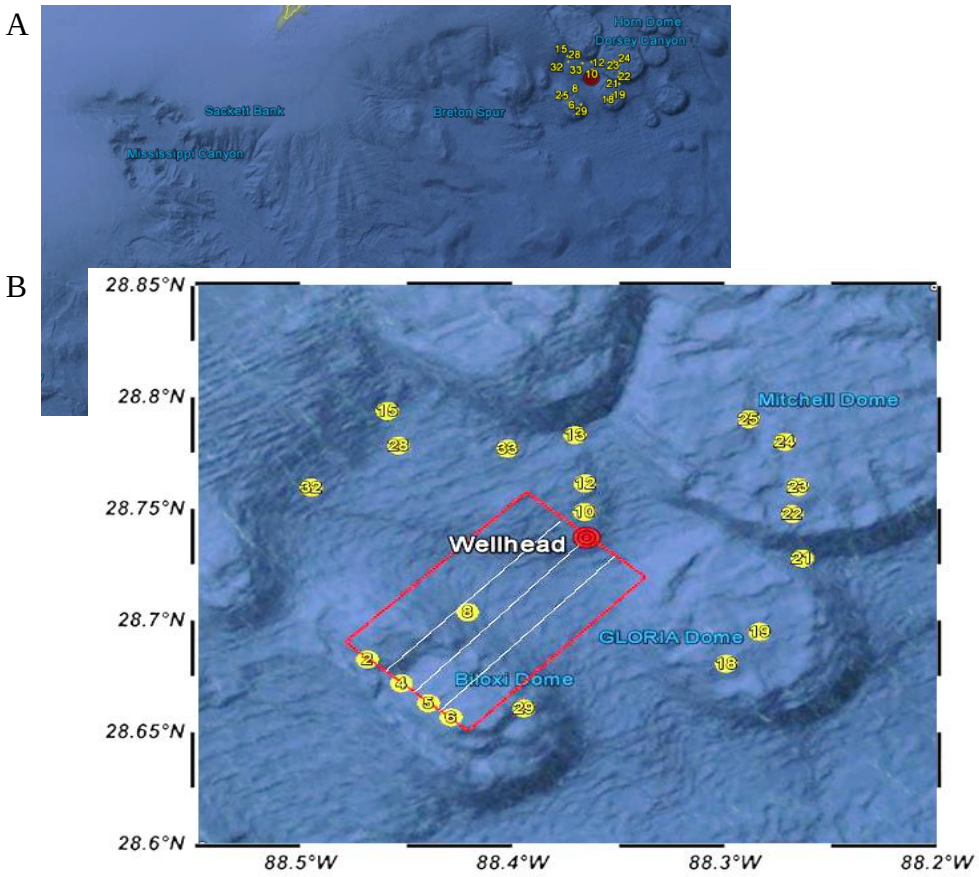

Figure 3.1 (A) Location of samples collected at 20 stations located from 1 to 12 km from the wellhead on the R/V Cape Hatteras from 11 June through 20 June 2010; (B) Blow-up of (A) highlighting the stations with a four box model for characterizing the dynamics of CH_4 in the system.

As the substrate for bacterial respiration, CH_4 residing in the deep waters of the Gulf of Mexico sustained a bacterial bloom for several months [*Du and Kessler*, 2012; *Hazen et al.*, 2010; *Valentine et al.*, 2012]. Consider two reactions in this system as pseudo first order reactions:

$$2^{13}CH_4\ (A_{Hi}) + O_2 \overset{k_H}{\rightarrow} 2^{13}CH_2\ + 2H_2\ O \qquad \text{(Eq. 3.1)}$$

$$2^{12}CH_4\ (A_{Li}) + O_2 \overset{k_L}{\rightarrow} 2^{12}CH_2\ + 2H_2\ O \qquad \text{(Eq. 3.2)}$$

where, A_{Hi} and A_{Li} are the concentrations of the lighter and heavier isotopes, respectively; k_H and k_L are the reaction rate constants for the lighter and heavier isotopes, respectively.

Assuming that the majority of released CH_4 dissolved at about 300 to 500m above the wellhead (i. e., 1000 to 1200m depth; a negligible amount of CH_4 was released from the deep water to the atmosphere [*Yvon-Lewis et al.*, 2011]), this area can be seen as a half-open system. Then the CH_4 retained above the wellhead was transported from this point source to surrounding areas by currents. The surrounding areas can be seen as a full-open system where the residual CH_4 over an area continually mixes with the continually added "fresh" CH_4 (Figure 3.2).

3.2.1 Half-open System Model

A half-open system describes continuous addition of the reactant (i.e., CH_4) into a system but no export of residual reactant or products from the system (Figure 3.2; [*Kessler et al.*, 2006].

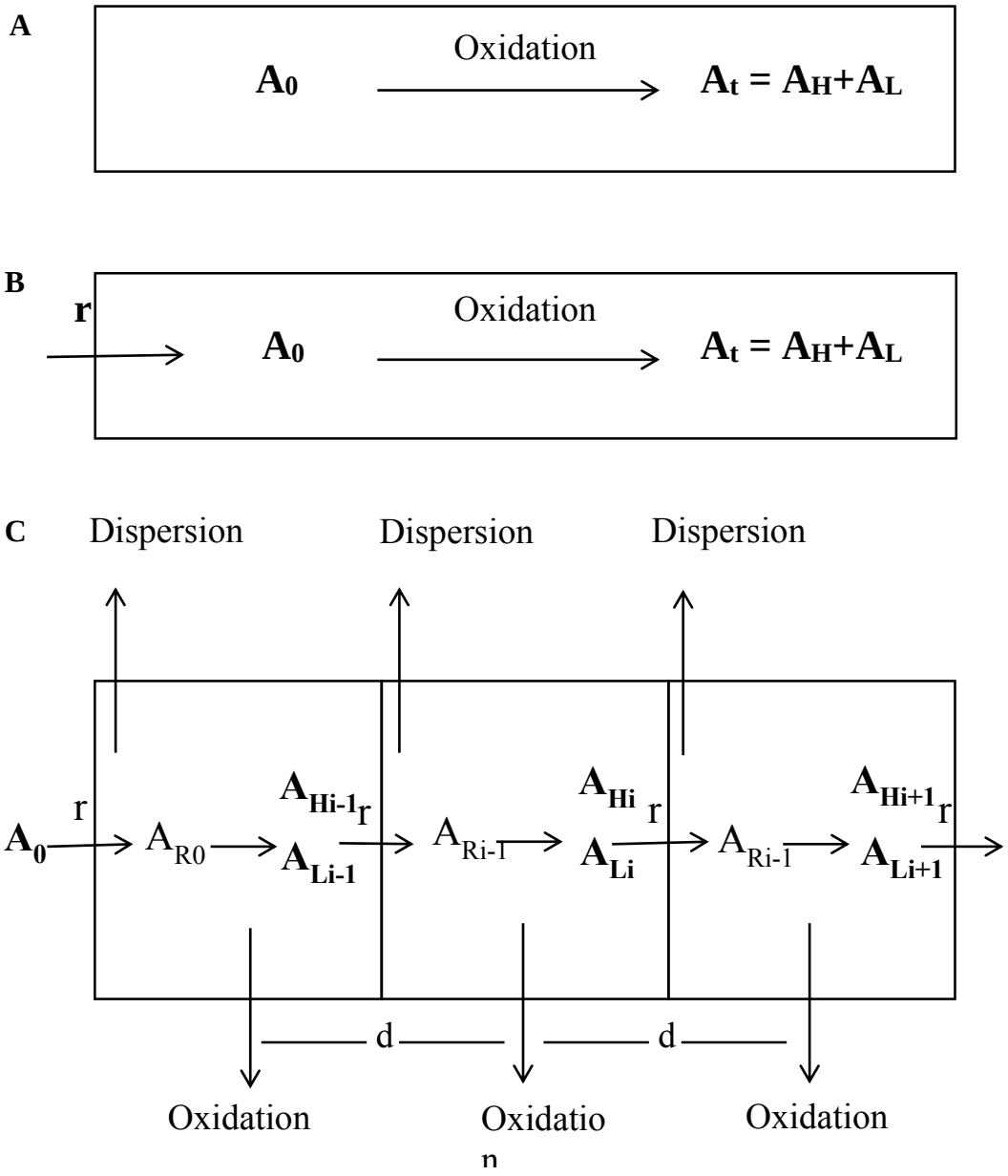

Figure 3.2 Schematic of kinetic isotope fractionation in three systems. (A) a closed system; (B) a half-open system; (C) a full-open Syatem.

Thus non-steady state equations can be written as:

$$\frac{dA_{Ht}}{dt} = r_H - k_H A_{Ht} \quad \text{(Eq. 3.3)}$$

$$\frac{dA_{Lt}}{dt} = r_L - k_L A_{Lt} \quad \text{(Eq. 3.4)}$$

where r_H and r_L are the constant rate of addition of the heavier molecules A_H and the lighter molecules A_L.

Then the exact equation can be derived as:

$$\delta A_0 = \frac{f(\delta A_t + 1000)}{\alpha - \alpha(1-f)^{1/\alpha}} - 1000 \quad \text{(Eq. 3.5)}$$

$$f = 1 - \left(\frac{\delta A_t + 1000}{\delta A_0 + 1000}\right)^{\frac{\alpha}{1-\alpha}} \quad \text{(Eq. 3.6)}$$

$$\alpha = \frac{k_L}{k_H} \quad \text{(Eq. 3.7)}$$

where, α is the isotopic fractionation factor; f is the fraction of the initial amount of reactant that has reacted; δA_0 is the δ^{13}C-CH_4 of source reactant.

In the steady state case (i.e. f = 1, the chemical reaction rate equals the addition rate of the reactant)

$$\delta A_0 = \frac{1}{\alpha}(\delta A_t + 1000) - 1000 \quad \text{(Eq. 3.8)}$$

Since no sample was taken from the station above the wellhead for concentration and isotope analysis, the δ^{13}C-CH_4 at that station was assumed to be the same as the source CH_4 ($\delta A_0 = -57.5‰$, [*Reddy et al.*, 2012]).

3.2.2 Full-open System Model

A full-open system describes continuous input and output of a reactant into the system where a reaction occurs (Figure 3.2). The model assumes a steady-state over the sampling time under the following condition: (1) the input of reactant is equal to the export and reaction loss terms so that the concentration of reactant in the system is constant, (2) the rates in and out of fluid are assumed equal and constant, so that no net changes in the reservoir volume are observed, and (3) the confines of the system are well mixed.

Thus, steady-state equations can be written as:

$$\frac{\mathrm{dA_{Hi}}}{dt} = \frac{r \times A_{Hi-1} - r \times A_{Hi}}{d} - k_H A_{Hi} = 0 \qquad \text{(Eq. 3.9)}$$

$$\frac{\mathrm{dA_{Li}}}{dt} = \frac{r \times A_{Li-1} - r \times A_{Li}}{d} - k_L A_{Li} = 0 \qquad \text{(Eq. 3.10)}$$

where r is the average velocity over the sampling time, r = 3 km d^{-1}; d is the distance between the adjacent boxes.

Then the exact equation can be derived as:

$$\delta \mathrm{A_i} = (\delta A_{i-1} + 1000)\left(\frac{\alpha}{f+\alpha-\alpha f}\right) - 1000 \qquad \text{(Eq. 3.11)}$$

$$f = \frac{\alpha}{1-\alpha}\left(\frac{\delta A_{i-1}+1000}{\delta A_i+1000} - 1\right) \qquad \text{(Eq. 3.12)}$$

Rate into Box_i that is available for reaction = $F_{INi} = (r \times A_{Ri-1})/d$ (Eq. 3.13)

Rate out from $Box_i = F_{INi} = (r \times A_i)/d$ (Eq. 3.14)

Oxidation loss rate in $Box_i = F_{OXi} = (r \times (A_{Ri-1} - A_i))/d$ (Eq. 3.15)

Dispersion loss rate in $Box_i = F_{DISPi} = (r \times (A_{i-1} - A_{Ri-1}))/d$ (Eq. 3.16)

where A_{Ri-1} is the concentration that is available for reaction after dispersion has occurred, $A_{Ri-1} = A_i/(1\text{-}f)$.

This model is applicable for the stations surrounding the wellhead showing high CH_4 concentrations (> 500 nM) at 1000m to 1200 m depth. The isotopic fractionation factor ($\alpha = 1.0265 \pm 0.0039$) has been previously determined for aerobic CH_4 oxidation in ocean waters adjacent to an active seep field [*Kinnaman et al.*, 2007]. When individual one-box model was applied to each of the surrounding stations (i.e., $\delta A_{i-1} = \delta A_0 = -57.5‰$, [*Reddy et al.*, 2012]; δA_i is the measured δ^{13}C-CH_4 at a station; d is the distance between the wellhead and the station), CH_4 oxidation rates can be determined at each of the station during the sampling time (Figure 3.3, Table 3.1).

Figure 3.3 Correlations between CH_4 concentration in the plume (nM), oxidation rate (nM d^{-1}), $\delta^{13}C\text{-}CH_4$ (‰) and distance from the wellhead (km). (A) average CH_4 concentration in the plume vs. distance; (B) CH_4 oxidation rates vs. distance; (3) $\delta^{13}C\text{-}CH_4$ vs. distance; (D) $\delta^{13}C\text{-}CH_4$ vs. average CH_4 concentration in the plume.

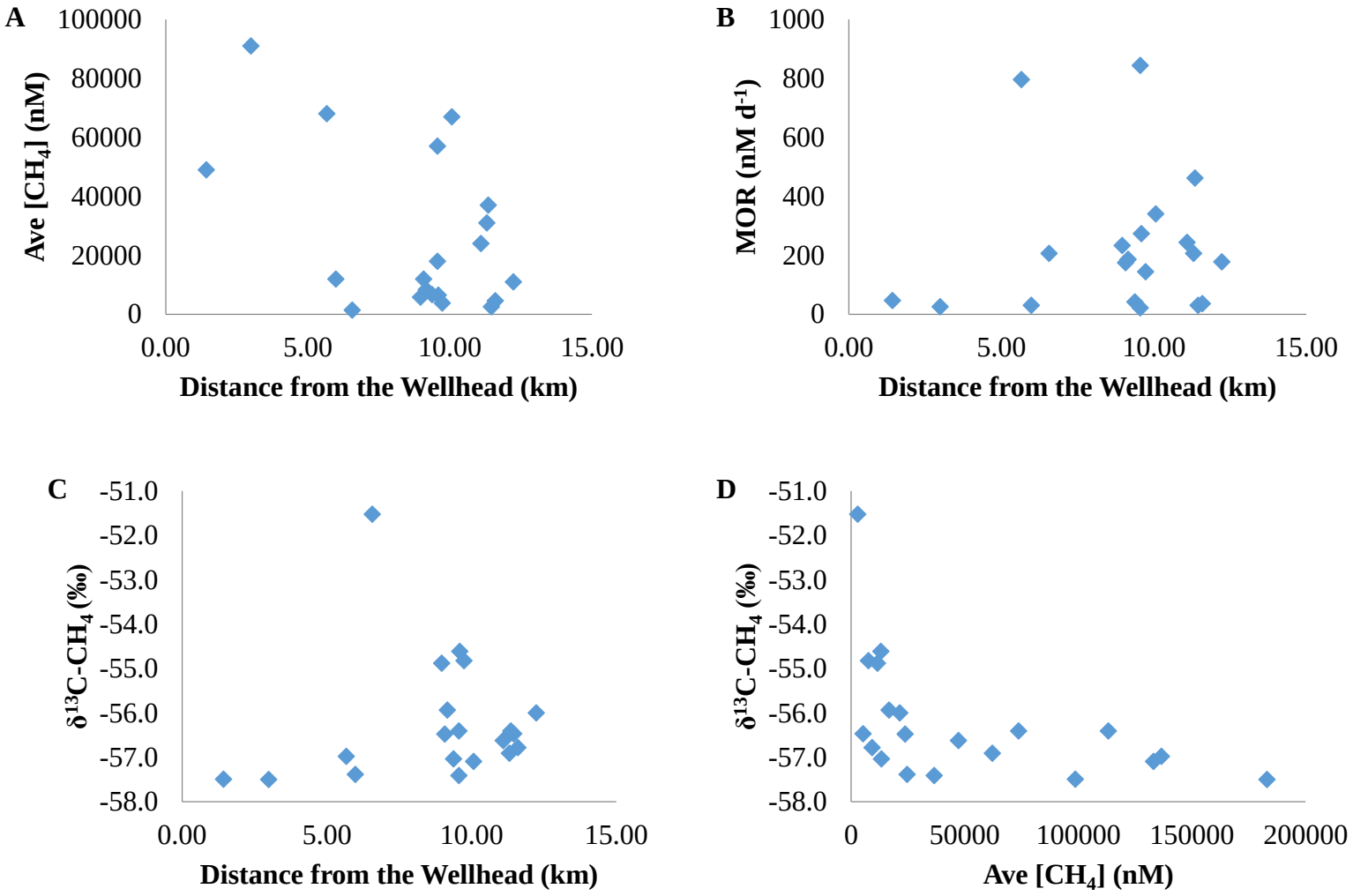
A
100000
80000
60000
40000
20000
0
Ave [CH4] (nM)
0.00
5.00
10.00
15.00
Distance from the Wellhead (km)
B
1000
800
600
400
200
0
MOR (nM d-1)
0.00
5.00
10.00
15.00
Distance from the Wellhead (km)
C
-51.0
-52.0
-53.0
-54.0
-55.0
-56.0
-57.0
-58.0
δ13C-CH4 (‰)
0.00
5.00
10.00
15.00
Distance from the Wellhead (km)
D
-51.0
-52.0
-53.0
-54.0
-55.0
-56.0
-57.0
-58.0
δ13C-CH4 (‰)
0
50000
100000
150000
200000
Ave [CH4] (nM)

Table 3.1 Methane oxidation rates at 20 stations located from 1 to 12 km from the wellhead.

Station	Lat	Lon	Max $[CH_4]$ Depth (m)	Max $[CH_4]$ (nM)	Ave $[CH_4]$ (nM)	$\delta^{13}C$-CH_4 (‰)	Distance (km)	f	Input (nM d^{-1})	MOR[a] (nM d^{-1})	MOR[b] (nM d^{-1})	Release ($\times 10^9$ moles)
2	28.6857	-88.4686	1080	9138	4600	-56.8	11.59	0.030	1227.234	37	1	0.47
4	28.6728	-88.4547	1089	62059	31000	-56.9	11.30	0.025	8436.79	207		3.5
5	28.6622	-88.4437	1102	73676	37000	-56.4	11.35	0.045	10242.02	462	0-25	2.8
6	28.6545	-88.4344	1080	5239	2600	-56.5	11.45	0.042	711.3463	30		0.17
8	28.7056	-88.4221	1025	2819	1400	-51.5	6.56	0.244	846.9999	207	2	
10	28.7510	-88.3658	1108	98681	49000	-57.5	1.43	0.000	103132.2	47	12	
12	28.7650	-88.3641	1080	182940	91000	-57.5	2.99	0.000	91390.82	25		
13	28.7891	-88.3662	1095	136478	68000	-57.0	5.66	0.022	36832.6	797		
15	28.8072	-88.4480	1120	47253	24000	-56.6	11.09	0.036	6736.007	244		
18	28.6717	-88.3105	1100	16651	8300	-55.9	9.16	0.064	2905.856	187		
19	28.6863	-88.2942	1079	23781	12000	-56.5	9.07	0.042	4144.067	175		
21	28.7210	-88.2718	1090	13319	6700	-57.0	9.37	0.019	2186.886	42		
22	28.7432	-88.2742	1100	11516	5800	-54.9	8.96	0.108	2175.418	234	44	
23	28.7563	-88.2702	1144	36574	18000	-57.4	9.55	0.004	5674.06	22		
24	28.7789	-88.2739	1160	133063	67000	-57.1	10.06	0.017	20321.14	341		
25	28.7912	-88.2888	1148	113180	57000	-56.4	9.56	0.045	18738.37	844		
28	28.7898	-88.4447	1040	13079	6500	-54.6	9.59	0.119	2307.395	274	820	
29	28.6565	-88.4018	1080	7631	3800	-54.8	9.73	0.110	1316.376	145		
32	28.7720	-88.4853	1072	21393	11000	-56.0	12.23	0.062	2876.073	178		
33	28.7847	-88.3967	1110	24622	12000	-57.4	5.98	0.005	6050.275	30		
										22 to 844	0 to 820	Total: 6.9

[a]methane oxidation rates determined here; [b]methane oxidation rates measured by Valentine et al. 2010

The dominant plume resulted from the DWH incident was formed at 1000m to 1200m depth with an average plume height of 200m [*Camilli et al.*, 2010; *Du and Kessler*, 2012; *Joye et al.*, 2011; *Kessler et al.*, 2011b; *Ryerson et al.*, 2012; *Valentine et al.*, 2010; *Yvon-Lewis et al.*, 2011]. The general migration of the plume was toward the southwest [*Du and Kessler*, 2012; *Kessler et al.*, 2011b] with an average δ of 3 km d^{-1} [*NDBC*, 2010]. Thus a four box model incorporating measurements of CH_4 concentrations and stable isotopic values from four stations along the plume transect was developed to characterize the dynamics of CH_4 in the system. Assuming that the majority of the CH_4 released from the wellhead was transported toward the southwest, and that the CH_4 added to each of the four boxes had an identical isotopic value (-57.5‰) with the CH_4 exiting the wellhead [*Reddy et al.*, 2012], summation of F_{in} calculated from all the four boxes determines the total flux of CH_4 from the wellhead (Table 3.1).

3.3 Results and Discussion

This model produced values for CH_4 oxidation rate and flux from the seafloor that are consistent with previous estimates (Table 3.1). The CH_4 oxidation rate determined here ranged from 22 to 844 nM d^{-1}, which is in agreement with previous estimates at the same time period using radio tracer addition technique [*Valentine et al.*, 2010]. The flow rate of CH_4 was 8.4×10^7 moles d^{-1} (i.e. total environmental release of 6.9×10^9 moles), which is within the range of previous estimates of 7.6 to 10.6 $\times 10^7$ moles d^{-1} [*Camilli et al.*, 2010; *Crone and Tolstoy*, 2010; *McNutt et al.*, 2012; *Reddy et al.*, 2012]. It should be noted that the CH_4 oxidation rates determined here represent the average oxidation rates between the

point source (i.e., wellhead) and the sampling stations, while the rates determined previously [*Valentine et al.*, 2010] represent the instantaneous CH_4 oxidation rates. The higher oxidation rates determined from this model most likely resulted from CH_4 oxidation prior to the sampling points.

The results from 20 stations surround the wellhead display a general pattern of enrichment of ^{13}C in CH_4 with increasing distance from the wellhead except at station 8 (Figure 3.3). Possible reasons for the abnormally heavy CH_4 at station 8 could be either that oxidation occurred prior to this station, or that reversal current transported plumes backward and mixed in heavier plume CH_4 at this station seeing that station 8 is located right below the Biloxi Dome.

This stable isotope model provides an easy and effective approach of assessing both the biodegradation of CH_4 and the total environmental release following the Deepwater Horizon oil spill. Errors may arise from unknown variations in modeling parameters with a coarse sampling grid. A fine sampling campaign incorporating the measurements of CH_4 concentration, CH_4 isotopes, ocean currents, as well as the fractionation factors, would help better characterize the dynamics of an oceanic CH_4 system.

4. HIGH RESOLUTION MEASUREMENTS OF METHANE AND CARBON DIOXIDE IN SURFACE WATERS OVER A NATURAL SEEP REVEAL DYNAMICS OF AIR-SEA FLUX*

Marine hydrocarbon Marine hydrocarbon seeps are sources of methane and carbon dioxide to the ocean, and potentially to the atmosphere, though the magnitude of the fluxes and dynamics of these systems are poorly defined. To better constrain these variables in natural environments, we conducted the first high-resolution measurements of sea surface methane and carbon dioxide concentrations in the massive natural seep field near Coal Oil Point, California. The corresponding high resolution fluxes were calculated, and the total dissolved phase air-sea fluxes over the surveyed plume area (~363 km^2) were 6.66 $\times 10^4$ to 6.71 $\times 10^4$ mol day^{-1} with respect to CH_4 and -6.01 $\times 10^5$ to -5.99 $\times 10^5$ mol day^{-1} with respect to CO_2. The mean and standard deviation of the dissolved phase air-sea fluxes of methane and carbon dioxide from the contour gridding analysis were estimated to be 0.18 $\pm$ 0.19 mmol m^{-2} day^{-1} and -1.65 $\pm$ 1.23 mmol m^{-2} day^{-1}, respectively,. This methane flux is consistent with previous, lower-resolution estimates and was used, in part, to conservatively estimate the total area of the dissolved methane plume at 8400 km^2. The influx of carbon dioxide to the surface water refutes the hypothesis that COP seep methane appreciably influencing carbon dioxide dynamics. Seeing that the COP seep field is one

*Reprinted with permission from Du, M., S. Yvon-Lewis, F. Garcia-Tigreros, D. L. Valentine, S. D. Mendes and J. D. Kessler (2014), High resolution measurements of methane and carbon dioxide in surface waters over a natural seep reveal dynamics of air-sea flux. Environmental science & technology.

of the biggest natural seeps, a logical conclusion could be drawn that microbial oxidation of methane from natural seeps is of insufficient magnitude to change the resulted plume area from a sink of atmospheric carbon dioxide to a source.

4.1 Introduction

The atmospheric concentrations of greenhouse gases CH_4 and CO_2 have increased to levels unparalleled in the last 0.8 million years [*IPCC*, 2013]. In 2011 the concentrations of CH_4 and CO_2 have exceeded the pre-industrial levels by about 150% and 40%, respectively [*IPCC*, 2013]. Though the present concentration of CH_4 in the atmosphere is ~200 times lower than that of CO_2, on a per molecule basis CH_4 is 23 times more potent in warming the earth than CO_2 over a 100-year timescale [*Forster et al.*, 2007; *Ramaswamy et al.*, 2001]. Despite the fact that the ocean contributes only ~1% to the global atmospheric budget [*Wuebbles and Hayhoe*, 2002], the marine sediments are the largest global reservoir of CH_4 and has the potential to increase its emissions with changing oceanographic conditions as implied from the geologic record [*Dickens et al.*, 1995].

At continental margins, CH_4 is produced by microbial and thermogenic processes. Methane that migrates to the seabed is either oxidized or escapes to the water column in dissolved or gaseous form [*Martens and Berner*, 1977; *McGinnis et al.*, 2006; *William S Reeburgh*, 1980]. Some of the CH_4 may enter the atmosphere through ebullition at sea surface. Some of the CH_4 may be lost to the water column while gas bubbles migrate

upward toward the sea surface, a process that is dependent on the initial bubble size, water depth, upwelling, and the surface conditions of the bubble (e.g. oil or hydrate coatings on the bubble surface) [McGinnis *et al.*, 2006]. In locations with seafloor depths greater than 100 m, CH_4 in rising bubbles may be completely replaced by DO and nitrogen from the water [*McGinnis et al.*, 2006]. The dissolved CH_4 is either utilized by microbes as part of their metabolic processes [*Mau et al.*, 2012; *Mau et al.*, 2007] or emitted to the atmosphere from the mixed layer [*Hu et al.*, 2012]. CO_2 produced from oxidation of oil and gas may dissolve into the water and react with dissolved Ca & Mg cations, forming insoluble carbonates, or be removed through photosynthesis in surface waters. Nevertheless, microbial oxidation of dissolved CH_4 to CO_2 provides a possibility to influence the dynamics of the greenhouse gas [Dickens 2000; Elliott *et al.*, 2011; Zachos *et al.*, 2008].

The Coal Oil Point (COP) seep field is located at a water depth of 5m to 70 m along the northern continental shelf of the Santa Barbara Channel (Figure 1). It has been reported to release up to 6.0×10^6 moles methane per day to the overlying waters, thereby establishing it as one of the World's most active seeps. [*Hornafius et al.*, 1999; *Quigley*, 1999]. Circulation pattern of the sub-mesoscale currents in the Santa Barbara Basin (SBB) generally shows a cyclonic eddy pattern [Beckenbach 2004; Emery et al., 2004; Harms and Winant 1998; Heintz *et al.*, 2012; Mau *et al.*, 2007; Nishimoto and Washburn 2002]. The cyclonic eddy in SBB transports the methane saturated waters from the massive seep field near Coal Oil Point (COP) toward the west and the center of the Santa Barbara

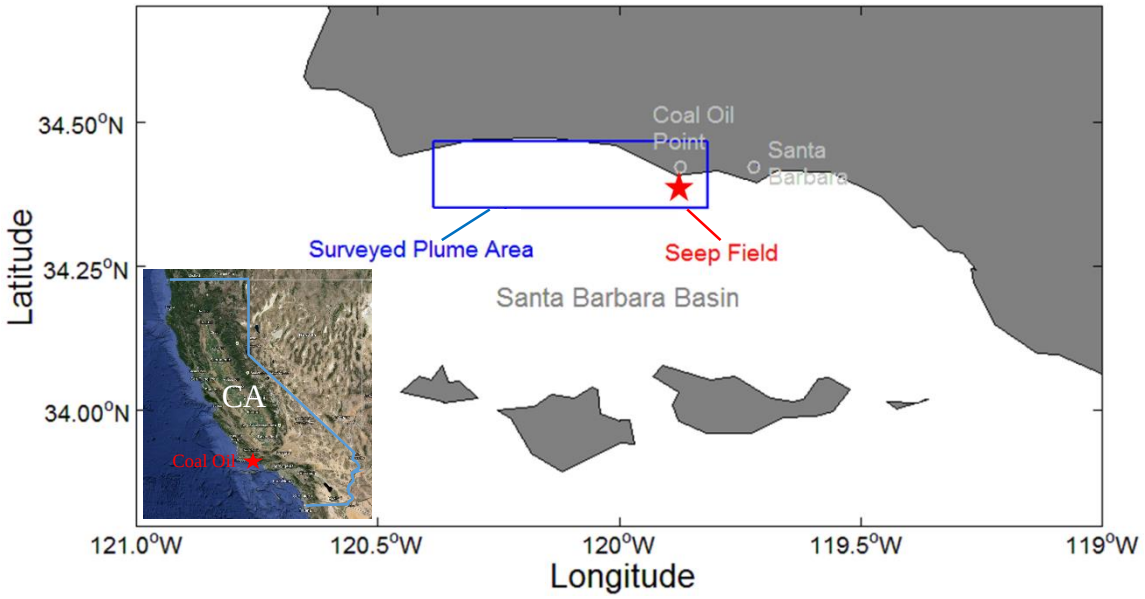

Figure 4.1 Location of the study area within the Santa Barbara Basin. The red star indicates the seep field near the Coal Oil Point; the blue box indicates the surveyed plume area (i.e. seep field and the down-current area); a map inset of CA is at the bottom left corner.

Chanel, resulting in two distinct methane plumes: one centered at ~40m and one centered at ~200m over a surveyed area of ~198 km^2 [Mau *et al.*, 2012]. Advection dominates in the plume area, allowing the dissolved methane to be transported out of the surveyed plume area for further microbial oxidation or exchange with atmosphere. The evolving sub-mesoscale currents in SBB play an important role in regulating the concentrations of methane. The cyclonic eddy weakens in Fall, resulting in higher methane concentrations along the coast [Mau *et al.*, 2007]. And a small anticyclonic eddy that lasts a few days

occurs several times a year [Bassin *et al.,* 2005; Mau *et al.,* 2007] resulting in much lower methane concentrations. Apparently the speeds and directions of the currents have the potential to regulate the concentrations of methane in the waters; however the prior estimates of air-sea fluxes have not shown large discrepancies under distinct current conditions [Clark *et al.,* 2012; Clark *et al.,* 2000; Mau *et al.,* 2007].

Since the majority of emitted CH_4 is dissolved in the overlying waters and thus available for both equilibration with the atmosphere and microbial oxidation at COP, we hypothesize that microbial oxidation of CH_4 changes this region from a sink of atmospheric CO_2 to a source. Here we investigate the dissolved phase net air-sea fluxes of CH_4 in the plume area that resulted from the COP seeps, and report the first study of dissolved phase air-sea fluxes of CO_2 from this region. Both CH_4 and CO_2 fluxes were measured concurrently using a new integrated nozzle-type equilibrator [*Pierrot et al.*, 2009] and Cavity Ring-down Spectrometer (CRDS) enabling high spatial resolution measurements (Figure 4.2). This study provides a view of high-resolution distributions of CH_4 and CO_2 in the air and in the surface water within the Santa Barbara Basin, which contributes to a better understanding of the fate of CH_4 injected into the water above seeps and its contributions to atmospheric greenhouse gas budgets.

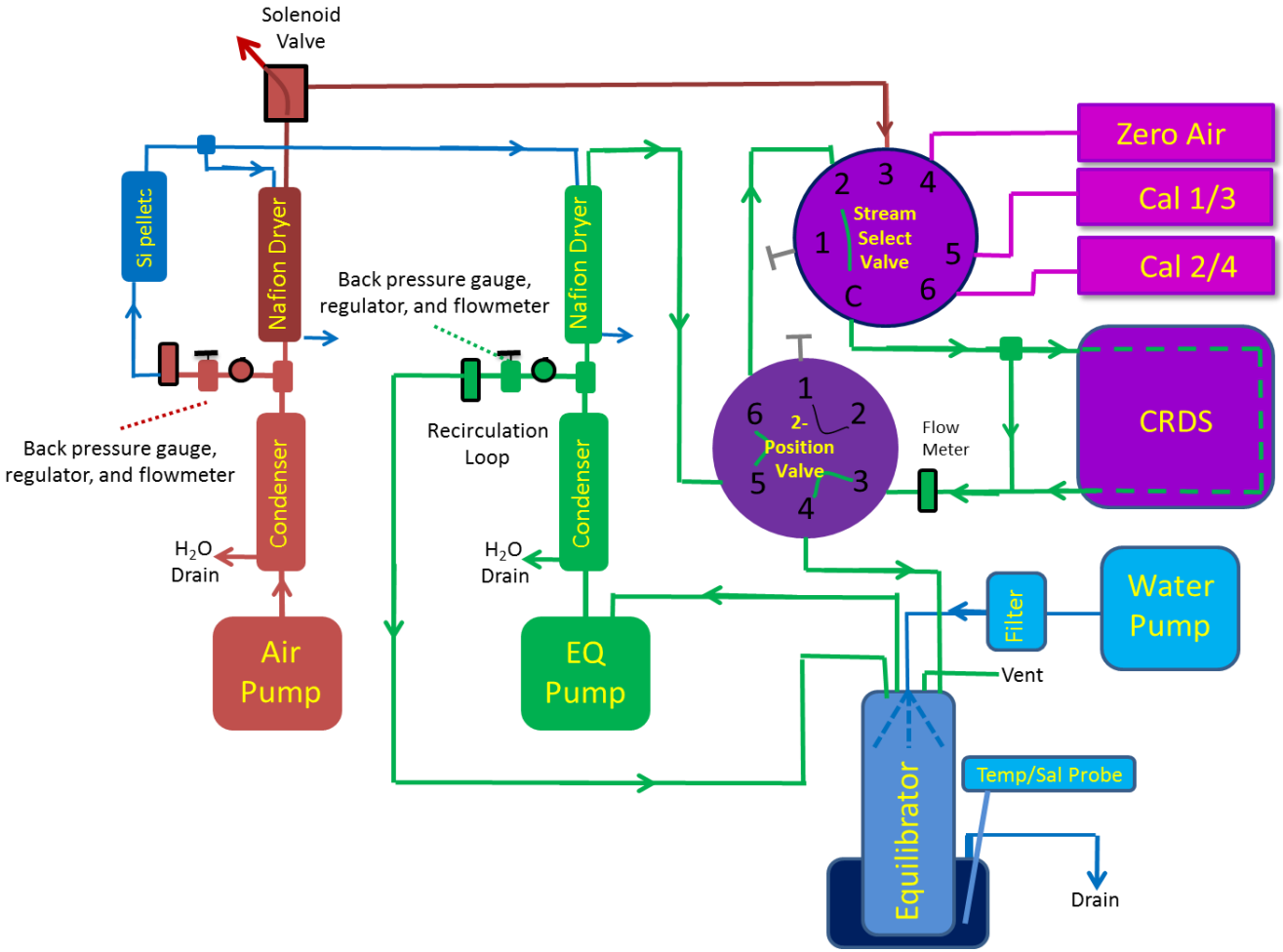

Figure 4.2 Integrated nozzle-type equilibrator and cavity ring-down spectrometer (CRDS): the equilibrator mode (green), the air mode (red), and the standard mode (purple).

4.2 Methods

4.2.1 Measurements

Flux measurements of CH_4 and CO_2 within the Santa Barbara Basin were made onboard the *R/V Atlantis* from 12 September to 29 September 2011 (Figure 4.1A). The concentrations of CH_4 and CO_2 in the air and surface seawater were continuously measured through a new integrated equilibrator and Cavity Ring-down Spectrometer (EQ/CRDS) system (Figure 4.2) [*Gülzow et al.*, 2011]. The headspace of the equilibrator was plumbed to the CRDS in a closed-loop, and since CRDS is a non-destructive technique, this EQ/CRDS system can be viewed as a nearly-closed system (Figure 4.2). In addition, some plumbing internal to the CRDS (e.g. pumps, fittings, and tubing) were vacuum sealed to minimize leaks we previously identified. Ship positions were continuously recorded by the onboard Global Positioning System (GPS). Sea surface temperature and salinity were continuously recorded by a thermosalinograph (SBE-45) located in the bow thruster room (~5 m below the sea level). Concurrent air temperature, humidity, wind speeds and wind directions were continuously recorded by an IMET sensor mounted on the bow (21 m above the sea level).

Surface seawater was continuously pumped from ~5 m below the sea level into the equilibrator at a rate of 1.9 to 2.9 L/min through a spiral nozzle. The mixed layer depth ranged from 8 to 18 m within the surveyed plume area. The nozzle created a spray of seawater that maximized the rate of equilibration of CH_4 and CO_2 between the headspace and the water phase in the equilibrator. The headspace inside the equilibrator was

maintained at ambient pressure by a vent, however, continuous leak checking of the system plumbing confirmed the vent flow to be insignificant. Air was continuously pumped through a Synflex tube mounted on the flying bridge on the bow. The bow air and equilibrator headspace were pumped through condensers and Nafion dryers to quantitatively remove water moisture, and then were alternately analyzed by the CRDS (100-minute continuous measurement of the equilibrator headspace samples followed by 10-minute continuous measurement of bow air samples).

The CH_4 concentration recorded by the EQ/CRDS system was routinely verified by analyzing discrete samples via Gas Chromatography with Flame Ionization Detection (GC-FID). In order to validate the EQ/CRDS technique, surface seawater samples were collected periodically in 160 ml crimp-top bottles for analysis of CH_4 with a GC-FID [*Valentine et al.*, 2001]. All sample bottles were flushed with at least 3 volumes of seawater and filled completely without bubbles. The bottles were immediately capped with butyl rubber stoppers, crimp sealed, and poisoned with mercuric chloride. Then a 10 ml nitrogen headspace was introduced into each bottle via displacement [*Valentine et al.*, 2001]. After the dissolved gas was allowed to fully equilibrate with the nitrogen headspace for at least 12 hours, two aliquots of the headspace were analyzed to determine the concentration of CH_4 with a GC-FID. A comparison of the CH_4 concentrations in discrete samples analyzed by GC/FID with those measured using the EQ/CRDS showed good agreement, with residuals randomly distributed around zero (average value of the residuals ($\mu mol\ L^{-1}$) = 0.00, sum of the residual = -0.23; standard deviation of the residuals = 0.11,

n = 54) indicating that the EQ/CRDS measurements were not systematically higher or lower than the GC measurements.

4.2.2 Calculations

Seawater equilibrators have been used for the study of dissolved gases in the ocean such as CO_2, CH_4, halocarbons and other soluble gases for many years e.g., [*Bates et al.*, 1995; *Butler et al.*, 2007; *Gülzow et al.*, 2011; *Hu et al.*, 2012; *Kourtidis et al.*, 2006; *Pierrot et al.*, 2009; *Takahashi et al.*, 2009; *Wanninkhof and Thoning*, 1993; *Yvon-Lewis et al.*, 2011]. The measurement assumes that the gas reaches complete and instantaneous equilibration between the headspace and the water phase, and that the water sampled is representative of the water in contact with the atmosphere [*Johnson*, 1999]. However, the dissolution/exsolution rates of the gases are rarely instantaneous and need to be taken into account when calculating true seawater concentrations. The true concentrations of CH_4 and CO_2 in surface seawater can be determined from the equilibrator measurement:

$$C_w = \frac{\alpha(C_e - e^{-\frac{t}{\tau}} C_i)}{1 - e^{-\frac{t}{\tau}}} \qquad \text{(Eq. 4.1)}$$

where, C_w is gas concentration in the incoming seawater; C_e is the gas concentration in the headspace measured by the CRDS and averaged over 1 minute; C_i is the previous gas concentration in the headspace measured by the CRDS and averaged over 1 minute; t is the time between the measurement of C_i and C_e, 1 min; τ is an empirically-derived e-folding time constant for equilibration and was measured in the lab at different solubilities, τ = 1.1 min when the concentration is increasing (i.e. $C_e > C_i$) and τ = 6.03 min when the

concentration is decreasing (i.e. $C_e < C_i$) with respect to CH_4, and is negligible with respect to CO_2 (i.e., CO_2 in the headspace rapidly comes to full equilibrium in this equilibrator).

When either surface seawater or air samples were not being measured (i.e. when the other parameter was being measured), the concentrations of CH_4 and CO_2 were linearly interpolated between measurements in order to calculate the saturation anomalies (SA) and air-sea fluxes (F):

$$SA = [(p_w - p_a)/p_a] \times 100 \quad \text{(Eq. 4.2)}$$

$$F = k\,(C_w - p_a \times k_H) \quad \text{(Eq. 4.3)}$$

where p_w is the partial pressure (atm) of the gas in the surface seawater, $p_w = C_w/k_H$; k_H is the Henry's law constant (mol L^{-1} atm^{-1}) [*Lide*, 1995]; p_a is the partial pressure (atm) of the gas in the air; $k = 0.27\, u_{10}^2\, (Sc/600)^{-0.5}$ is the gas transfer velocity (cm h^{-1}) [*Sweeney et al.*, 2007]; Sc is the Schmidt Number of the gas in seawater [*Wanninkhof*, 1992]; u_{10} is the wind speed adjusted to 10 m above the sea level (m s^{-1}) [*Large and Pond*, 1982].

4.3 Results

In this study, we measured CH_4 and CO_2 concentrations in the air and surface seawater and calculated their respective air-sea fluxes over a ~363 km^2 area in the Santa Barbara Basin (Figure 4.3-4.5; Table 4.1). Enriched CH_4 concentrations in the air correlate with more enriched concentrations in the surface seawater suggesting that the major source of atmospheric CH_4 in the study area was the ocean. For CO_2 however, enrichment in the

atmosphere and in the surface water was not correlated, possibly due to continental sources of atmospheric CO_2.

Concentrations of CH_4 ranged from 1.91 to 11.31 ppm with a mean of 2.16 ppm in the air and 0.00 to 1.55 μmol L^{-1} with a mean of 0.22 μmol L^{-1} in the surface seawater within the surveyed plume area. Concentrations of CO_2 ranged from 383.3 to 425.2 ppm with a mean of 390.7 ppm in the air and 9.29 to 10.68 μmol L^{-1} with a mean of 9.72 μmol L^{-1} in the surface seawater within the surveyed plume area. The saturation anomalies ranged from 390 to 37598 % with a mean of 7811 % with respect to CH_4 and from -19.36 to -2.18% with a mean of -11.94 % with respect to CO_2 within the surveyed plume area. The diffusive air-sea fluxes ranged from 0 to 0.83 mmol m^{-2} day^{-1} with a mean of 0.11 mmol m^{-2} day^{-1} with respect to CH_4 and from -6.90 to 0.00 mmol m^{-2} day^{-1} with a mean of -0.95 mmol m^{-2} day^{-1} with respect to CO_2 in the surveyed plume area.

Figure 4.3 (A) Concentrations of CH_4 in the surface seawater and in the air, yellow dots are the discrete seawater samples measured with GC-FID; (B) saturation anomalies and air-sea fluxes of CH_4; (C) concentration of CO_2 in the surface seawater and in the air; (D) saturation anomalies and air-sea fluxes of CO_2; (E) wind speed and humidity; (F) salinity and seawater temperature and air temperature from the surveyed plume area; the grey shadows indicate the time periods over the seep field.

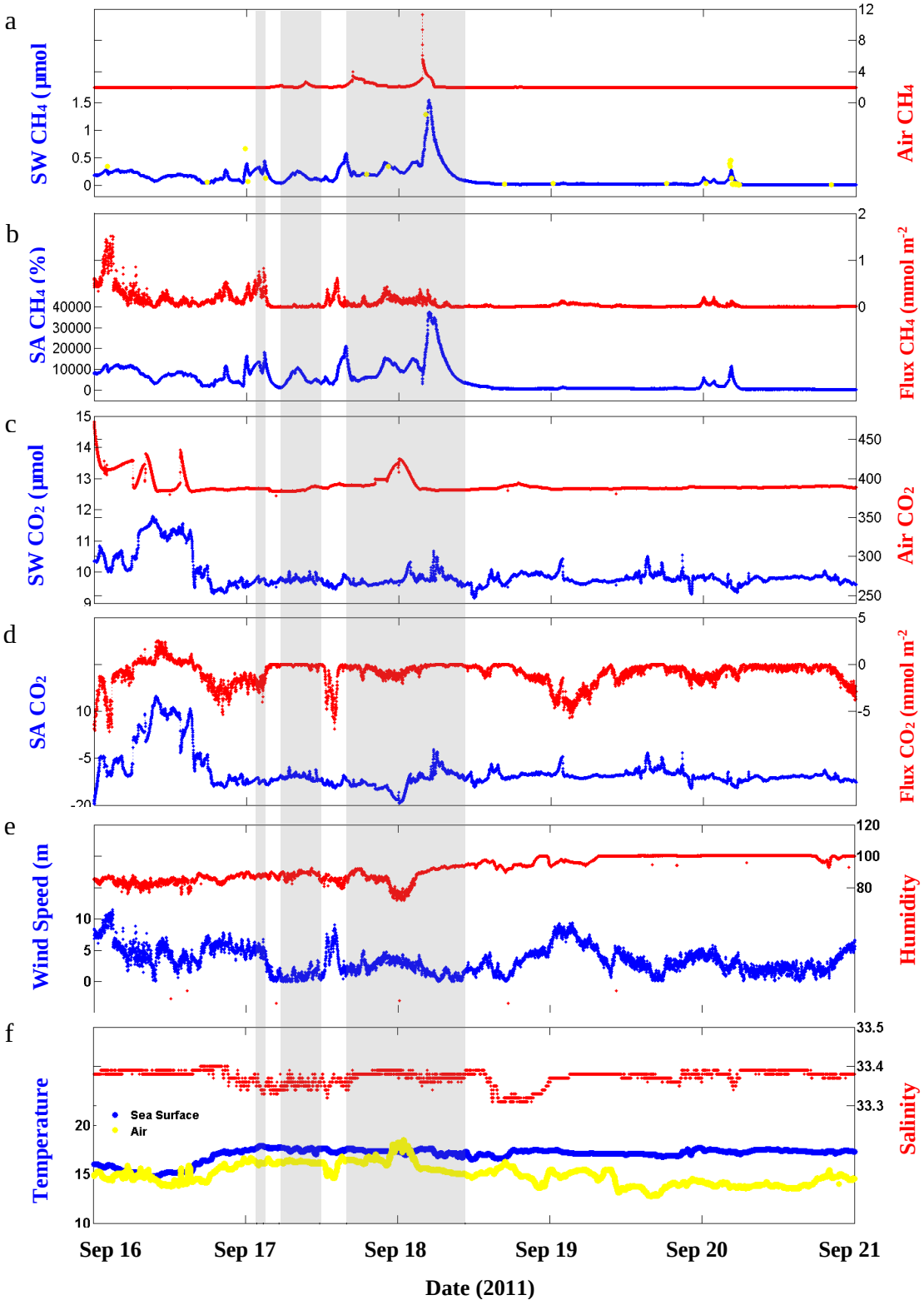
a
SW CH4 (µmol
Air CH4
b
SA CH4 (%)
Flux CH4 (mmol m-2
c
SW CO2 (µmol
Air CO2
d
SA CO2
Flux CO2 (mmol m-2
e
Wind Speed (m
Humidity
f
Temperature
Salinity
Sea Surface
Air
Sep 16
Sep 17
Sep 18
Sep 19
Sep 20
Sep 21
Date (2011)

Figure 4.4 Spatial distribution of concentrations, SA and fluxes of CH_4. (A) CH_4 concentration in the air; (B) CH_4 concentration in the surface seawater; (C) saturation anomaly of CH_4; (D) air-sea flux of CH_4 from the surveyed plume area.

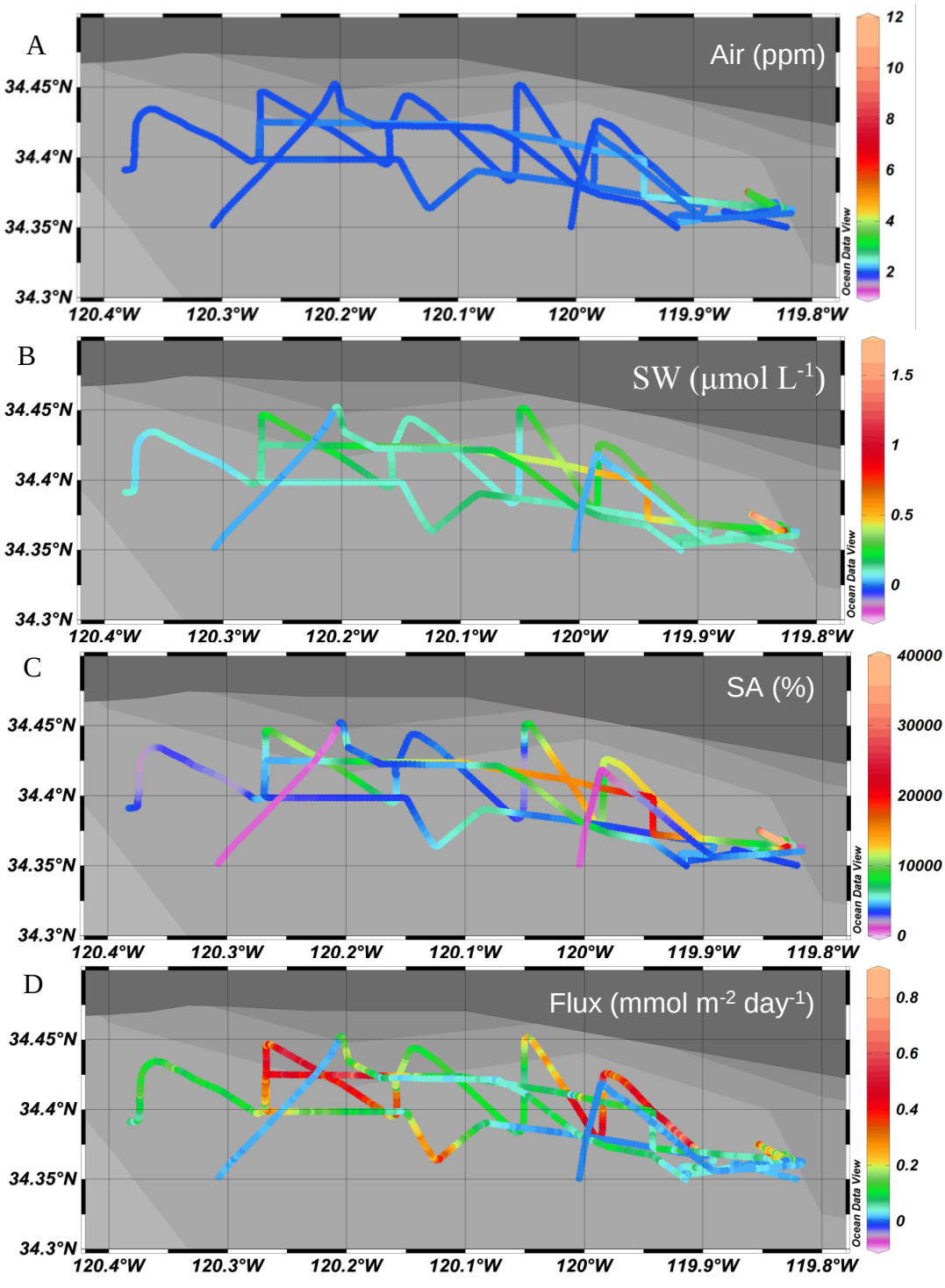
A
Air (ppm)
34.45°N
34.4°N
34.35°N
34.3°N
120.4°W
120.3°W
120.2°W
120.1°W
120°W
119.9°W
119.8°W
12
10
8
6
4
2
Ocean Data View
B
SW (µmol L-1)
1.5
1
0.5
0
C
SA (%)
40000
30000
20000
10000
0
D
Flux (mmol m-2 day-1)
0.8
0.6
0.4
0.2
0

Figure 4.5 Spatial distribution of concentrations, SA and fluxes of CO_2. (A) CO_2 concentration in the air; (B) CO_2 concentration in the surface seawater; (C) saturation anomaly of CO_2; (D) air-sea flux of CO_2 from the surveyed plume area.

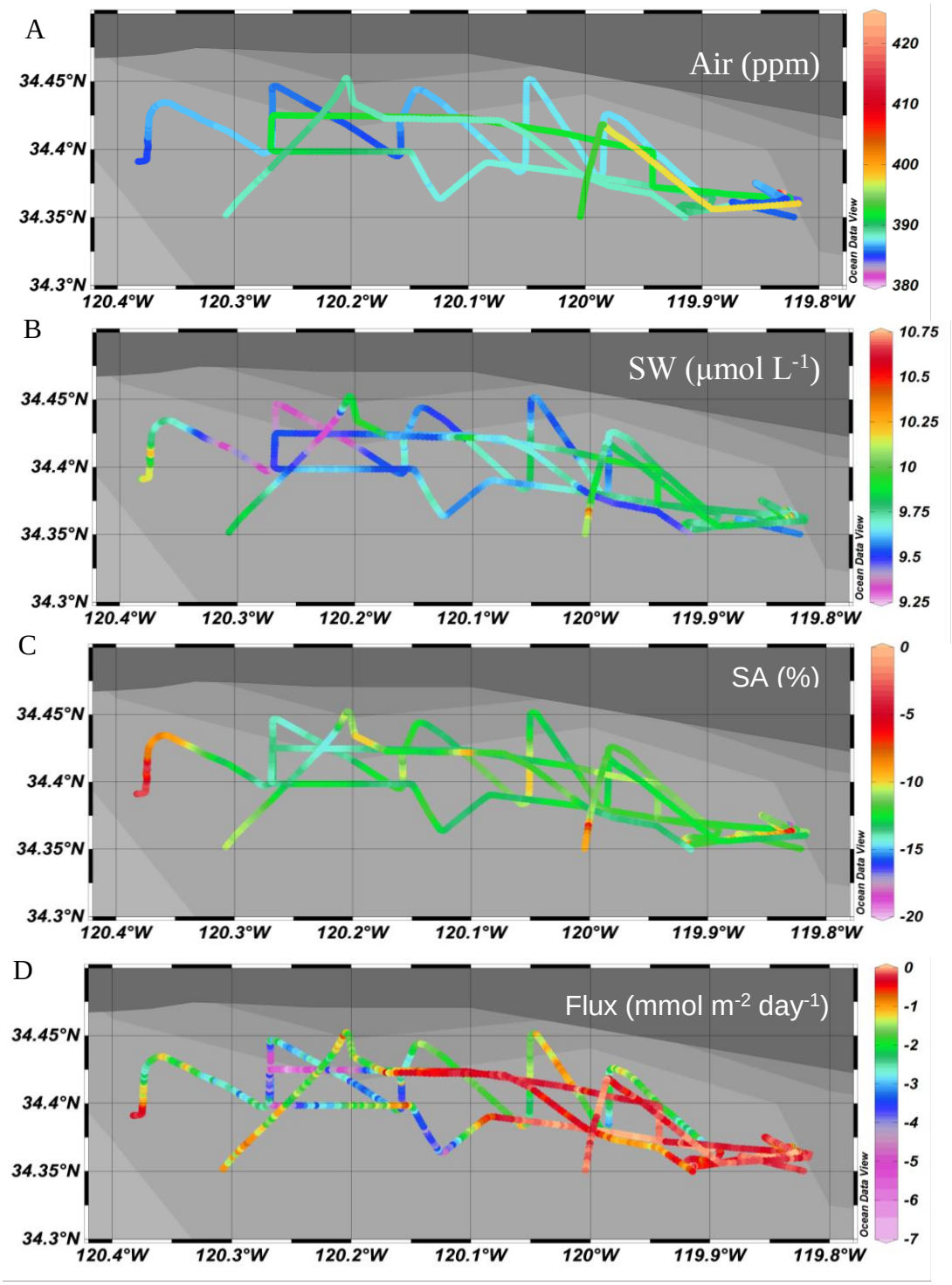
A
Air (ppm)
34.45°N
34.4°N
34.35°N
34.3°N
120.4°W
120.3°W
120.2°W
120.1°W
120°W
119.9°W
119.8°W
420
410
400
390
380
Ocean Data View
B
SW (µmol L-1)
10.75
10.5
10.25
10
9.75
9.5
9.25
C
SA (%)
0
-5
-10
-15
-20
D
Flux (mmol m-2 day-1)
-1
-2
-3
-4
-5
-6
-7

Table 4.1 CH_4 and CO_2 concentrations in the air and surface seawater, saturation anomalies and air-sea fluxes over the surveyed plume area of ~363 km^2.

	pa (ppm)	C_w (μmol L-1)	SA (%)	Flux Measured (mmol m^{-2} day^{-1})	Flux Interpolated (mmol m^{-2} day^{-1})
			CH_4		
min	1.91	0.01	390	0.00	0.00
max	11.31	1.55	37598	0.83	0.83
[a]μ	2.16	0.22	7811	0.11	0.18
[b]σ	0.48	0.22	6680	0.12	0.19
[c]σ_{mean}	0.01	0.004	121	0.002	0.000
			CO_2		
min	383.3	9.29	-19.36	-6.90	-6.90
max	425.2	10.68	-2.18	0.00	0.00
[a]μ	390.7	9.72	-11.94	-0.95	-1.65
[b]σ	10.6	0.25	2.39	1.05	1.23
[c]σ_{mean}	0.2	0.004	0.04	0.02	0.002

[a]μ is the average
[b]σ is the standard deviation
[c]σ_{mean} is the standard deviation of the mean

The results indicate that the surface waters of the Santa Barbara Basin was mainly supersaturated with CH_4 and undersaturated with CO_2 (Figure 4.3-4.5; Table 4.1). The maximum saturation anomaly of CH_4 was observed within the seep field, whereas the maximum diffusive air-sea flux of CH_4 was observed southwest to the seep field due to stronger winds in that area during the sampling time (Figure 4.5). The Santa Barbara Basin acted as a net source of atmospheric CH_4 and a net sink of atmospheric CO_2.

4.4 Discussion

4.4.1 Diffusive Air-sea Flux

Four different contouring methods were used to interpolate the diffusive air-sea flux of CH_4 and CO_2: empirical Bayesian kriging (EBK), inverse distance weighted (IDW), radial basis functions (RBF), and diffusion kernel (DK). These interpolation methods produced similar results except DK. EBK had the lowest prediction errors for both CO_2 and CH_4 among the three methods that generally agreed, and was, therefore, selected as the primary contouring method (Figure 4.6). In consideration of the multiple measurements at some locations, the contour gridding was repeated using the minimum value, the mean value, and the maximum value, respectively. The results suggest that the integrated air-sea flux over the surveyed plume area (~363 km^2) was 6.66 $\times 10^4$ to 6.71 $\times 10^4$ mol day^{-1} with respect to CH_4 with a mean per area flux of 0.18 mmol m^{-2} day^{-1} (standard deviation σ = 0.19; standard deviation of the mean σ_{mean} = 0.0003), and -6.01 $\times 10^5$ to -5.99 $\times 10^5$ mol day^{-1} with respect to CO_2 with a mean per area flux of -1.65 mmol m^{-2} day^{-1} (standard deviation σ = 1.23; standard deviation of the mean σ_{mean} = 0.002). The mean, standard deviation and the standard deviation of the mean of the interpolation results, which are based on data more evenly distributed through the surveyed plume area, were seen as more representative of the plume than those calculated from the measured data points. Nonetheless, the fluxes calculated from the interpolated data are similar to those from the measured data (Table 4.1).

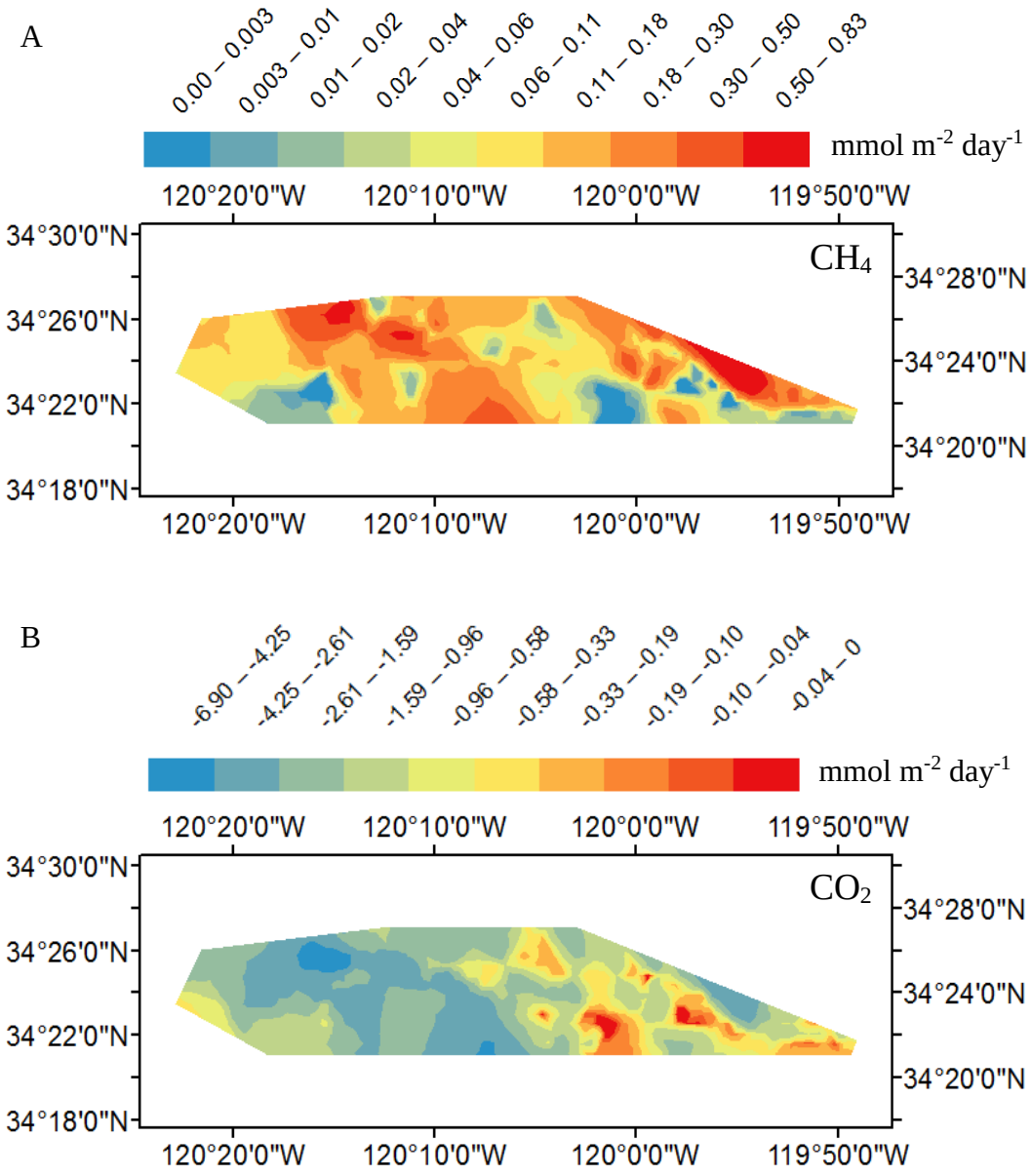

Figure 4.6 Contour plots of air-sea fluxes of (A) CH_4 and (B) CO_2 using empirical Bayesian kriging from the surveyed plume area.

While no CO_2 fluxes have been reported previously with which to compare, this estimate of the diffusive air-sea flux of CH_4 (6.71×10^4 mol day^{-1} over an area of ~363 km^2 with a mean per area flux of 0.18 mmol m^{-2} day^{-1}) is consistent with previously published estimates. A previous study [*Mau et al.*, 2007] estimated the air-sea flux to be on the order of 5×10^4 mol day^{-1} from dissolved CH_4 over an area of ~280 km^2 (0.18 mmol m^{-2} day^{-1}). While there is close agreement between these studies, each representing a different snapshot in time, uncertainties in both estimates may arise from gas transfer parameterization, sampling density, and interpolation method. (1) Uncertainties in the gas transfer parameterization derive primarily from wind speed variability [*Mau et al.*, 2007]. For example, variation in wind speed from 4 m s^{-1} to 5 m s^{-1} may cause the total flux to change by 50% [*Mau et al.*, 2007]. Rather than using an average wind speed over the whole study area (e.g. [*Mau et al.*, 2007]), wind speed and CH_4 concentration were recorded synchronously and used for the flux calculations in this study. However, neither study included a surfactant layer in the flux calculations though the occurrence of thick oil slicks are common at COP seep field [*Kraus and Estes*, 1977a; b]. (2) Variations in surface water CH_4 concentration within a plume may not be captured with a coarse sampling grid (e.g. [*Mau et al.*, 2007]), while high-density sampling in this study provides a higher spatial resolution view of the concentration changes. (3) Contoured results vary with interpolation method and corresponding parameterization. Four interpolation methods were tested in this study and corresponding error analyses suggest that the four methods did not produce significantly different results; however, much smaller sampling campaigns may produce different results using different interpolation methods. Finally,

variations in gas solubilities, seafloor emission rates, current velocities and mixing rates at different sampling times could also lead to temporal variations in CH_4 fluxes.

A contour, gridding, and summation analysis was then conducted on the concentration of CH_4 in the surface water to estimate the total amount of dissolved CH_4 in the mixed layer and its turnover time. If we assume that the top 13m (i.e., the median of the mixed layer depths measured at 20 CTD stations) of the surveyed area was well-mixed, a total amount of 1.1×10^6 mol CH_4 would be dissolved in the mixed layer. This result suggests that 6% of the mixed layer CH_4 would diffuse to the atmosphere in one day, and that it would take 16 days for all of the CH_4 in the mixed layer to diffuse to the atmosphere; this calculation assumes a steady-state mixed layer where the atmospheric flux is constant and balanced by CH_4 sources from below. If we use the lower/upper bonds of the measured mixed layer depths (8 m/18 m) as the mean mixed layer depth in the surveyed plume area, 10%/4% of the mixed layer CH_4 would diffuse to the atmosphere per day and it would take 10 days/23 days for all of the CH_4 in the mixed layer to diffuse to the atmosphere.

4.4.2 *Fate of CH_4 Released at Seafloor*

Seepage CH_4 is released to the atmosphere either directly through direct bubble injection to the atmosphere or indirectly through diffusion from dissolved CH_4 in the surface water mixed layer. Previous studies indicate approximately 6×10^6 mol day^{-1} of CH_4 is released at the seafloor from the COP seep field [*Clark et al.*, 2003; *Hornafius et al.*, 1999; *Leifer et al.*, 2000; *Quigley*, 1999] of which 60% (3.6×10^6 mol day^{-1}) was dissolved into the

overlying water and 40% (2.4×10^6 mol day^{-1}) was directly emitted to the atmosphere through bubble injection [*Clark et al.*, 2000]. This study estimated a total diffusive air-sea flux on the order of 6.66×10^4 mol day^{-1} from dissolved CH_4 over an area of ~363 km^2 (i.e. 2% of the dissolved CH_4). This result implies that 3.53×10^6 mol day^{-1} of the CH_4 released at the sea floor (i.e., 98% of the dissolved CH_4) is either oxidized in the water column within the study area or dispersed followed by further oxidization and/or air-sea exchange outside of our survey area. Assuming that the CH_4 oxidation rate during the sampling time in this study is similar to what was measured previously (average of 3.3 nM d^{-1} for waters shallower than 75 m) [*Mau et al.*, 2012], then only 2% of the dissolved CH_4 would be microbially oxidized in this study area, leaving a significant fraction available for further oxidation or atmospheric equilibration outside of regions studied here and previously.

Since a closed budget for CH_4 released from the COP seep field cannot be established from the regions investigated here and previously (e.g. [*Mau et al.*, 2012]), we provide a first-order estimate of the area impacted by COP CH_4, which must extend beyond regions investigated here. If we assume that the mean atmospheric flux value determined here is representative of the entire plume, not just the surveyed plume area (Figure 4.1A), then an estimate for the area of the COP CH_4 plume can be made by dividing the rate at which COP CH_4 dissolves in seawater (3.6×10^6 mol day^{-1}) by the sum of the diffusive air-sea flux (0.18 mmol m^{-2} day^{-1}) and oxidation flux (0.25 mmol m^{-2} day^{-1}) [*Mau et al.*, 2012]; this calculation assumes the COP CH_4 plume extends between the surface and 75 m and

has an average oxidation rate similar to what was measured previously [*Mau et al.*, 2012]. This plume area estimate (8,400 km^2) is likely an underestimate since both the oxidation rates and diffusive air-sea flux will likely decrease as the plume extends beyond the surveyed plume area and the dissolved CH_4 concentration decreases. To find the true boundary of the plume area, radiocarbon analysis of CH_4 from this region could be done since as all of the CH_4 coming from the seeps must be fossil [*Kessler et al., 2008*].

Interestingly, this conservatively estimated plume area (8,400 km^2) is an order of magnitude less than the CH_4 plume which resulted from the Deepwater Horizon (DWH) oil spill in 2010 (73,200 km^2) [*Du and Kessler*, 2012]. At the same time the daily emission rate of CH_4 from the COP seep field (6×10^6 mol day^{-1}) [*Clark et al.*, 2003; *Hornafius et al.*, 1999; *Leifer et al.*, 2000; *Quigley*, 1999] is also an order of magnitude less than that from the DWH oil spill (94×10^6 mol day^{-1}) [*McNutt et al.*, 2012; *Ryerson et al.*, 2012]. Since no DWH CH_4 was emitted to the atmosphere [*Ryerson et al.*, 2011; *Yvon-Lewis et al.*, 2011] but instead had an ultimate fate of microbial oxidation [*Kessler et al.*, 2011b], a logical conclusion from this comparison would be that microbial oxidation also provides the dominant sink of CH_4 in COP. Nonetheless, there are significant uncertainties and differences that make such a comparison less straightforward. (1) Assumptions in the COP plume area calculation lead to a conservative estimate of the area, (2) The area of the COP seep field is much larger than the pipe (inner diameter 0.5 m) in the DWH oil spill [*FRTG*, 2010; *Hornafius et al.*, 1999; *Quigley et al.*, 1999]. (3) The COP seep field is much

shallower than the depth of the blowout (1500 m below the surface) in the Gulf of Mexico [*Hornafius et al.*, 1999; *Lehr; et al.*, 2010; *Quigley et al.*, 1999].

We hypothesized that the aerobic oxidation of CH_4 to CO_2 would influence the dissolved CO_2 reservoir, potentially making it a source of CO_2 to the atmosphere. This hypothesis was based on a simple mass balance. The maximum surface water CH_4 concentration measured is 1.55 μmol L^{-1}, and if quantitatively converted to CO_2, would increase a background CO_2 concentration of 9 μmol L^{-1} by 17%. However, our measurements did not support this hypothesis. (1) The dissolved CO_2 concentrations were understaturated, indicating this region is a sink of atmospheric CO_2 rather than a source. (2) Our data do not refute the possibility that CH_4 oxidation increased the dissolved concentration of CO_2 above background levels, thus decreasing the ocean's ability to absorb atmospheric CO_2. If we assume that the average surface concentrations of CH_4 and CO_2 measured here are representative of the entire COP CH_4 plume and that all surface water CH_4 is converted to CO_2 without loss to the atmosphere, the surface water concentration of CO_2 would increase by only 2%. (3) Our actual measurements of dissolved CO_2 concentration are not significantly outside normal background values for the ocean, further arguing against the hypothesis of COP seep CH_4 appreciably influencing CO_2 dynamics.

At shallower seep fields, a greater portion of the CH_4 released at seafloor would be expected to enter the atmosphere through ebullition and a smaller portion would be dissolved to the water. Thus a smaller portion of the dissolved phase CH_4 may be

converted to CO_2. Seeing that the COP seep field is one of the biggest natural seeps, a logical conclusion could be drawn that microbial oxidation of methane from natural seeps is of insufficient magnitude to change the resulted plume area from a sink of atmospheric carbon dioxide to a source.

5. CONCLUSIONS

CH_4 dynamics from two sites were investigated: the DWH oil spill in the GoM, and a shallow natural seep field at COP, CA. A suite of measurements have been conducted on DO concentrations, CH_4 concentrations and stable isotopic ratios, and air-sea fluxes of CH_4. Analyses have been done to quantify the mass of CH_4 as well as total hydrocarbons released to the GoM, to track the microbial respiration of deep plume CH_4 and hydrocarbons temporally and spatially, and to evaluate the diffusive air-sea fluxes of CH_4 from the seeps at COP. The results provide a clear view of depth on the influence of CH_4 evasion to the atmosphere as well as microbial response. The results also speak to the regional differences (i.e. shallow shelf vs. base of the continental slope) in the atmospheric flux of CO_2 produced from CH_4 oxidation.

The DO and CH_4 stable isotope approaches produced values for the CH_4 oxidation rates and total environmental release of CH_4 that are consistent with previous estimates (Table 5.1). Approximately 40% of the CH_4 release by the shallow seeps at COP escaped to the atmosphere directly as bubbles, however, negligible amounts of CH_4 were able to reach to the surface when released into deep waters. Interestingly the daily emission rate of CH_4 from the seeps at COP, CA (6×10^6 mol day^{-1}) is an order of magnitude less than that from the DWH oil spill in the GoM (7.6 - 10.6 $\times 10^7$ mol day^{-1}). The estimates produced here of the total area impacted by CH_4 plumes from the seeps at COP, CA (8,400 km^2) is also an order of magnitude less than that from the DWH oil spill in the GoM (73,200 km^2).

Since no DWH CH_4 was emitted to the atmosphere but instead had an ultimate fate of microbial oxidation, these results suggest that microbial oxidation provides the dominant sink of the dissolved CH_4 from COP seeps as well.

Table 5.1 Comparison of the fate of CH_4 released from the DWH oil spill and the shallow seeps at COP.

	DWH Oil Spill	Shallow Seeps at COP
CH_4 Release Depth (m)	[a]1500	[d]5-70
Flux of CH_4 at Seafloor (mol d^{-1})	[a]7.6- 10.6 $\times 10^7$	[d]6.0 $\times 10^6$
Dissolved into seawater (mol d^{-1})	[a]7.6- 10.6 $\times 10^7$	[e]3.6 $\times 10^6$
Area of Plumes (km^2)	[b]73,200	8,400
Flux of CH_4 to the Atmosphere (mol d^{-1})	[c]22.8	[f]2.5 $\times 10^6$
Percent of Emission to the Atmosphere (%)	0	42

[a]Camilli et al., 2010; Crone and Tolstoy, 2010; McNutt et al., 2012; Reddy et al., 2012; [b]Du and Kessler, 2012; [c]Yvon-Lewis et.al., 2011; [d]Clark et.al., 2003; Hornafius et.al., 1999; Leifer et.al., 2000; Quigley 1999; [e]Clark et.al., 2000; [e]total flux of CH_4 from the seawater to the atmosphere is contributed from direct bubble injection of 2.4 $\times 10^6$ mol d^{-1} [Clark et.al., 2000] and indirect diffusive air-sea flux of 1 $\times 10^5$ mol d^{-1}.

While CO_2 is produced during microbial oxidation of CH_4 near COP seeps, it is not emitted to the atmosphere because primary production reduces pCO_2 to understaturated values. Interestingly, this is true for most shallow water environments where the productivity is normally high and the CH_4 released from the seafloor can dissolve to the

surface mixed layer and. But in deep water environments, CH_4 tends to dissolve into the deep waters and make insignificant contribution to these atmospheric greenhouse gas budget.

6. FUTURE WORK

Future studies of geologic CH_4 at more sites (e.g. the natural seeps in the South China Sea) is needed to provide a global view of CH_4 dynamics. Future work for all investigations of CH_4 seeps should include a well-organized sampling regime along plume transects, including sampling multiple depths to provide high resolution views of CH_4 plumes temporally and spatially. The DO approach presented has been proven successful for assessing the bulk hydrocarbon respiration following the DWH oil spill. However a potential error occurs when DO samples were not adequately or randomly analyzed throughout the intrusion area and may not capture the true location of the plumes. An organized fine-grid network would help better assess the fate of released HCs. The stable isotope model successfully estimated the total environmental release of CH_4 and the CH_4 oxidation rates in June 2010. However a bigger data set is essential for providing information such as the spatial and temporal change of the oxidation rate.

It has been recognized that CH_4 escaping from shallow-water seeps tends to enter the atmosphere, whereas CH_4 escaping from deep-sea seeps tends to be lost to the hydrosphere. However a critical depth is unknown. High resolution mapping of the spatial distribution of CH_4 plumes at a seep site or a comprehensive comparison among natural seeps at various depths will be a boon for understanding the dynamics of the global oceanic CH_4 system.

REFERENCES

Aminot, A. (1997), Anomalies in the Coastal Hydrobiological System After the Amoco Cadiz Grounding. Qualitative and Quantitative Considerations on Hydrocarbons In Situ Biodegradation *Rep., 1*, 223-242.

Aminot, A. K., R. (1978), First results on hydrology, dissolved oxygen and photosynthetic pigments in the western English Channel after the stranding of the Amoco Cadiz *Rep., 1*, 51-68.

Barker, J. F., and P. Fritz (1981), Carbon isotope fractionation during microbial methane oxidation, *Nature*, *293*, 289-291.

Bates, T. S., K. C. Kelly, J. E. Johnson, and R. H. Gammon (1995), Regional and seasonal variations in the flux of oceanic carbon monoxide to the atmosphere, *Journal of Geophysical Research: Atmospheres (1984–2012)*, *100*(D11), 23093-23101.

Beolchini, F., L. Rocchetti, F. Regoli, and A. Dell'Anno (2010), Bioremediation of marine sediments contaminated by hydrocarbons: experimental analysis and kinetic modeling, *Journal of hazardous materials*, *182*(1-3), 403-407.

Bigeleisen, J., and M. Wolfsberg (1958), Theoretical and experimental aspects of isotope effects in chemical kinetics, *Adv. Chem. Phys*, *1*, 15-76.

Boles, J., J. Clark, I. Leifer, and L. Washburn (2001), Temporal variation in natural methane seep rate due to tides, Coal Oil Point area, California, *Journal of Geophysical Research: Oceans (1978–2012)*, *106*(C11), 27077-27086.

Broecker, W. S., and V. M. Oversby (1971), Chemical equilibria in the earth. E*arth & Planetary Science, 1*, 1-2.

Butler, J. H., D. B. King, J. M. Lobert, S. A. Montzka, S. A. Yvon-Lewis, B. D. Hall, N. J. Warwick, D. J. Mondeel, M. Aydin, and J. W. Elkins (2007), Oceanic distributions and emissions of short-lived halocarbons, *Global Biogeochem Cy*, *21*(1), 1-2.

Camilli, R., C. M. Reddy, D. R. Yoerger, B. A. S. Van Mooy, M. V. Jakuba, J. C. Kinsey, C. P. McIntyre, S. P. Sylva, and J. V. Maloney (2010), Tracking Hydrocarbon Plume Transport and Biodegradation at Deepwater Horizon, *Science*, *330*(6001), 201-204.

Camilli, R., D. Di Iorio, A. Bowen, C. M. Reddy, A. H. Techet, D. R. Yoerger, L. L. Whitcomb, J. S. Seewald, S. P. Sylva, and J. Fenwick (2012), Acoustic measurement of the Deepwater Horizon Macondo well flow rate, *Proceedings of the National Academy of Sciences*, *109*(50), 20235-20239.

Clark, J. F., L. Washburn, J. S. Hornafius, and B. P. Luyendyk (2000), Dissolved hydrocarbon flux from natural marine seeps to the southern California Bight, *Journal of Geophysical Research: Oceans (1978–2012), 105*(C5), 11509-11522.

Clark, J. F., I. Leifer, L. Washburn, and B. P. Luyendyk (2003), Compositional changes in natural gas bubble plumes: observations from the Coal Oil Point marine hydrocarbon seep field, *Geo-Mar Lett*, *23*(3-4), 187-193.

Cranston, R., G. Ginsburg, V. Soloviev, and T. Lorenson (1994), Gas venting and hydrate deposits in the Okhotsk Sea, *Bulletin of the Geological Society of Denmark, 41*(1), 80-85.

Crone, T. J., and M. Tolstoy (2010), Magnitude of the 2010 Gulf of Mexico oil leak, *Science*, *330*(6004), 634-634.

Das, N., and P. Chandran (2010), Microbial degradation of petroleum hydrocarbon contaminants: an overview, *Biotechnology research international*, *2011*.

de Gouw, J. A., et al. (2011), Organic aerosol formation downwind from the Deepwater Horizon oil spill, *Science*, *331*(6022), 1295-1299.

Dickens, G. R. (2000), Methane oxidation during the late Palaeocene thermal maximum, *Bulletin de la Société géologique de France*, *171*(1), 37-49.

Dickens, G. R., J. R. O'Neil, D. K. Rea, and R. M. Owen (1995), Dissociation of oceanic methane hydrate as a cause of the carbon isotope excursion at the end of the Paleocene, *Paleoceanography*, *10*(6), 965-971.

DiMarco, S. F., M. K. Howard, and A. E. Jochens (2001), Deepwater Gulf of Mexico Historical Physical Oceanography Data Report: Quality Assurance and Quality Control Procedures and Data Inventory; Technical Report No. 01-01-D; Department of Oceanography, Texas A&M University: College Station, TX, 2001.

Dimitrov, L. (2002), Contribution to atmospheric methane by natural seepages on the Bulgarian continental shelf, *Continental Shelf Research*, *22*(16), 2429-2442.

Du, M., and J. D. Kessler (2012), Assessment of the spatial and temporal variability of bulk hydrocarbon respiration following the Deepwater Horizon oil spill, *Environ Sci Technol*, *46*(19), 10499-10507.

Elliott, S., M. Maltrud, M. Reagan, G. Moridis, and P. Cameron-Smith (2011), Marine methane cycle simulations for the period of early global warming, *Journal of Geophysical Research: Biogeosciences (2005–2012)*, *116*.

Emery, B. M., L. Washburn, and J. A. Harlan (2004) Evaluating radial current measurements from CODAR high-frequency radars with moored current meters, *Journal of Atmospheric and Oceanic Technology 21(8),* 1259-1271.

Floodgate, G., and A. Judd (1992), The origins of shallow gas, *Continental Shelf Research*, *12*(10), 1145-1156.

Forster, P., V. Ramaswamy, P. Artaxo, T. Berntsen, R. Betts, D. W. Fahey, and R. Van Dorland (2007), Changes in atmospheric constituents and in radiative forcing. Chapter 2. In *Climate change 2007*. The physical Science Basis, 60-62.

Fritsche, W., and M. Hofrichter (2009), Aerobic degradation by microorganisms, *Biotechnology Set, Second Edition*, 144-167.

FRTG (2010), Deepwater Horizon Release, Estimate by PIV, 2010; http://www.doi.gov/deepwaterhorizon/loader.cfm?csModule=security/getfile&PageID=68011 (accessed April 1, 2014).

Grossman, E. L. (1997), Stable carbon isotopes as indicators of microbial activity in aquifers, *Manual of environmental microbiology*, 565-576.

Gülzow, W., G. Rehder, B. Schneider, J. S. v. Deimling, and B. Sadkowiak (2011), A new method for continuous measurement of methane and carbon dioxide in surface waters using off-axis integrated cavity output spectroscopy (ICOS): An example from the Baltic Sea, *Limnol. Oceanogr. Methods, 9*, 176-184.

Harms, S., and C. D. Winant (1998) Characteristic patterns of the circulation in the Santa Barbara Channel, *Journal of Geophysical Reserch*,103(C2), 3041-3065.

Hazen T. C., E. A. Dubinsky, T. Z. DeSantis, G. L. Andersen, Y. M. Piceno, N. Singh, J. K. Jansson, A. Probst, S. E. Borglin, J. L. Fortney, W. T. Stringfellow, M. Bill, M. E. Conrad, L. M. Tom, K. L. Chavarria, T. R. Alusi, R. Lamendella, D. C. Joyner, C. Spier, J. Baelum, M. Auer, M. L. Zemla, R. Chakraborty, E. L. Sonnenthal, P. D'haeseleer, H. N. Holman, S. Osman, Z. Lu, J. D. Van Nostrand, Y Deng, J. Zhou, O. U. Mason (2010), Deep-Sea Oil Plume Enriches Indigenous Oil-Degrading Bacteria, *Science*, *330*(6001), 204-208.

Heeschen, K. U., R. S. Keir, G. Rehder, O. Klatt, and E. Suess (2004), Methane dynamics in the Weddell Sea determined via stable isotope ratios and CFC-11, *Global Biogeochem Cy*, *18*(2), 1-18.

Heintz, M. B., Mau, S., and Valentine, D. L. (2012) Physical control on methanotrophic potential in waters of the Santa Monica Basin, Southern California. *Limnology and oceanography 57(2)*, 420-432.

Hinrichs, K., and A. Boetius (2002), The anaerobic oxidation of methane: new insights in microbial ecology and biogeochemistry, *Ocean margin systems*, 457-477.

Hornafius, J. S., D. Quigley, and B. P. Luyendyk (1999), The world's most spectacular marine hydrocarbon seeps (Coal Oil Point, Santa Barbara Channel, California): Quantification of emissions, *Journal of Geophysical Research: Oceans (1978-2012), 104*(C9), 20703-20711.

Hu, L., S. A. Yvon-Lewis, J. D. Kessler, and I. R. MacDonald (2012), Methane fluxes to the atmosphere from deepwater hydrocarbon seeps in the northern Gulf of Mexico, *Journal of Geophysical Research: Oceans (1978–2012), 117*.

IPCC (2013), (Intergovernmental Panel on Climate Change). Climate Change 2013: The Physical Basis. New York, NY: Cambridge University Press, 2013. *16-17*.

Johnson, J. E. (1999), Evaluation of a seawater equilibrator for shipboard analysis of dissolved oceanic trace gases, *Analytica chimica acta*, *395*(1), 119-132.

Joye, S. B., I. R. MacDonald, I. Leifer, and V. Asper (2011), Magnitude and oxidation potential of hydrocarbon gases released from the BP oil well blowout, *Nat Geosci*, *4*(3), 160-164.

Judd, A., G. Davies, J. Wilson, R. Holmes, G. Baron, and I. Bryden (1997), Contributions to atmospheric methane by natural seepages on the UK continental shelf, *Marine Geology*, *137*(1), 165-189.

Judd, A. G. (2004), Natural seabed gas seeps as sources of atmospheric methane, *Environmental Geology*, *46*(8), 988-996.

Judd, A. G., R. Sim, P. Kingston, and J. McNally (2002), Gas seepage on an intertidal site: Torry Bay, Firth of Forth, Scotland, *Continental Shelf Research*, *22*(16), 2317-2331.

Kadko, D., N. Rosenberg, J. Lupton, R. Collier, and M. Lilley (1990), Chemical reaction rates and entrainment within the Endeavour Ridge hydrothermal plume, *Earth and Planetary Science Letters*, *99*(4), 315-335.

Kessler, J. D., and W. S. Reeburgh (2005), Preparation of natural methane samples for stable isotope and radiocarbon analysis, *Limnology and Oceanography: Methods*, *3*, 408-418.

Kessler, J., W. Reeburgh, and S. Tyler (2006), Controls on methane concentration and stable isotope (δ^2H-CH_4 and δ^{13}C-CH_4) distributions in the water columns of the Black Sea and Cariaco Basin, *Global Biogeochem Cy*, *20*(4), 1-13.

Kessler, J. D., W. S. Reeburgh, D. L. Valentine, F. S. Kinnaman, E. T. Peltzer, P. G. Brewer, J. Southon, and S C. Tyler (2008), A survey of methane isotope abundance (^{14}C, ^{13}C, ^{2}H) from five nearshore marine basins that reveals unusual radiocarbon levels in subsurface waters. *Journal of Geophysical Research: Oceans (1978-2012)*, 113(C12), 1-13.

Kessler, J. D., D. L. Valentine, M. C. Redmond, and M. R. Du (2011a), Response to Comment on "A Persistent Oxygen Anomaly Reveals the Fate of Spilled Methane in the Deep Gulf of Mexico", *Science*, *332*(6033), 1033.

Kessler, J. D., et al. (2011b), A Persistent Oxygen Anomaly Reveals the Fate of Spilled Methane in the Deep Gulf of Mexico, *Science*, *331*(6015), 312-315.

Kinnaman, F. S., D. L. Valentine, and S. C. Tyler (2007), Carbon and hydrogen isotope fractionation associated with the aerobic microbial oxidation of methane, ethane, propane and butane, *Geochim Cosmochim Ac*, *71*(2), 271-283.

Knittel, K., and A. Boetius (2009), Anaerobic oxidation of methane: progress with an unknown process, *Annual review of microbiology*, *63*, 311-334.

Kourtidis, K., I. Kioutsioukis, and S. Rapsomanikis (2006), Effects of methane outgassing on the Black Sea atmosphere, *Atmospheric Chemistry and Physics Discussions*, *6*(3), 3611-3626.

Kraus, S., and J. Estes (1977a), Oil seep survey over Coal Oil Point and Santa Barbara Channel, California, October 1976, *California Offshore Gas, Oil, and Tar Seeps*, 323-346.

Kraus, S., and J. Estes (1977b), Radar detection of surface oil slicks, *Photogramm. Eng. Remote Sens.*, *43*, 1523-1531.

Kujawinski, E. B., M. C. K. Soule, D. L. Valentine, A. K. Boysen, K. Longnecker, and M. C. Redmond (2011), Fate of Dispersants Associated with the Deepwater Horizon Oil Spill, *Environ Sci Technol*, *45*(4), 1298-1306.

Large, W., and S. Pond (1982), Sensible and latent heat flux measurements over the ocean, *Journal of Physical Oceanography*, *12*(5), 464-482.

Lehr, B., S. Bristol, and A. Possolo (2010), Oil Budget Calculator Deepwater Horizon, Technical Documentation, A Report to the National Incident Command, November 2010, *Available at h ttp://www. restorethegulf. gov/sites/default/files/documents/pdf/OilBudgetCalc_Full_HQ-Print_111110. pdf. (Accessed January, 21*, 2012).

Lehr, B. B., Sky; Possolo, Antonio (2010), Deepwater Horizon Technical Documentation: A Report to the National Incident Command; The Federal Interagency Solutions Group, Oil Budget Calculator Science and Engineering Team 2010; http://www.restorethegulf.gov/sites/default/files/documents/pdf/OilBudgetCalc_Full_HQ-Print_111110.pdf (accessed April 1, 2014).

Leifer, I., J. F. Clark, and R. F. Chen (2000), Modifications of the local environment by natural marine hydrocarbon seeps, *Geophys Res Lett*, *27*(22), 3711-3714.

Lide, D. R. (1995), CRC Handbook of Chemistry and Physics, 76th Edition. CRC Press, Inc., Boca Raton, FL, 19-20.

Martens, C. S., and R. A. Berner (1977), Interstitial water chemistry of anoxic Long Island Sound sediments. 1. Dissolved gases, *Limnol. Oceanogr*, *22*(1), 10-25.

Mau, S., M. B. Heintz, and D. L. Valentine (2012), Quantification of CH< sub> 4</sub> loss and transport in dissolved plumes of the Santa Barbara Channel, California, *Continental Shelf Research*, *32*, 110-120.

Mau, S., D. L. Valentine, J. F. Clark, J. Reed, R. Camilli, and L. Washburn (2007), Dissolved methane distributions and air-sea flux in the plume of a massive seep field, Coal Oil Point, California, *Geophys Res Lett*, *34*(22), 1-5.

McGinnis, D., J. Greinert, Y. Artemov, S. Beaubien, and A. Wüest (2006), Fate of rising methane bubbles in stratified waters: How much methane reaches the atmosphere?, *Journal of Geophysical Research: Oceans (1978–2012)*, *111*(C9), 1-15.

McNutt, M. K., R. Camilli, T. J. Crone, G. D. Guthrie, P. A. Hsieh, T. B. Ryerson, O. Savas, and F. Shaffer (2012), Review of flow rate estimates of the Deepwater

Horizon oil spill, *Proceedings of the National Academy of Sciences*, *109*(50), 20260-20267.

NDBC (2010), National Data Buoy Center, National Oceanic and Atmospheric Administration. http:///ndbc.noaa.gov/. (accessed May 1, 2014).

NODC (2011), "Ocean Profile Data: Deepwater Horizon Support." http://www.nodc.noaa.gov/General/DeepwaterHorizon/oceanprofile.html (accessed February 1, 2012).

Nishimoto, M. M., and L. Washburn (2002), Patterns of coastal eddy circulation and abundance of pelagic juvenile fish in the Santa Barbara Channel, California, USA, *Marine Ecology Progress Series*, *241*, 183-199.

Nowlin Jr., W. D. J., A. E.; DiMarco, S. F.; Reid, R. O.; Howard, M. K (2001), Deepwater Physical Oceanography Reanalysis and Synthesis of Historical Data: Synthesis Report; OCS Study MMS 2001-064; U.S. Dept. of the Interior, Mineral Management Service, Gulf of Mexico OCS Region: New Orleans, LA, 2001.

Pack, M. A., M. B. Heintz, W. S. Reeburgh, S. E. Trumbore, D. L. Valentine, X. M. Xu, and E. R. M. Druffel (2011), A method for measuring methane oxidation rates using low-levels of C-14-labeled methane and accelerator mass spectrometry, *Limnol Oceanogr-Meth*, *9*, 245-260.

Parkes, R., B. Cragg, J. Fry, R. Herbert, J. Wimpenny, J. Allen, and M. Whitfield (1990), Bacterial Biomass and Activity in Deep Sediment Layers from the Peru Margin [and Discussion], *Philosophical Transactions of the Royal Society of London. Series A, Mathematical and Physical Sciences*, *331*(1616), 139-153.

Plume Modeling Team (2010) Deepwater Horizon Release Estimate of Rate by PIV. Report to the Flow Rate Technical Group. Available at http://www.doi.gov/deepwaterhorizon/loader.cfmcsModule=security/getfile&PageID=68011. (accessed May 5, 2014).

Pierrot, D., C. Neill, K. Sullivan, R. Castle, R. Wanninkhof, H. Lüger, T. Johannessen, A. Olsen, R. A. Feely, and C. E. Cosca (2009), Recommendations for autonomous underway pCO_2 measuring systems and data-reduction routines, *Deep Sea Research Part II: Topical Studies in Oceanography*, *56*(8), 512-522.

Pohlman, J. W., J. E. Bauer, W. F. Waite, C. L. Osburn, and N. R. Chapman (2010), Methane hydrate-bearing seeps as a source of aged dissolved organic carbon to the oceans, *Nat Geosci*, *4*(1), 37-41.

Quigley, D. C., J. S. Hornafius, B. P. Luyendyk, R. D. Francis, J. Clark, and L. Washburn (1999), Decrease in natural marine hydrocarbon seepage near Coal Oil Point, California, associated with offshore oil production, *Geology*, *27*(11), 1047-1050.

Rabalais, N. N., & Turner, R. E. (2001). Hypoxia in the northern Gulf of Mexico: description, causes and change. *American Geophysical Union*, 1-36.

Ramaswamy, V., O. Boucher, J. Haigh, D. Hauglustine, J. Haywood, G. Myhre, T. Nakajima, G. Shi, and S. Solomon (2001), Radiative forcing of climate, *Climate change*, 349-416.

Rayleigh, L. (1896), L. Theoretical considerations respecting the separation of gases by diffusion and similar processes, *The London, Edinburgh, and Dublin Philosophical Magazine and Journal of Science*, *42*(259), 493-498.

Reddy, C. M., J. S. Arey, J. S. Seewald, S. P. Sylva, K. L. Lemkau, R. K. Nelson, C. A. Carmichael, C. P. McIntyre, J. Fenwick, and G. T. Ventura (2012), Composition and fate of gas and oil released to the water column during the Deepwater Horizon oil spill, *Proceedings of the National Academy of Sciences*, *109*(50), 20229-20234.

Reeburgh, W. S. (1980), Anaerobic methane oxidation: rate depth distributions in Skan Bay sediments, *Earth and Planetary Science Letters*, *47*(3), 345-352.

Reeburgh, W. S. (2007), Oceanic methane biogeochemistry, *Chem Rev*, *107*(2), 486-513.

Rehder, G., R. S. Keir, E. Suess, and M. Rhein (1999), Methane in the northern Atlantic controlled by microbial oxidation and atmospheric history, *Geophys Res Lett*, *26*(5), 587-590.

Ruppel, C. (2011), Methane hydrates and contemporary climate change, *Nature Education Knowledge*, *3*(10), 29.

Ryerson, T., K. Aikin, W. Angevine, E. Atlas, D. Blake, C. Brock, F. Fehsenfeld, R. S. Gao, J. de Gouw, and D. Fahey (2011), Atmospheric emissions from the Deepwater Horizon spill constrain air-water partitioning, hydrocarbon fate, and leak rate, *Geophys Res Lett*, *38*(7), 1-6.

Ryerson, T. B., R. Camilli, J. D. Kessler, E. B. Kujawinski, C. M. Reddy, D. L. Valentine, E. Atlas, D. R. Blake, J. de Gouw, and S. Meinardi (2012), Chemical data quantify Deepwater Horizon hydrocarbon flow rate and environmental distribution, *Proceedings of the National Academy of Sciences*, *109*(50), 20246-20253.

Sassen, R., S. Losh, L. Cathles III, H. Roberts, J. Whelan, A. Milkov, S. Sweet, and D. DeFreitas (2001), Massive vein-filling gas hydrate: relation to ongoing gas

migration from the deep subsurface in the Gulf of Mexico, *Marine and Petroleum Geology*, *18*(5), 551-560.

Scranton, M. I., and P. G. Brewer (1978), Consumption of dissolved methane in the deep ocean, *Limnol. Oceanogr*, *23*(6), 1207-1213.

Socolofsky, S. A., and E. E. Adams (2005), Role of slip velocity in the behavior of stratified multiphase plumes, *Journal of Hydraulic Engineering*, *131*(4), 273-282.

Socolofsky, S. A., E. E. Adams, and C. R. Sherwood (2011), Formation dynamics of subsurface hydrocarbon intrusions following the Deepwater Horizon blowout, *Geophys Res Lett*, *38*(9), 1-6.

Sweeney, C., E. Gloor, A. R. Jacobson, R. M. Key, G. McKinley, J. L. Sarmiento, and R. Wanninkhof (2007), Constraining global air-sea gas exchange for CO2 with recent bomb 14C measurements, *Global Biogeochem Cy*, *21*(2), 1-10.

Takahashi, T., S. C. Sutherland, R. Wanninkhof, C. Sweeney, R. A. Feely, D. W. Chipman, B. Hales, G. Friederich, F. Chavez, and C. Sabine (2009), Climatological mean and decadal change in surface ocean pCO2, and net sea–air CO2 flux over the global oceans, *Deep Sea Research Part II: Topical Studies in Oceanography*, *56*(8), 554-577.

Treude, T., A. Boetius, K. Knittel, K. Wallmann, and B. Barker Joergensen (2003), Anaerobic oxidation of methane above gas hydrates at Hydrate Ridge, NE Pacific Ocean, *Marine Ecology Progress Series*, *264*, 1-14.

Valentine, D. L., D. C. Blanton, W. S. Reeburgh, and M. Kastner (2001), Water column methane oxidation adjacent to an area of active hydrate dissociation, Eel River Basin, *Geochim Cosmochim Ac*, *65*(16), 2633-2640.

Valentine, D. L., I. Mezić, S. Maćešić, N. Črnjarić-Žic, S. Ivić, P. J. Hogan, V. A. Fonoberov, and S. Loire (2012), Dynamic autoinoculation and the microbial ecology of a deep water hydrocarbon irruption, *Proceedings of the National Academy of Sciences*, *109*(50), 20286-20291.

Valentine, D. L., et al. (2010), Propane respiration jump-starts microbial response to a deep oil spill, *Science*, *330*(6001), 208-211.

Wang, X. C., R. F. Chen, J. Whelan, and L. Eglinton (2001), Contribution of "old" carbon from natural marine hydrocarbon seeps to sedimentary and dissolved organic carbon pools in the Gulf of Mexico, *Geophys Res Lett*, *28*(17), 3313-3316.

Wanninkhof, R. (1992), Relationship between wind speed and gas exchange over the ocean, *Journal of Geophysical Research: Oceans (1978–2012)*, *97*(C5), 7373-7382.

Wanninkhof, R., and K. Thoning (1993), Measurement of fugacity of CO2 in surface water using continuous and discrete sampling methods, *Marine Chemistry*, *44*(2), 189-204.

Ward, B. B., K. A. Kilpatrick, P. C. Novelli, and M. I. Scranton (1987), Methane Oxidation and Methane Fluxes in the Ocean Surface-Layer and Deep Anoxic Waters, *Nature*, *327*(6119), 226-229.

Whiticar, M. J. (1999), Carbon and hydrogen isotope systematics of bacterial formation and oxidation of methane, *Chem Geol*, *161*(1), 291-314.

Wuebbles, D. J., and K. Hayhoe (2000), Atmospheric methane: trends and impacts, in *Non-CO2 Greenhouse Gases: Scientific Understanding, Control and Implementation*, edited, Springer, 1-44.

Wuebbles, D. J., and K. Hayhoe (2002), Atmospheric methane and global change, *Earth-Science Reviews*, *57*(3), 177-210.

Yapa, P. D., and F. Chen (2004), Behavior of oil and gas from deepwater blowouts, *Journal of Hydraulic Engineering*, *130*(6), 540-553.

Yerushalmi, L., and S. Guiot (1998), Kinetics of biodegradation of gasoline and its hydrocarbon constituents, *Applied microbiology and biotechnology*, *49*(4), 475-481.

Yvon-Lewis, S. A., L. Hu, and J. Kessler (2011), Methane flux to the atmosphere from the Deepwater Horizon oil disaster, *Geophys Res Lett*, *38*(1), 1-5.

Zachos, J. C., G. R. Dickens, and R. E. Zeebe (2008), An early Cenozoic perspective on greenhouse warming and carbon-cycle dynamics, *Nature*, *451*(7176), 279-283.

APPENDIX

Table A.1 Integrated Dissolved Oxygen Anomalies (*indicates station within the Mississippi Canyon)

Date	R/V	Longitude	Latitude	DO Anomaly [mol m^{-2}]
20100511	Pelican	-88.3648	28.7052	-0.3548
20100511	Pelican	-88.2798	28.7015	0.0000
20100512	Pelican	-88.3885	28.7252	-2.7952
20100512	Pelican	-88.4090	28.7160	-2.6227
20100512	Pelican	-88.3785	28.7158	-1.2728
20100512	Pelican	-88.3910	28.7328	-0.9279
20100512	Pelican	-88.3655	28.7128	-0.3568
20100513	Pelican	-88.4605	28.7317	-2.3080
20100513	Pelican	-88.6275	28.6352	-2.1594
20100513	Pelican	-88.4373	28.6787	-1.9983
20100513	Pelican	-88.5607	28.6990	-1.7100
20100513	Pelican	-88.3900	28.6980	-0.9575
20100513	Pelican	-88.4127	28.7337	-0.9312
20100513	Pelican	-88.5078	28.6233	-0.7068
20100513	Pelican	-88.4157	28.6565	-0.5435
20100513	Pelican	-88.3883	28.7453	-0.5407
20100513	Pelican	-88.3462	28.6588	0.0000
20100513	Pelican	-88.3830	28.6552	0.0000
20100514	Pelican	-88.7143	28.6023	-1.2983
20100514	Pelican	-88.6318	28.6733	-0.6052
20100514	Pelican	-88.7953	28.5673	-0.3201
20100514	Pelican	-88.6867	28.5572	-0.0188
20100514	Pelican	-88.3673	28.7040	0.0000
20100519	Brooks McCall	-88.4847	28.7093	-0.3017
20100519	Brooks McCall	-88.4267	28.6441	0.0000
20100521	Brooks McCall	-88.3668	28.7520	-0.3330
20100521	Brooks McCall	-88.3870	28.7383	-0.0429
20100524	Jack Fitz	-88.4045	28.7538	-0.1498
20100526	Walton Smith	-88.4093	28.7307	-0.0246

Table A.1. Continued

Date	R/V	Longitude	Latitude	DO Anomaly [mol m^{-2}]
20100526	Walton Smith	-88.4083	28.7158	0.0000
20100526	Walton Smith	-88.4067	28.7143	0.0000
20100526	Walton Smith	-88.4070	28.7137	0.0000
20100527	Jack Fitz	-88.3837	28.7493	-0.3845
20100527	Walton Smith	-88.4840	28.7235	-2.2993
20100527	Walton Smith	-88.4823	28.7230	-2.0291
20100527	Walton Smith	-88.5165	28.7072	-0.9597
20100527	Walton Smith	-88.4328	28.7245	-0.4339
20100527	Walton Smith	-88.4422	28.7232	-0.3760
20100527	Walton Smith	-88.4492	28.7208	-0.3161
20100527	Walton Smith	-88.4577	28.7187	-0.2423
20100527	Walton Smith	-88.4653	28.7182	-0.1919
20100527	Walton Smith	-88.4085	28.7410	-0.0848
20100527	Walton Smith	-88.4263	28.7257	-0.0637
20100527	Walton Smith	-88.4203	28.7297	-0.0596
20100527	Walton Smith	-88.4083	28.7240	0.0000
20100528	Jack Fitz	-88.3923	28.7543	-0.0507
20100528	Walton Smith	-88.5397	28.7018	-2.5913
20100528	Walton Smith	-88.5600	28.6972	-2.4962
20100528	Walton Smith	-88.5777	28.6922	-1.7927
20100528	Walton Smith	-88.5650	28.7123	-1.6315
20100528	Walton Smith	-88.4890	28.7268	-1.2165
20100528	Walton Smith	-88.6872	28.6842	-0.2053
20100528	Walton Smith	-88.6878	28.6685	-0.1780
20100528	Walton Smith	-88.5950	28.6898	-0.1604
20100528	Walton Smith	-88.6142	28.6858	-0.0213
20100528	Walton Smith	-88.6318	28.6805	0.0000
20100528	Walton Smith	-88.6510	28.6757	0.0000
20100528	Walton Smith	-88.6688	28.6720	0.0000
20100529	Gordon Gunter	-87.9486	29.0050	0.0000
20100529	Gordon Gunter	-88.0173	28.8960	0.0000
20100529	Jack Fitz	-88.3875	28.7083	0.0000
20100530	Brooks McCall	-88.3768	28.7324	-0.8300
20100530	Brooks McCall	-88.3879	28.7580	-0.1997
20100530	Gordon Gunter	-87.9817	28.9063	0.0000
20100530	Gordon Gunter	-88.2292	28.8029	0.0000

Table A.1. Continued

Date	R/V	Longitude	Latitude	DO Anomaly [mol m^{-2}]
20100530	Jack Fitz	-88.3772	28.7240	-0.1697
20100530	Walton Smith	-88.4088	28.7102	-0.5952
20100530	Walton Smith	-88.4742	28.7032	-0.4216
20100530	Walton Smith	-88.3875	28.7122	-0.3516
20100530	Walton Smith	-88.3972	28.7123	-0.2135
20100530	Walton Smith	-88.3470	28.7668	-0.0945
20100530	Walton Smith	-88.4373	28.7093	-0.0782
20100530	Walton Smith	-88.3860	28.7627	-0.0078
20100530	Walton Smith	-88.3267	28.7395	0.0000
20100530	Walton Smith	-88.3482	28.7095	0.0000
20100530	Walton Smith	-88.4052	28.6908	0.0000
20100531	Brooks McCall	-88.4016	28.7051	-1.8235
20100531	Brooks McCall	-88.4359	28.6727	-0.5649
20100531	Brooks McCall	-88.4149	28.7236	-0.2758
20100531	Brooks McCall	-88.4713	28.6389	0.0000
20100531	Gordon Gunter	-88.2645	28.8500	-0.3507
20100531	Gordon Gunter	-88.3460	28.6539	0.0000
20100531	Jack Fitz	-88.3572	28.7603	-0.2413
20100531	Walton Smith	-88.4012	28.7323	-2.5694
20100531	Walton Smith	-88.4325	28.6938	-2.2666
20100531	Walton Smith	-88.4335	28.6948	-2.0010
20100531	Walton Smith	-88.6172	28.6500	-1.9828
20100531	Walton Smith	-88.3973	28.7208	-1.7082
20100531	Walton Smith	-88.5713	28.6813	-1.2072
20100531	Walton Smith	-88.5345	28.6878	-0.9882
20100531	Walton Smith	-88.3878	28.7225	0.0000
20100531	Walton Smith	-88.4653	28.6837	0.0000
20100531	Walton Smith	-88.5453	28.6295	0.0000
20100601	Brooks McCall	-88.4487	28.7000	-0.2554
20100601	Brooks McCall	-88.4211	28.6640	-0.0457
20100601	Brooks McCall	-88.3719	28.7262	0.0000
20100601	Brooks McCall	-88.3850	28.6965	0.0000
20100601	Gordon Gunter	-88.4537	28.6814	-0.7348
20100601	Gordon Gunter	-88.4522	28.7947	-0.4947
20100601	Gordon Gunter	-88.2608	28.8455	-0.2297
20100601	Gordon Gunter	-88.4818	28.7046	-0.1920

Table A.1. Continued

Date	R/V	Longitude	Latitude	DO Anomaly [mol m^{-2}]
20100601	Gordon Gunter	-88.4328	28.8172	-0.1392
20100601	Gordon Gunter	-88.4847	28.7398	-0.1337
20100601	Gordon Gunter	-88.4818	28.7712	-0.0542
20100601	Gordon Gunter	-88.4249	28.6554	0.0000
20100601	Walton Smith	-88.3828	28.7372	-1.9315
20100601	Walton Smith	-88.3798	28.7372	-1.0563
20100601	Walton Smith	-88.3948	28.7362	-0.5695
20100601	Walton Smith	-88.3843	28.7333	-0.4440
20100601	Walton Smith	-88.3935	28.7285	-0.3395
20100601	Walton Smith	-88.4062	28.7192	-0.3283
20100601	Walton Smith	-88.3810	28.7215	0.0000
20100601	Walton Smith	-88.3647	28.7212	0.0000
20100601	Walton Smith	-88.3783	28.7163	0.0000
20100601	Walton Smith	-88.3937	28.7153	0.0000
20100602	Gordon Gunter	-88.4765	28.6627	-2.6781
20100602	Gordon Gunter	-88.4670	28.6672	-2.6287
20100602	Gordon Gunter	-88.3208	28.6780	0.0000
20100602	Gordon Gunter	-88.3532	28.6538	0.0000
20100602	Gordon Gunter	-88.3857	28.6522	0.0000
20100602	Gordon Gunter	-88.5328	28.6475	0.0000
20100602	Gordon Gunter	-88.4914	28.5533	0.0000
20100603	Gordon Gunter	-88.4531	28.7064	-0.9565
20100603	Gordon Gunter	-88.3380	28.7008	-0.4072
20100603	Gordon Gunter	-88.2732	28.7028	0.0000
20100603	Gordon Gunter	-88.4351	28.6937	0.0000
20100604	Gordon Gunter	-88.4251	28.6784	0.0000
20100604	Thomas Jefferson	-88.4452	28.6915	0.0000
20100604	Thomas Jefferson	-88.4772	28.6460	0.0000
20100604	Walton Smith	-88.4235	28.7263	-1.9247
20100604	Walton Smith	-88.3847	28.7408	-0.9462
20100604	Walton Smith	-88.5557	28.6980	-0.7224
20100604	Walton Smith	-88.4357	28.7260	-0.4214
20100604	Walton Smith	-88.3857	28.7375	-0.2234
20100604	Walton Smith	-88.3972	28.7483	-0.2157
20100604	Walton Smith	-88.4620	28.7433	-0.2016
20100604	Walton Smith	-88.5292	28.6727	-0.1865

Table A.1. Continued

Date	R/V	Longitude	Latitude	DO Anomaly [mol m^{-2}]
20100604	Walton Smith	-88.4335	28.7427	-0.1552
20100604	Walton Smith	-88.5335	28.7338	-0.1348
20100604	Walton Smith	-88.6018	28.7180	0.0000
20100605	Brooks McCall	-88.3667	28.6934	-0.2905
20100605	Brooks McCall	-88.3768	28.7320	-0.2207
20100605	Brooks McCall	-88.3664	28.7295	0.0000
20100605	Thomas Jefferson	-88.5377	28.7085	-0.3571
20100605	Thomas Jefferson	-88.5332	28.7075	-0.2012
20100605	Walton Smith	-88.3837	28.7332	-0.3079
20100605	Walton Smith	-88.3825	28.7262	-0.2736
20100605	Walton Smith	-88.3570	28.7223	-0.2320
20100605	Walton Smith	-88.3852	28.7283	-0.1684
20100605	Walton Smith	-88.3957	28.7202	-0.1522
20100605	Walton Smith	-88.3785	28.7400	-0.1058
20100605	Walton Smith	-88.3485	28.7322	-0.0901
20100605	Walton Smith	-88.3773	28.7270	-0.0526
20100605	Walton Smith	-88.3462	28.7442	-0.0488
20100605	Walton Smith	-88.3792	28.7498	-0.0419
20100605	Walton Smith	-88.3690	28.7553	0.0000
20100605	Walton Smith	-88.3550	28.7528	0.0000
20100606	Brooks McCall	-88.3468	28.6971	-0.5252
20100606	Brooks McCall	-88.3666	28.6482	-0.4120
20100606	Brooks McCall	-88.3305	28.7068	0.0000
20100606	Thomas Jefferson	-88.4503	28.7202	-0.0528
20100606	Walton Smith	-88.5210	28.7745	-0.1365
20100606	Walton Smith	-88.4890	28.8510	0.0000
20100607	Brooks McCall	-88.3735	28.7230	-0.4668
20100607	Brooks McCall	-88.3774	28.7482	-0.2538
20100607	Brooks McCall	-88.4183	28.6881	-0.0352
20100611	Brooks McCall	-88.4149	28.7236	-0.4284
20100611	Brooks McCall	-88.4172	28.7324	-0.2353
20100611	Brooks McCall	-88.4176	28.7414	-0.1705
20100611	Brooks McCall	-88.4159	28.7503	-0.1558
20100612	Brooks McCall	-88.4123	28.7588	-0.5740
20100612	Brooks McCall	-88.3919	28.7355	-0.3706
20100612	Brooks McCall	-88.3893	28.7487	-0.2983

Table A.1. Continued

Date	R/V	Longitude	Latitude	DO Anomaly [mol m^{-2}]
20100612	Brooks McCall	-88.3766	28.7400	-0.2042
20100613	Brooks McCall	-88.3819	28.7816	-0.8007
20100613	Brooks McCall	-88.4068	28.7664	-0.7120
20100613	Brooks McCall	-88.3997	28.7729	-0.6821
20100613	Brooks McCall	-88.3913	28.7781	-0.5786
20100613	Brooks McCall	-88.4272	28.7476	-0.2756
20100613	Cape Hatteras	-88.4602	28.6787	-1.4032
20100613	Cape Hatteras	-88.4702	28.6863	-1.1734
20100613	Cape Hatteras	-88.4793	28.6930	-0.1634
20100614	Cape Hatteras	-88.4438	28.6627	-1.4873
20100614	Cape Hatteras	-88.4577	28.6742	-1.3904
20100614	Cape Hatteras	-88.4222	28.7035	-0.4120
20100614	Cape Hatteras	-88.4337	28.6537	-0.4051
20100614	Cape Hatteras	-88.3800	28.7382	-0.2117
20100614	Cape Hatteras	-88.3795	28.7302	-0.1187
20100614	Jack Fitz	-88.3668	28.7485	-0.7910
20100615	Cape Hatteras	-88.4485	28.8053	-1.3890
20100615	Cape Hatteras	-88.3643	28.7692	-0.8048
20100615	Cape Hatteras	-88.3655	28.7890	-0.6016
20100615	Cape Hatteras	-88.3148	28.8435	-0.5762
20100615	Cape Hatteras	-88.3655	28.7508	-0.2662
20100615	Cape Hatteras	-88.3657	28.7268	-0.1633
20100616	Cape Hatteras	-88.3112	28.6737	-1.1644
20100616	Cape Hatteras	-88.2947	28.6878	-1.1134
20100616	Cape Hatteras	-88.2727	28.7218	-1.1090
20100616	Cape Hatteras	-88.3233	28.6562	-0.5030
20100616	Cape Hatteras	-88.2795	28.7032	-0.3543
20100616	Jack Fitz	-88.3652	28.7572	-0.1348
20100617	Brooks McCall	-88.3461	28.7385	-0.6323
20100617	Brooks McCall	-88.3869	28.7387	-0.2327
20100617	Brooks McCall	-88.3664	28.7295	-0.1632
20100617	Cape Hatteras	-88.2745	28.7790	-2.7719
20100617	Cape Hatteras	-88.2712	28.7558	-1.4853
20100617	Cape Hatteras	-88.2737	28.7450	-0.9011
20100617	Cape Hatteras	-88.2882	28.7913	-0.7740
20100617	Jack Fitz	-88.3648	28.7618	-0.1138

Table A.1. Continued

Date	R/V	Longitude	Latitude	DO Anomaly [mol m^{-2}]
20100618	Brooks McCall	-88.3666	28.8015	-0.3431
20100619	Brooks McCall	-88.2938	28.8025	-1.7804
20100619	Brooks McCall	-88.3913	28.7781	-1.2287
20100619	Brooks McCall	-88.3816	28.7626	-0.6446
20100619	Brooks McCall	-88.4385	28.8029	-0.3132
20100619	Jack Fitz	-88.3810	28.7522	-0.6056
20100619	Jack Fitz	-88.4093	28.8132	-0.2943
20100620	Jack Fitz	-88.3728	28.7725	-1.0931
20100620	Jack Fitz	-88.3822	28.7878	-0.3448
20100621	Endevour	-88.3630	28.7110	-2.7201
20100621	Endevour	-88.3810	28.7500	-0.6692
20100623	Brooks McCall	-88.3714	28.7150	0.0000
20100623	Brooks McCall	-88.3850	28.6965	0.0000
20100623	Brooks McCall	-88.3667	28.6934	0.0000
20100623	Thomas Jefferson	-88.3632	28.7713	-0.1704
20100624	Brooks McCall	-88.4384	28.7439	-0.4866
20100624	Brooks McCall	-88.3878	28.7401	0.0000
20100624	Brooks McCall	-88.4178	28.7382	0.0000
20100624	Brooks McCall	-88.4166	28.7293	0.0000
20100624	Thomas Jefferson	-88.3333	28.8175	-0.1050
20100625	Brooks McCall	-88.3902	28.7296	-0.9889
20100625	Brooks McCall	-88.3863	28.7214	-0.3855
20100625	Brooks McCall	-88.3768	28.7320	-0.0957
20100625	Brooks McCall	-88.4074	28.7115	-0.0224
20100625	Brooks McCall	-88.5616	28.7561	0.0000
20100625	Thomas Jefferson	-88.4200	28.7250	-0.4278
20100625	Thomas Jefferson	-88.3340	28.8328	0.0000
20100626	Endevour	-88.5430	28.6570	-0.8446
20100626	Ocean Varitas	-88.4033	28.7078	-0.6613
20100626	Ocean Varitas	-88.4033	28.6957	-0.1077
20100626	Ocean Varitas	-88.3865	28.7383	0.0000
20100626	Ocean Varitas	-88.3809	28.7260	0.0000
20100626	Ocean Varitas	-88.3806	28.7206	0.0000
20100626	Thomas Jefferson	-88.4272	28.7070	-0.2623
20100627	Ocean Varitas	-88.4138	28.7060	-0.5747
20100627	Ocean Varitas	-88.3958	28.7017	-0.1094

Table A.1. Continued

Date	R/V	Longitude	Latitude	DO Anomaly [mol m^{-2}]
20100627	Ocean Varitas	-88.4108	28.7162	-0.1029
20100627	Ocean Varitas	-88.4169	28.7303	0.0000
20100627	Ocean Varitas	-88.4169	28.7303	0.0000
20100628	Endevour	-88.6750	28.5780	-2.3473
20100628	Endevour	-88.3500	28.7310	-2.2488
20100628	Endevour	-88.3450	28.7500	-1.9688
20100628	Endevour	-88.5570	28.6320	-1.7397
20100628	Endevour	-88.4040	28.7300	-1.5520
20100628	Endevour	-88.4410	28.7350	-1.5352
20100628	Endevour	-88.5430	28.6560	-0.8227
20100628	Endevour	-88.5790	28.6630	-0.5584
20100628	Endevour	-88.5290	28.6990	-0.3465
20100628	Endevour	-88.6340	28.6630	-0.1196
20100628	Endevour	-88.3530	28.7490	-0.1051
20100628	Endevour	-88.3900	28.7350	-0.0465
20100628	Endevour	-88.3900	28.7360	0.0000
20100628	Endevour	-88.5360	28.5990	0.0000
20100628	Endevour	-88.3890	28.3760	0.0000
20100628	Ocean Varitas	-88.3809	28.7263	-0.3914
20100628	Ocean Varitas	-88.3671	28.7202	-0.0746
20100628	Ocean Varitas	-88.3768	28.7320	0.0000
20100702	Ocean Varitas	-88.3966	28.7383	-0.7853
20100702	Ocean Varitas	-88.3865	28.7383	-0.6635
20100702	Ocean Varitas	-88.3800	28.7511	-0.5638
20100702	Ocean Varitas	-88.4169	28.7393	-0.3724
20100702	Ocean Varitas	-88.3678	28.7320	-0.0558
20100702	Ocean Varitas	-88.4375	28.7398	0.0000
20100703	Ocean Varitas	-88.4164	28.7575	-1.0747
20100703	Ocean Varitas	-88.4166	28.7484	-0.9056
20100703	Ocean Varitas	-88.4078	28.7778	-0.2625
20100705	Brooks McCall	-88.3478	28.7458	0.0000
20100705	Brooks McCall	-88.3463	28.7414	0.0000
20100706	Brooks McCall	-88.3576	28.7223	-1.3901
20100706	Brooks McCall	-88.3462	28.7368	-0.0545
20100711	Brooks McCall	-88.3829	28.7156	-0.5008
20100711	Brooks McCall	-88.3974	28.7379	-0.3884

Table A.1. Continued

Date	R/V	Longitude	Latitude	DO Anomaly [mol m^{-2}]
20100711	Brooks McCall	-88.3876	28.7198	0.0000
20100711	Brooks McCall	-88.3651	28.7115	0.0000
20100711	Brooks McCall	-88.3887	28.7080	0.0000
20100712	Brooks McCall	-88.3758	28.7128	0.0000
20100712	Brooks McCall	-88.3774	28.7084	0.0000
20100712	Brooks McCall	-88.3788	28.7042	0.0000
20100713	Brooks McCall	-88.3718	28.7120	0.0000
20100713	Brooks McCall	-88.3826	28.7051	0.0000
20100713	Brooks McCall	-88.4417	28.7000	0.0000
20100713	Brooks McCall	-88.3820	28.6955	0.0000
20100717	Brooks McCall	-88.4670	28.6364	-1.9780
20100717	Brooks McCall	-88.4861	28.6681	-1.3237
20100717	Brooks McCall	-88.4738	28.6548	-1.0563
20100717	Nancy Foster	-88.3992	28.7568	-1.1051
20100717	Nancy Foster	-88.1738	28.0052	-0.8610
20100717	Nancy Foster	-88.4367	28.6178	-0.8517
20100717	Nancy Foster	-88.2465	28.6300	-0.8204
20100718	Brooks McCall	-88.4172	28.6205	0.0000
20100719	Brooks McCall	-88.2929	28.6298	-1.5673
20100719	Brooks McCall	-88.2088	28.6730	-0.2195
20100719	Brooks McCall	-88.2249	28.7289	-0.1017
20100719	Brooks McCall	-88.2276	28.7062	0.0000
20100725	Ferrel	-88.3228	28.5702	0.0000
20100726	Ferrel	-88.1106	28.6592	-1.0438
20100727	Ocean Varitas	-88.5802	28.4261	-1.8006
20100727	Ocean Varitas	-88.6310	28.3521	-0.8658
20100727	Ocean Varitas	-88.8357	28.4469	0.0000
20100728	Ocean Varitas	-88.5121	28.4661	-2.9862
20100728	Ocean Varitas	-88.5060	28.4097	-2.5436
20100728	Ocean Varitas	-88.6800	28.5065	-2.4776
20100728	Ocean Varitas	-88.7411	28.5956	-1.4748
20100728	Ocean Varitas	-88.6006	28.5630	-0.7209
20100728	Ocean Varitas	-88.7986	28.4193	-0.4175
20100729	Brooks McCall	-88.3665	28.7566	0.0000
20100729	Brooks McCall	-88.3461	28.7385	0.0000
20100729	Brooks McCall	-88.3870	28.7383	0.0000

Table A.1. Continued

Date	R/V	Longitude	Latitude	DO Anomaly [mol m^{-2}]
20100729	Brooks McCall	-88.3665	28.7206	0.0000
20100730	Brooks McCall	-88.2360	28.7705	0.0000
20100730	Brooks McCall	-88.3303	28.7066	0.0000
20100730	Brooks McCall	-88.4027	28.7066	0.0000
20100731	Brooks McCall	-88.7589	28.4469	-1.2224
20100731	Brooks McCall	-88.7778	28.3457	-0.9543
20100731	Brooks McCall	-89.1290	28.2357	0.0000
20100731	Brooks McCall	-88.9988	28.1311	0.0000
20100801	Ocean Veritas *	-89.4070	28.1411	0.0000
20100802	Ferrel	-88.7787	28.3452	-1.5764
20100802	Ferrel	-88.7594	28.4472	-0.9163
20100802	Ocean Varitas	-88.8550	28.1450	-2.1741
20100802	Ocean Varitas	-88.8118	28.2906	-1.4878
20100802	Ocean Varitas	-88.7714	28.2896	-0.7462
20100802	Ocean Varitas	-88.8175	28.1357	-0.6030
20100802	Ocean Varitas	-88.8714	28.2911	-0.5318
20100802	Ocean Varitas	-89.0057	28.2873	0.0000
20100803	Henry Bigelow	-88.3223	28.7223	-0.4307
20100803	Henry Bigelow	-88.3362	28.7020	0.0000
20100803	Henry Bigelow	-88.3362	28.7020	0.0000
20100804	Brooks McCall	-88.8252	28.1825	-1.4180
20100804	Brooks McCall	-88.8252	28.1825	-1.1716
20100804	Brooks McCall	-88.7949	28.2188	-0.9719
20100804	Brooks McCall	-88.8252	28.1825	-0.7085
20100804	Ferrel	-88.8440	27.6789	0.0000
20100804	Henry Bigelow	-88.2247	28.6970	0.0000
20100805	Brooks McCall	-88.7892	28.1503	-1.5559
20100805	Brooks McCall	-88.7537	28.1922	-1.2182
20100805	Brooks McCall	-88.7168	28.2244	-0.9029
20100805	Brooks McCall	-88.7594	28.2544	-0.2354
20100805	Gordon Gunter	-88.3935	28.6475	-0.0742
20100805	Gordon Gunter	-88.5848	28.5353	-0.0086
20100805	Gordon Gunter	-88.3527	28.6428	0.0000
20100805	Henry Bigelow	-88.2645	28.8510	0.0000
20100805	Henry Bigelow	-88.2998	28.8178	0.0000
20100806	Brooks McCall	-88.8996	28.2338	-0.3524

Table A.1. Continued

Date	R/V	Longitude	Latitude	DO Anomaly [mol m^{-2}]
20100806	Brooks McCall	-88.9709	28.3128	0.0000
20100806	Ferrel	-88.4171	28.7417	0.0000
20100806	Gordon Gunter	-88.7475	28.1522	-2.1612
20100806	Gordon Gunter	-88.7955	28.3458	-0.9591
20100806	Gordon Gunter	-88.5555	28.0838	-0.2852
20100806	Gordon Gunter	-88.9088	28.2532	-0.2453
20100806	Gordon Gunter	-88.6905	28.4582	-0.0457
20100806	Henry Bigelow	-88.3235	28.7233	-0.0589
20100806	Pisces	-88.3662	28.4682	-0.4410
20100806	Pisces	-88.2872	28.4765	-0.3167
20100806	Pisces	-88.1533	28.5440	0.0000
20100806	Pisces	-88.2150	28.5025	0.0000
20100807	Ocean Veritas *	-89.3973	28.2262	-0.0779
20100807	Gordon Gunter	-88.2647	28.8675	0.0000
20100807	Gordon Gunter	-88.2755	28.8527	0.0000
20100807	Henry Bigelow	-88.3958	28.7055	-0.6050
20100807	Henry Bigelow	-88.3950	28.7040	-0.2448
20100807	Henry Bigelow	-88.4123	28.7362	-0.2103
20100807	Henry Bigelow	-88.3998	28.7667	-0.0775
20100807	Henry Bigelow	-88.3412	28.7713	-0.0554
20100807	Henry Bigelow	-88.3360	28.7083	-0.0392
20100807	Henry Bigelow	-88.3708	28.7802	0.0000
20100807	Ocean Varitas	-88.9015	28.2580	-0.1360
20100807	Pisces	-88.0958	28.8653	-0.1390
20100807	Pisces	-88.1423	28.9220	0.0000
20100807	Pisces	-88.0688	28.8010	0.0000
20100807	Pisces	-88.0600	28.7323	0.0000
20100807	Pisces	-88.0715	28.6638	0.0000
20100807	Pisces	-88.1030	28.5997	0.0000
20100808	Ferrel	-88.4175	28.7326	0.0000
20100808	Ferrel	-88.4150	28.7236	0.0000
20100808	Henry Bigelow	-88.3558	28.6963	-0.0864
20100808	Henry Bigelow	-88.2952	28.6742	-0.0649
20100808	Henry Bigelow	-88.3655	28.7782	0.0000
20100808	Henry Bigelow	-88.3308	28.7580	0.0000

Table A.1. Continued

Date	R/V	Longitude	Latitude	DO Anomaly [mol m^{-2}]
20100808	Henry Bigelow	-88.2660	28.7373	0.0000
20100808	Henry Bigelow	-88.3935	28.7038	0.0000
20100808	Henry Bigelow	-88.3587	28.7015	0.0000
20100808	Ocean Varitas	-88.8621	27.9822	-1.6286
20100808	Ocean Varitas	-89.0296	28.1160	-1.1544
20100808	Pisces	-88.3657	28.3320	-0.6021
20100808	Pisces	-87.9662	28.9393	-0.1704
20100808	Pisces	-88.0397	29.0242	0.0000
20100808	Pisces	-87.9208	28.8425	0.0000
20100808	Pisces	-87.9055	28.7363	0.0000
20100808	Pisces	-87.9213	28.6320	0.0000
20100808	Pisces	-87.9685	28.5335	0.0000
20100808	Pisces	-88.0410	28.4508	0.0000
20100808	Pisces	-88.1357	28.3868	0.0000
20100808	Pisces	-88.2455	28.3460	0.0000
20100809	Ferrel	-88.9692	28.0907	-0.2915
20100809	Henry Bigelow	-88.4660	28.7455	-0.2276
20100809	Henry Bigelow	-88.2247	28.6960	-0.1131
20100809	Henry Bigelow	-88.4382	28.6768	-0.0379
20100809	Henry Bigelow	-88.2930	28.6708	-0.0258
20100809	Henry Bigelow	-88.3722	28.6503	-0.0134
20100809	Henry Bigelow	-88.2653	28.7337	0.0000
20100809	Ocean Varitas	-88.7585	28.0540	-2.1509
20100809	Ocean Varitas	-88.8421	28.1660	-0.7274
20100809	Ocean Varitas	-88.9271	28.2790	-0.5419
20100809	Ocean Varitas	-88.6739	27.9410	0.0000
20100809	Pisces	-88.6933	28.2818	-0.3298
20100809	Pisces	-88.4848	28.3455	-0.2233
20100809	Pisces	-87.8502	28.4473	0.0000
20100809	Pisces	-88.0842	28.2587	0.0000
20100809	Pisces	-88.2323	28.2110	0.0000
20100810	Brooks McCall	-88.8447	28.1925	-0.7176
20100810	Brooks McCall	-88.5905	27.8282	0.0000
20100810	Brooks McCall	-88.7172	27.7537	0.0000
20100810	Ferrel	-88.8854	27.9794	-1.9857

Table A.1. Continued

Date	R/V	Longitude	Latitude	DO Anomaly [mol m^{-2}]
20100810	Ferrel	-88.8565	28.1445	-1.1995
20100810	Ferrel	-88.8013	27.8660	0.0000
20100810	Henry Bigelow	-88.2252	28.6965	-0.2232
20100810	Pisces	-88.0142	28.1387	0.0000
20100811	Brooks McCall	-89.0119	27.9041	-1.1097
20100811	Brooks McCall	-89.1809	28.1294	0.0000
20100811	Brooks McCall	-89.0952	28.0153	0.0000
20100813	Ocean Veritas *	-89.4343	27.9789	0.0000
20100813	Ocean Varitas	-88.9238	27.7900	0.0000
20100813	Pisces	-88.4565	28.4802	-0.5132
20100814	Ocean Veritas *	-89.2641	27.7537	0.0000
20100814	Ferrel	-88.8859	27.4908	0.0000
20100814	Henry Bigelow	-88.4633	28.7462	-0.6994
20100814	Henry Bigelow	-88.2932	28.6685	-0.1131
20100814	Henry Bigelow	-88.3658	28.6465	-0.0796
20100814	HOS Davis	-88.9663	28.0864	-0.4498
20100814	HOS Davis	-89.0538	28.2043	-0.1149
20100814	Ocean Varitas	-89.1790	27.6406	-0.1071
20100814	Ocean Varitas	-89.0974	27.5300	0.0000
20100815	Ferrel	-89.1381	27.8286	-0.3506
20100815	Ferrel	-89.0533	27.7154	0.0000
20100815	Ferrel	-88.9698	27.6043	0.0000
20100815	Henry Bigelow	-88.4390	28.6747	-0.0999
20100815	Henry Bigelow	-88.2690	28.7392	-0.0733
20100815	Henry Bigelow	-88.3232	28.7405	-0.0729
20100815	Henry Bigelow	-88.3280	28.7100	-0.0142
20100815	Henry Bigelow	-87.6848	29.0473	0.0000
20100815	Henry Bigelow	-87.8295	28.9888	0.0000
20100815	Henry Bigelow	-88.4118	28.7392	0.0000
20100815	Henry Bigelow	-88.3998	28.7015	0.0000
20100815	HOS Davis	-88.9447	28.1835	0.0000
20100815	HOS Davis	-88.9054	28.1284	0.0000
20100815	Ocean Varitas	-89.6001	27.7130	-0.1983
20100815	Ocean Varitas	-89.5167	27.6027	-0.0733
20100815	Ocean Varitas	-89.6879	27.8278	0.0000
20100815	Ocean Varitas	-89.3905	27.6783	0.0000

Table A.1. Continued

Date	R/V	Longitude	Latitude	DO Anomaly [mol m^{-2}]
20100815	Ocean Varitas	-89.3055	27.5650	0.0000
20100816	Ferrel *	-89.3076	28.0545	-0.6306
20100816	Brooks McCall *	-89.3475	27.8642	-0.2246
20100816	Brooks McCall *	-89.3973	28.0908	0.0000
20100816	Brooks McCall	-89.0538	28.2843	0.0000
20100816	Brooks McCall	-88.9687	28.0908	0.0000
20100816	Henry Bigelow	-88.5890	28.5558	-0.4007
20100816	Henry Bigelow	-87.4725	28.9157	0.0000
20100816	Henry Bigelow	-87.6218	28.8873	0.0000
20100816	Henry Bigelow	-87.6038	28.7123	0.0000
20100816	Henry Bigelow	-87.4528	28.7002	0.0000
20100816	HOS Davis	-89.0117	27.9016	-1.0629
20100816	HOS Davis	-88.8853	27.9792	-0.1437
20100817	Henry Bigelow	-88.7025	28.4627	-0.0922
20100817	Henry Bigelow	-88.3685	28.6078	-0.0281
20100817	Henry Bigelow	-88.3653	28.5400	0.0000
20100817	HOS Davis	-88.8009	27.8660	-1.2650
20100818	Brooks McCall *	-89.1753	27.7536	0.0000
20100818	Brooks McCall	-89.4312	27.4895	-0.3941
20100818	Brooks McCall	-89.8136	27.7535	0.0000
20100818	Brooks McCall	-89.7248	27.6363	0.0000
20100818	Brooks McCall	-89.6421	27.5271	0.0000
20100818	Bunny Bordelon	-90.3849	27.5913	0.0000
20100818	Henry Bigelow	-88.5887	28.0950	-0.9623
20100818	Henry Bigelow	-88.3678	28.7110	-0.4789
20100818	Henry Bigelow	-88.3662	28.6698	-0.1799
20100818	Henry Bigelow	-88.3670	28.6905	-0.1461
20100818	Henry Bigelow	-88.3842	28.7972	0.0000
20100818	HOS Davis	-88.9272	27.7910	-1.3212
20100818	Jack Fitz	-90.6813	27.5327	0.0000
20100819	HOS Davis *	-89.3075	28.0660	0.0000
20100819	Bunny Bordelon	-90.2968	27.2356	-2.4688
20100819	Henry Bigelow	-88.9308	27.7932	-1.4778
20100819	Henry Bigelow	-89.4237	27.4930	-0.1489
20100819	Henry Bigelow	-89.3097	27.5637	-0.1195
20100819	Henry Bigelow	-88.4062	27.9290	0.0000

Table A.1. Continued

Date	R/V	Longitude	Latitude	DO Anomaly [mol m^{-2}]
20100819	Henry Bigelow	-88.7997	27.8647	0.0000
20100819	Jack Fitz	-90.6577	27.4378	-1.6241
20100819	Ocean Varitas	-89.3864	27.1897	-0.4541
20100819	Ocean Varitas	-89.5566	27.4138	-0.3862
20100819	Ocean Varitas	-89.4737	27.3038	-0.1665
20100819	Ocean Varitas	-89.3024	27.0751	0.0000
20100819	Pisces	-87.3764	29.0863	-0.7047
20100819	Pisces	-88.0350	29.0189	-0.2821
20100819	Pisces	-87.3300	28.9862	-0.1013
20100819	Pisces	-87.9173	29.1080	-0.1000
20100819	Pisces	-87.4288	29.2093	0.0000
20100819	Pisces	-87.6024	29.1649	0.0000
20100819	Pisces	-87.7534	29.1384	0.0000
20100819	Pisces	-87.5497	29.1129	0.0000
20100819	Pisces	-87.9686	28.9368	0.0000
20100820	HOS Davis *	-89.3479	27.8639	0.0000
20100820	Bunny Bordelon	-90.2749	27.1477	-2.3715
20100820	Bunny Bordelon	-90.2536	27.0617	-2.0967
20100820	HOS Davis	-89.4735	27.7883	-0.4098
20100820	Jack Fitz	-90.5920	27.1760	-2.7060
20100820	Jack Fitz	-90.5698	27.0882	-2.3577
20100820	Jack Fitz	-90.5483	27.0028	-0.9636
20100820	Ocean Varitas	-89.1777	27.1512	-0.1583
20100820	Ocean Varitas	-89.3477	27.3805	-0.1196
20100820	Ocean Varitas	-89.2631	27.2653	-0.1145
20100820	Ocean Varitas	-89.2240	27.4532	0.0000
20100820	Ocean Varitas	-89.1385	27.3393	0.0000
20100820	Ocean Varitas	-89.2169	26.9623	0.0000
20100820	Pisces	-87.2930	28.7430	-0.5351
20100820	Pisces	-88.3305	28.6103	-0.5306
20100820	Pisces	-87.3080	28.8593	-0.3851
20100820	Pisces	-88.4096	28.6106	-0.0946
20100820	Pisces	-87.8683	28.9762	0.0000
20100820	Pisces	-87.8685	28.6365	0.0000
20100820	Pisces	-88.4468	28.6236	0.0000
20100820	Pisces	-88.3700	28.6054	0.0000

Table A.1. Continued

Date	R/V	Longitude	Latitude	DO Anomaly [mol m^{-2}]
20100820	Wes Bordelon	-89.9794	27.2066	-1.2430
20100820	Wes Bordelon	-89.9582	27.1198	-1.1688
20100820	Wes Bordelon	-89.9364	27.0307	-0.8477
20100821	Bunny Bordelon	-90.2313	26.9721	-1.5795
20100821	Bunny Bordelon	-90.2097	26.8841	0.0000
20100821	Bunny Bordelon	-90.1879	26.7959	0.0000
20100821	Cape Hatteras	-88.4147	28.8092	0.0000
20100821	Ferrel	-90.8871	27.2895	-0.3933
20100821	HOS Davis	-90.6584	27.4369	-1.0866
20100821	Jack Fitz	-90.5260	26.9127	-1.2841
20100821	Jack Fitz	-90.5042	26.8247	0.0000
20100821	Jack Fitz	-90.4822	26.7365	0.0000
20100821	Ocean Varitas	-89.4271	26.9994	-0.5722
20100821	Ocean Varitas	-89.3411	26.8844	-0.1885
20100821	Ocean Varitas	-89.0523	27.2268	0.0000
20100821	Ocean Varitas	-88.9661	27.1122	0.0000
20100821	Ocean Varitas	-89.0907	27.0374	0.0000
20100821	Pisces	-88.4782	28.6455	-0.3887
20100821	Pisces	-88.5840	28.5485	-0.2953
20100821	Pisces	-88.4992	28.6717	-0.2139
20100821	Pisces	-88.6632	28.6712	-0.0452
20100821	Pisces	-88.5005	28.7050	0.0000
20100821	Pisces	-88.6322	28.6043	0.0000
20100821	Pisces	-88.5193	28.5046	0.0000
20100821	Pisces	-88.4463	28.4777	0.0000
20100821	Pisces	-88.3672	28.4681	0.0000
20100821	Wes Bordelon	-89.9149	26.9427	-1.0247
20100821	Wes Bordelon	-89.8934	26.8545	0.0000
20100821	Wes Bordelon	-89.8505	26.6783	0.0000
20100822	Brooks McCall *	-89.6879	28.4630	-0.9603
20100822	Brooks McCall *	-89.6001	28.5482	-0.3650
20100822	Brooks McCall	-88.7030	28.4629	-0.3434
20100822	Brooks McCall	-88.7718	28.5483	0.0000
20100822	Brooks McCall	-88.6118	28.3960	0.0000
20100822	Bunny Bordelon	-89.6459	27.0889	-0.2894
20100822	Bunny Bordelon	-89.6833	27.2649	0.0000

Table A.1. Continued

Date	R/V	Longitude	Latitude	DO Anomaly [mol m^{-2}]
20100822	Bunny Bordelon	-89.6621	27.1774	0.0000
20100822	Cape Hatteras	-88.4560	28.7198	-0.3935
20100822	Ferrel	-90.8871	27.1170	0.0000
20100822	Ferrel	-90.8647	27.0289	0.0000
20100822	HOS Davis	-88.9278	27.7907	-0.4639
20100822	HOS Davis	-88.8855	27.7350	0.0000
20100822	HOS Davis	-88.8456	27.6748	0.0000
20100822	Jack Fitz	-91.2733	27.4125	-1.6282
20100822	Jack Fitz	-91.2495	27.3200	-0.2398
20100822	Jack Fitz	-90.9778	27.4738	0.0000
20100822	Pisces	-88.8853	27.9791	-1.0217
20100822	Pisces	-89.1382	27.8290	-0.9171
20100822	Pisces	-89.3905	27.6782	-0.7821
20100822	Pisces	-89.0118	27.9043	-0.6716
20100822	Pisces	-89.2644	27.7537	-0.5570
20100822	Pisces	-88.7585	28.0541	-0.5494
20100822	Pisces	-88.7505	28.1518	-0.4692
20100822	Pisces	-88.6725	28.2680	-0.2367
20100822	Pisces	-88.5963	28.3870	-0.0654
20100822	Pisces	-88.3692	28.3327	0.0000
20100822	Wes Bordelon	-89.8293	26.5902	0.0000
20100822	Wes Bordelon	-89.8079	26.5021	0.0000
20100823	Brooks McCall *	-89.4737	28.2817	-0.4532
20100823	Brooks McCall *	-89.3864	28.3511	0.0000
20100823	Brooks McCall *	-89.5566	28.2219	0.0000
20100823	Brooks McCall	-88.6934	28.2818	-0.4431
20100823	Brooks McCall	-88.8150	28.3710	0.0000
20100823	Brooks McCall	-88.5018	28.3511	0.0000
20100823	Brooks McCall	-88.5468	28.2220	0.0000
20100823	Bunny Bordelon	-91.5451	27.2601	-2.0498
20100823	Bunny Bordelon	-91.5688	27.3516	-0.6881
20100823	Cape Hatteras	-89.1752	27.7663	-2.4526
20100823	Cape Hatteras	-89.2915	27.6313	0.0000
20100823	Cape Hatteras	-89.4060	27.4968	0.0000
20100823	Jack Fitz	-91.2042	27.1432	-0.2064
20100823	Jack Fitz	-91.2268	27.2317	-0.0212

Table A.1. Continued

Date	R/V	Longitude	Latitude	DO Anomaly [mol m^{-2}]
20100823	Pisces	-90.4446	27.2078	-1.9853
20100823	Pisces	-90.5920	27.1783	-1.7632
20100823	Pisces	-90.2970	27.2371	-1.4081
20100823	Pisces	-90.0012	27.2953	-0.8907
20100823	Pisces	-89.5163	27.6026	-0.5040
20100823	Pisces	-89.6421	27.5270	-0.4989
20100823	Pisces	-89.8507	27.3247	-0.4528
20100823	Pisces	-90.7398	27.1477	-0.4477
20100823	Pisces	-89.7678	27.4512	-0.0921
20100823	Pisces	-90.1492	27.2662	0.0000
20100824	Brooks McCall *	-89.2631	28.1659	-0.6069
20100824	Brooks McCall *	-89.3477	28.2789	-0.0938
20100824	Brooks McCall *	-89.2169	27.9409	0.0000
20100824	Brooks McCall	-88.8422	28.1660	-0.5669
20100824	Brooks McCall	-88.7586	28.0540	-0.2304
20100824	Brooks McCall	-88.9267	28.2789	-0.0843
20100824	Brooks McCall	-88.6743	27.9410	0.0000
20100824	Cape Hatteras	-90.4148	27.0767	-0.9798
20100824	Cape Hatteras	-89.0607	27.9030	-0.4897
20100824	Ferrel	-89.6192	27.0007	-1.0669
20100824	Ferrel	-89.5762	26.8246	-0.5656
20100824	Ferrel	-89.5977	26.9127	-0.3732
20100824	Pisces	-91.6851	27.2251	-1.0305
20100824	Pisces	-91.6652	27.1362	-0.4138
20100824	Pisces	-92.0236	27.3387	-0.3541
20100824	Pisces	-91.6439	27.0482	-0.2822
20100824	Pisces	-92.0023	27.2500	-0.0356
20100824	Pisces	-91.7073	27.3125	0.0000
20100824	Pisces	-90.8871	27.1169	0.0000
20100824	Pisces	-91.0347	27.0861	0.0000
20100824	Pisces	-91.1815	27.0550	0.0000
20100824	Pisces	-91.3287	27.0237	0.0000
20100824	Pisces	-91.4758	26.9923	0.0000
20100825	Ocean Veritas *	-89.1385	27.8662	0.0000
20100825	Ocean Veritas *	-89.2240	27.7535	0.0000
20100825	Cape Hatteras	-90.4190	26.7417	0.0000

Table A.1. Continued

Date	R/V	Longitude	Latitude	DO Anomaly [mol m^{-2}]
20100825	Ferrel	-89.5337	26.6483	0.0000
20100825	Ocean Varitas	-88.8849	27.9791	-1.0030
20100825	Ocean Varitas	-88.9688	28.0905	-0.3170
20100825	Ocean Varitas	-89.0537	28.2044	0.0000
20100825	Ocean Varitas	-88.8006	27.8662	0.0000
20100825	Ocean Varitas	-88.7173	27.7535	0.0000
20100825	Pisces	-90.5920	27.1760	-1.9484
20100825	Pisces	-91.9168	26.8990	-0.9150
20100825	Pisces	-90.6578	27.4377	-0.7005
20100825	Pisces	-91.9380	26.9868	-0.5703
20100825	Pisces	-91.8742	26.7222	-0.4337
20100825	Pisces	-91.8955	26.8102	-0.2655
20100825	Pisces	-91.9594	27.0742	-0.1933
20100825	Pisces	-91.9805	27.1624	0.0000
20100826	Ocean Veritas *	-89.3411	27.9040	-0.3384
20100826	Ocean Veritas *	-89.4271	28.0148	0.0000
20100826	Cape Hatteras	-90.4182	26.8287	-2.9641
20100826	Cape Hatteras	-90.4147	26.7423	-0.9441
20100826	Cape Hatteras	-90.4187	26.7442	-0.7083
20100826	Cape Hatteras	-90.4197	26.6633	0.0000
20100826	Ferrel	-89.5126	26.5605	0.0000
20100826	Ferrel	-89.4911	26.4729	0.0000
20100826	HOS Davis	-88.8860	27.9793	-0.5133
20100826	Ocean Varitas	-89.0116	27.9040	-0.4888
20100826	Ocean Varitas	-89.0971	28.0148	0.0000
20100826	Pisces	-90.5698	27.0880	-1.2654
20100826	Pisces	-90.5041	26.8247	-1.1751
20100826	Pisces	-90.5261	26.9126	-1.1217
20100826	Pisces	-90.4803	26.7368	-0.7177
20100826	Pisces	-90.5485	27.0027	-0.5448
20100826	Pisces	-90.4583	26.6478	0.0000
20100826	Pisces	-90.4380	26.5613	0.0000
20100827	Cape Hatteras	-90.4052	26.9778	-1.6386
20100827	HOS Davis	-89.0120	27.9038	-0.5750
20100827	Ocean Varitas	-88.9262	27.7903	-0.4616
20100827	Ocean Varitas	-89.0467	27.7039	0.0000

Table A.1. Continued

Date	R/V	Longitude	Latitude	DO Anomaly [mol m^{-2}]
20100827	Ocean Varitas	-88.8428	27.6786	0.0000
20100827	Ocean Varitas	-88.7414	27.5779	0.0000
20100827	Pisces	-91.5824	26.7845	-0.4016
20100827	Pisces	-92.1935	26.7440	-0.1051
20100827	Pisces	-91.3080	26.9335	0.0000
20100827	Pisces	-91.1375	26.8793	0.0000
20100827	Pisces	-90.7976	26.7627	0.0000
20100827	Pisces	-91.8530	26.6338	0.0000
20100827	Pisces	-91.8313	26.5457	0.0000
20100828	Pisces	-92.4958	27.2844	-0.0405
20100828	Pisces	-92.4958	27.1492	0.0000
20100828	Pisces	-92.4956	27.0141	0.0000
20100828	Pisces	-92.4949	26.8788	0.0000
20100828	Pisces	-92.4947	26.7440	0.0000
20100828	Pisces	-92.7957	26.7440	0.0000
20100828	Pisces	-92.4958	26.6088	0.0000
20100828	Pisces	-92.4959	26.4736	0.0000
20100828	Pisces	-92.4960	26.3384	0.0000
20100829	Pisces	-91.2656	27.4077	-1.5794
20100829	Pisces	-91.1375	26.8793	-0.2239
20100829	Pisces	-91.0934	26.7032	-0.0796
20100829	Pisces	-91.2230	27.2312	0.0000
20100829	Pisces	-91.0344	27.0860	0.0000
20100829	Pisces	-91.1817	27.0552	0.0000
20100829	Pisces	-91.0492	26.5249	0.0000
20100829	Pisces	-90.8646	26.3809	0.0000
20100830	Cape Hatteras	-90.4953	27.0337	-2.2352
20100830	Cape Hatteras	-90.4162	27.0375	-1.9390
20100830	Cape Hatteras	-90.4155	27.0353	-1.7889
20100830	Cape Hatteras	-90.5137	27.0345	-1.4087
20100830	Cape Hatteras	-90.5035	27.0303	-1.2788
20100830	Cape Hatteras	-90.6103	27.0360	-0.8542
20100830	Cape Hatteras	-90.4180	26.9073	-0.5520
20100830	HOS Davis	-89.0113	27.9043	-0.7706
20100830	Pisces	-90.4442	27.2060	-2.2556
20100830	Pisces	-90.5918	27.1760	-1.2794

Table A.1. Continued

Date	R/V	Longitude	Latitude	DO Anomaly [mol m^{-2}]
20100830	Pisces	-90.7398	27.1477	-0.7537
20100830	Pisces	-89.7428	27.4369	-0.4704
20100830	Pisces	-89.8202	27.6025	-0.1156
20100830	Pisces	-89.7056	27.3530	0.0000
20100830	Pisces	-90.8872	27.1170	0.0000
20100831	HOS Davis *	-89.2640	27.7538	-0.9289
20100831	HOS Davis *	-89.1568	27.8217	-0.1489
20100831	Ocean Varitas	-91.1510	27.5298	0.0000
20100831	Pisces	-89.6247	27.1870	-0.5261
20100831	Pisces	-89.5082	26.9375	-0.2784
20100831	Pisces	-89.5468	27.0200	-0.2652
20100831	Pisces	-88.9841	27.3783	-0.0180
20100831	Pisces	-89.0952	27.5260	0.0000
20100831	Pisces	-89.0396	27.4518	0.0000
20100831	Pisces	-89.6644	27.2706	0.0000
20100831	Pisces	-89.5853	27.1039	0.0000
20100831	Pisces	-89.4687	26.8518	0.0000
20100831	Pisces	-89.4285	26.7706	0.0000
20100901	Pisces *	-89.3216	27.8289	-1.2194
20100901	Pisces *	-89.3781	27.9025	-0.3409
20100901	Pisces *	-89.4343	27.9795	0.0000
20100901	Cape Hatteras	-88.2678	28.7368	0.0000
20100901	Cape Hatteras	-88.4577	28.7235	0.0000
20100901	Cape Hatteras	-88.3675	28.6537	0.0000
20100901	HOS Davis	-89.3907	27.6785	-0.8777
20100901	Ocean Varitas	-90.0622	26.9130	-0.9675
20100901	Ocean Varitas	-90.0404	26.8251	-0.7924
20100901	Ocean Varitas	-90.0841	27.0014	-0.7301
20100901	Ocean Varitas	-90.1056	27.0895	-0.5693
20100901	Pisces	-89.2644	27.7538	-1.3738
20100901	Pisces	-89.6307	27.7510	-1.1610
20100901	Pisces	-89.2083	27.6784	-0.9315
20100901	Pisces	-89.3906	27.6783	-0.8265
20100901	Pisces	-89.5165	27.6193	-0.7958
20100901	Pisces	-89.1383	27.8290	-0.7012
20100901	Pisces	-89.5722	27.6758	-0.5854

Table A.1. Continued

Date	R/V	Longitude	Latitude	DO Anomaly [mol m^{-2}]
20100901	Pisces	-89.1527	27.6020	0.0000
20100901	Pisces	-89.4602	27.5275	0.0000
20100902	Cape Hatteras	-88.3672	28.8202	0.0000
20100902	HOS Davis	-89.6422	27.5268	-1.4692
20100902	HOS Davis	-89.5162	27.6025	-1.4531
20100902	Ocean Varitas	-91.5679	27.3512	-1.1350
20100902	Ocean Varitas	-91.5453	27.2616	-0.4600
20100902	Ocean Varitas	-91.5895	27.4388	-0.1669
20100902	Ocean Varitas	-91.5232	27.1757	0.0000
20100902	Pisces	-89.0123	27.9041	-0.0638
20100904	Jack Fitz	-88.8528	28.2513	0.0000
20100904	Meg Skansi	-88.8526	28.2505	-0.1569
20100904	Ocean Varitas	-88.8403	28.0466	-0.0885
20100904	Ocean Varitas	-88.6011	28.3935	0.0000
20100904	Ocean Varitas	-88.6802	28.2770	0.0000
20100904	Ocean Varitas	-88.7597	28.1620	0.0000
20100904	Ocean Varitas	-88.9202	27.9310	0.0000
20100905	Rachel Bordelon *	-89.3078	28.0545	0.0000
20100905	Bunny Bordelon *	-89.4346	27.9795	0.0000
20100905	Bunny Bordelon	-89.5161	27.6031	-0.3336
20100905	Cape Hatteras	-87.8560	28.9277	-0.1930
20100905	Cape Hatteras	-88.1582	28.7510	-0.0977
20100905	Cape Hatteras	-87.5030	29.1670	0.0000
20100905	Cape Hatteras	-87.6792	29.0492	0.0000
20100905	Cape Hatteras	-88.0593	28.8222	0.0000
20100905	Jack Fitz	-88.7000	28.1595	0.0000
20100905	Ocean Varitas	-88.8837	27.9793	-0.4199
20100905	Ocean Varitas	-88.9272	27.7905	-0.1241
20100905	Ocean Varitas	-89.0964	27.5292	0.0000
20100905	Ocean Varitas	-89.0103	27.4116	0.0000
20100905	Rachel Bordelon	-88.9747	28.1300	-0.4905
20100905	Ryan Chouest	-88.6800	28.5065	-0.1612
20100905	Ryan Chouest	-88.8565	28.1445	-0.0537
20100905	Wes Bordelon	-89.6192	27.0018	-0.6651
20100905	Wes Bordelon	-89.1736	26.6639	0.0000
20100906	Bunny Bordelon	-89.4306	27.4898	0.0000

Table A.1. Continued

Date	R/V	Longitude	Latitude	DO Anomaly [mol m^{-2}]
20100906	Cape Hatteras	-88.5633	28.2743	-0.2530
20100906	Cape Hatteras	-88.7492	28.5372	-0.1902
20100906	Cape Hatteras	-88.4747	28.6465	0.0000
20100906	Cape Hatteras	-88.6628	28.4192	0.0000
20100906	Jack Fitz	-88.8670	27.8703	0.0000
20100906	Jack Fitz	-88.9503	27.7260	0.0000
20100906	Meg Skansi	-88.2118	28.6491	-0.8423
20100906	Ocean Varitas	-90.2746	27.1495	-0.7816
20100906	Rachel Bordelon	-88.6506	28.4543	-0.4774
20100907	Bunny Bordelon	-89.7264	27.4423	-0.4970
20100907	Bunny Bordelon	-90.0665	27.5608	0.0000
20100907	Cape Hatteras	-89.1767	27.6398	-0.6322
20100907	Cape Hatteras	-89.0987	27.5305	-0.0830
20100907	Jack Fitz	-89.0338	27.5815	0.0000
20100907	Meg Skansi	-88.4078	28.8105	0.0000
20100907	Rachel Bordelon	-88.2824	28.5934	0.0000
20100907	Rachel Bordelon	-88.3659	28.4133	0.0000
20100907	Wes Bordelon	-90.4811	26.7368	-1.2584
20100907	Wes Bordelon	-89.8934	26.8545	-0.4606
20100908	Cape Hatteras *	-89.3462	27.8640	-0.6700
20100908	Cape Hatteras *	-89.2645	27.7552	-0.4096
20100908	Cape Hatteras *	-89.5198	28.0842	0.0000
20100908	Cape Hatteras *	-89.4360	27.9763	0.0000
20100908	Bunny Bordelon	-90.7029	27.6196	0.0000
20100908	Bunny Bordelon	-91.2951	27.4997	0.0000
20100908	Jack Fitz	-89.2618	27.2662	-0.0540
20100908	Jack Fitz	-89.4262	27.0003	0.0000
20100908	Ocean Varitas	-90.5923	27.1795	-1.3540
20100908	Ocean Varitas	-90.5705	27.0917	-0.8001
20100908	Ocean Varitas	-90.5478	27.0031	-0.4837
20100908	Ocean Varitas	-90.6581	27.4437	-0.1808
20100908	Wes Bordelon	-91.6786	26.5833	-0.0964
20100908	Wes Bordelon	-91.0914	26.7054	0.0000
20100909	Bunny Bordelon	-91.8866	27.3769	0.0000
20100909	Bunny Bordelon	-92.4765	27.2518	0.0000
20100909	Cape Hatteras	-91.5917	27.4407	-0.1940

Table A.1. Continued

Date	R/V	Longitude	Latitude	DO Anomaly [mol m^{-2}]
20100909	Cape Hatteras	-90.4168	27.0342	-0.1184
20100909	Cape Hatteras	-91.5168	27.0057	-0.0560
20100909	HOS Davis	-89.9397	27.6779	0.0000
20100909	Jack Fitz	-89.5080	26.9375	0.0000
20100909	Meg Skansi	-88.7315	28.3732	-0.1841
20100909	Meg Skansi	-88.7835	28.0149	0.0000
20100909	Ocean Varitas	-90.5247	26.9126	-1.2697
20100909	Ocean Varitas	-90.5024	26.8251	-1.0211
20100909	Ocean Varitas	-90.4808	26.7370	-0.8250
20100909	Ocean Varitas	-90.4590	26.6490	0.0000
20100909	Ocean Varitas	-90.4378	26.5613	0.0000
20100909	Rachel Bordelon	-88.2738	28.7382	-0.7166
20100909	Wes Bordelon	-91.7715	26.9382	-0.3825
20100909	Wes Bordelon	-92.2652	26.4617	0.0000
20100910	Bunny Bordelon	-92.3588	26.8130	-0.3457
20100910	Bunny Bordelon	-92.3118	26.6374	-0.3215
20100910	Bunny Bordelon	-92.4058	26.9886	-0.3126
20100910	Cape Hatteras	-88.5032	28.5437	-0.9355
20100910	Cape Hatteras	-88.7000	28.5468	-0.4050
20100910	Cape Hatteras	-88.1232	28.5415	-0.0367
20100910	Cape Hatteras	-88.3117	28.5432	0.0000
20100910	HOS Davis	-89.8532	27.3239	-0.6181
20100910	HOS Davis	-89.7055	27.3529	0.0000
20100910	Jack Fitz	-90.5923	27.1797	-1.4984
20100910	Jack Fitz	-89.9800	27.2085	-1.1374
20100910	Meg Skansi	-88.5353	28.1060	0.0000
20100910	Meg Skansi	-88.6200	27.7899	0.0000
20100910	Ocean Varitas	-90.7523	26.5899	-1.1995
20100910	Ocean Varitas	-90.7305	26.5011	-1.0903
20100910	Ocean Varitas	-90.7975	26.7650	0.0000
20100910	Ocean Varitas	-90.7245	26.6767	0.0000
20100910	Pisces	-90.7617	27.2379	-1.0823
20100910	Pisces	-90.5918	27.1795	-0.6731
20100910	Pisces	-90.5476	27.0035	-0.1758
20100910	Pisces	-90.6362	27.3556	0.0000
20100910	Pisces	-90.7172	27.0619	0.0000

Table A.1. Continued

Date	R/V	Longitude	Latitude	DO Anomaly [mol m^{-2}]
20100910	Rachel Bordelon	-88.3242	28.8105	0.0000
20100910	Wes Bordelon	-92.9453	26.6859	0.0000
20100910	Wes Bordelon	-92.5578	26.3986	0.0000
20100911	Bunny Bordelon	-91.7245	26.7593	-1.8622
20100911	Bunny Bordelon	-91.5688	27.3511	-0.1775
20100911	Bunny Bordelon	-91.8177	27.1140	-0.1769
20100911	Cape Hatteras	-87.9310	28.7097	-0.3376
20100911	Cape Hatteras	-87.9332	28.5410	-0.2095
20100911	Cape Hatteras	-87.9298	28.8792	-0.1837
20100911	Cape Hatteras	-88.1217	29.0442	0.0000
20100911	HOS Davis	-90.1489	27.2652	-1.6884
20100911	HOS Davis	-89.9000	27.2946	-1.1828
20100911	Jack Fitz	-91.1825	27.0603	0.0000
20100911	Meg Skansi	-88.3659	28.2509	-0.0876
20100911	Pisces	-90.5035	26.8274	-1.2187
20100911	Pisces	-90.6286	26.7098	-1.1383
20100911	Pisces	-90.4596	26.6514	-0.0682
20100911	Pisces	-90.6729	26.8858	0.0000
20100911	Pisces	-90.9449	26.7381	0.0000
20100911	Pisces	-91.0694	26.6201	0.0000
20100911	Pisces	-90.5845	26.5338	0.0000
20100911	Pisces	-90.4157	26.4753	0.0000
20100911	Wes Bordelon	-92.1583	27.2266	-0.1490
20100911	Wes Bordelon	-92.7234	27.0129	0.0000
20100911	Wes Bordelon	-92.6522	26.7497	0.0000
20100912	Jack Fitz *	-89.2245	27.8792	-0.3569
20100912	Ocean Veritas *	-89.3040	27.7890	-0.1998
20100912	Bunny Bordelon	-89.8294	26.5901	0.0000
20100912	Bunny Bordelon	-90.4152	26.4727	0.0000
20100912	HOS Davis	-90.2966	27.2356	-1.3034
20100912	Jack Fitz	-89.6873	27.8288	0.0000
20100912	Ocean Varitas	-89.3906	27.6780	-0.6915
20100912	Ocean Varitas	-89.4721	27.7890	-0.5575
20100912	Ocean Varitas	-89.3040	27.5652	-0.2114
20100912	Pisces	-91.1594	26.9719	-0.4900
20100912	Pisces	-91.5223	27.1749	-0.2204

Table A.1. Continued

Date	R/V	Longitude	Latitude	DO Anomaly [mol m^{-2}]
20100912	Pisces	-91.2045	27.1478	-0.1750
20100912	Pisces	-91.2498	27.3237	-0.0716
20100912	Pisces	-91.8402	27.2013	-0.0696
20100912	Pisces	-92.1583	27.2269	-0.0221
20100912	Pisces	-91.0345	27.0900	0.0000
20100912	Pisces	-90.9896	26.9141	0.0000
20100912	Pisces	-91.1143	26.7960	0.0000
20100912	Rachel Bordelon	-88.5979	28.6058	-0.4364
20100912	Ryan Chouest	-87.4066	29.0334	-0.1045
20100912	Ryan Chouest	-87.8683	28.9762	0.0000
20100912	Wes Bordelon	-90.5924	27.1797	-2.6976
20100912	Wes Bordelon	-90.6590	27.4438	-0.4642
20100913	Meg Skansi *	-89.3388	27.7654	0.0000
20100913	Bunny Bordelon	-89.0509	27.2274	-0.0861
20100913	Bunny Bordelon	-88.7993	26.8904	0.0000
20100913	HOS Davis	-90.5260	26.9127	-1.1822
20100913	HOS Davis	-90.5698	27.0879	-0.7275
20100913	HOS Davis	-90.5485	27.0027	-0.2933
20100913	Jack Fitz	-88.3660	28.0883	0.0000
20100913	Meg Skansi	-89.0963	28.0086	-0.3634
20100913	Pisces	-91.6009	26.8806	-0.9285
20100913	Pisces	-91.4766	26.9991	-0.5301
20100913	Pisces	-91.9644	27.0824	-0.3954
20100913	Pisces	-91.1819	27.0599	-0.3021
20100913	Pisces	-91.7709	26.9377	-0.2976
20100913	Pisces	-91.4538	26.9112	-0.0879
20100913	Pisces	-90.8647	27.0320	-0.0706
20100913	Pisces	-91.3293	27.0296	0.0000
20100913	Pisces	-91.3066	26.9416	0.0000
20100913	Rachel Bordelon	-88.3831	28.7283	-0.0593
20100913	Ryan Chouest	-87.8687	29.1227	-0.2618
20100913	Wes Bordelon	-90.8775	26.4716	-1.1917
20100913	Wes Bordelon	-91.1257	26.2353	-0.2267
20100913	Wes Bordelon	-91.3956	26.0867	0.0000
20100914	Cape Hatteras	-87.9283	28.8818	-2.2924
20100914	Cape Hatteras	-87.9633	28.5268	-0.2929

Table A.1. Continued

Date	R/V	Longitude	Latitude	DO Anomaly [mol m^{-2}]
20100914	Cape Hatteras	-87.9322	28.5413	-0.0893
20100914	HOS Davis	-90.5260	26.9127	-1.4405
20100914	HOS Davis	-90.4812	26.7368	-1.0310
20100914	HOS Davis	-90.5041	26.8246	-0.8859
20100914	Pisces	-90.5697	27.0915	-0.7035
20100914	Pisces	-90.4222	27.1210	0.0000
20100914	Ryan Chouest	-87.8492	28.8803	-1.1208
20100915	Pisces *	-89.2665	27.7527	-0.2658
20100915	HOS Davis	-90.4153	26.4727	-0.2770
20100915	Pisces	-90.2745	27.1503	-0.8347
20100915	Pisces	-89.3901	27.6785	-0.7252
20100915	Pisces	-89.6417	27.5273	-0.4853
20100915	Pisces	-90.0224	27.3847	-0.4179
20100915	Pisces	-89.7477	27.5304	-0.3067
20100915	Pisces	-90.1486	27.2676	-0.2402
20100915	Pisces	-89.5160	27.6030	-0.1969
20100915	Pisces	-89.8743	27.4136	0.0000
20100916	Pisces *	-89.2217	27.9407	-0.0987
20100916	HOS Davis	-90.6282	26.7072	0.0000
20100916	Pisces	-88.6118	28.3960	-0.6679
20100916	Pisces	-88.5300	28.5101	-0.6080
20100916	Pisces	-88.4531	28.6711	-0.0431
20100916	Pisces	-88.0945	28.8637	0.0000
20100916	Pisces	-88.2888	28.7925	0.0000
20100916	Pisces	-88.3648	28.7652	0.0000
20100916	Pisces	-88.6934	28.2818	0.0000
20100916	Pisces	-88.8419	28.1662	0.0000
20100916	Pisces	-88.9685	28.0909	0.0000
20100916	Pisces	-89.0949	28.0155	0.0000
20100917	HOS Davis	-90.6504	26.7952	0.0000
20100917	Pisces	-87.6850	29.0507	-0.0884
20100917	Pisces	-87.8224	28.9886	-0.0858
20100917	Pisces	-87.9585	28.9262	0.0000
20100919	HOS Davis *	-89.4482	27.9534	0.0000
20100920	HOS Davis	-89.6906	27.5198	-0.4328